

Paraneoplastic cerebellar degeneration: Characterizing the Yo antibody antigens

Torbjørn Kråkenes

Thesis for the degree of Philosophiae Doctor (PhD)
University of Bergen, Norway
2021

UNIVERSITY OF BERGEN



Paraneoplastic cerebellar degeneration: Characterizing the Yo antibody antigens

Torbjørn Kråkenes



Thesis for the degree of Philosophiae Doctor (PhD)
at the University of Bergen

Date of defense: 16.03.2021

© Copyright Torbjørn Kråkenes

The material in this publication is covered by the provisions of the Copyright Act.

Year: 2021

Title: Paraneoplastic cerebellar degeneration: Characterizing the Yo antibody antigens

Name: Torbjørn Kråkenes

Print: Skipnes Kommunikasjon / University of Bergen

CONTENTS

SCIENTIFIC ENVIRONMENT.....	6
ACKNOWLEDGEMENTS	7
ABSTRACT	8
LIST OF PUBLICATIONS	11
ABBREVIATIONS.....	12
1. INTRODUCTION.....	13
<i>1.1 The Nervous System.....</i>	<i>13</i>
1.1.1 Anatomy of the brain	13
1.1.2 Cerebellum	13
<i>1.2 Cells of the Nervous System.....</i>	<i>15</i>
1.2.1 Neurons	15
1.2.2 Glial cells.....	18
<i>1.3. The Immune System.....</i>	<i>19</i>
1.3.1 The innate immune system	19
1.3.2 The adaptive immune system	20
1.3.3 Autoimmunity.....	22
1.3.4 Autoantibodies	23
1.3.5 Immune system and cancers	23
1.3.6 Immune system in the central nervous system.....	23
<i>1.4 Paraneoplastic Neurological Syndromes</i>	<i>25</i>
1.4.1 Onconeural antibodies	28
1.4.2 Paraneoplastic cerebellar degeneration	30
1.4.3 Yo-associated PCD	32
1.4.4 Cerebellar degeneration-related proteins.....	33
2. AIMS OF THE STUDY	35
3. METHODS.....	36
<i>3.1 Patient Samples</i>	<i>36</i>
<i>3.2 Cerebellar Tissue</i>	<i>36</i>

3.3 Cell Culturing	36
3.4 Immunostaining	36
3.5 Fluorescent Immunoblotting	37
3.6 Immunoprecipitation	37
3.7 Mass Spectrometry-based Proteomics.....	38
3.7.1 Database searching and criteria for protein identification	40
3.8 Recombinant DNA and Transfection	41
3.9 Super-Resolution Microscopy.....	41
3.10 Proximity Ligation Assay	41
3.11 Purkinje Neuron Culture	42
3.12 Methodological Considerations	46
4. RESULTS	47
4.1 Paper I	47
4.2 Paper II	49
4.3 Paper III	51
5. DISCUSSION.....	55
5.1 Paper I	55
5.2 Paper II	57
5.3 Paper III	59
6. ADVANCES AND FUTURE ASPECTS.....	62
7. CONCLUSIONS	64
8. SOURCE OF DATA	65
9. APPENDIX.....	75
9.1 CDR2.....	75
9.1.1 CDR2 mRNA sequence	75
9.1.2 CDR2 amino acid sequence.....	76
9.1.3 CDR2 amino acid profile	77
9.2 CDR2L.....	77
9.2.1 CDR2L mRNA sequence	77

9.2.2 CDR2L amino acid sequence.....	79
9.2.3 CDR2L amino acid profile.....	80
10. ORIGINAL PUBLICATIONS	81

SCIENTIFIC ENVIRONMENT

This work was carried out at the Neurology Research Laboratory, Haukeland University Hospital, Norway. The main funding was from Clinical Institute 1, University of Bergen, Norway.

ACKNOWLEDGEMENTS

First of all, I would like to thank my main supervisor and boss Prof. Christian A. Vedeler for including me as a master student at the Neurology Research Laboratory and encouraging me to pursue a PhD degree. Although exhausting at times, his everlasting enthusiasm made it an enjoyable ride.

I would also like to thank my PhD co-supervisor Manja Schubert and MSc co-supervisor Tilo Eichler for their excellent support and lab training, as well as for the countless discussions needed to understand the field of paraneoplastic neurological syndromes.

The technical and social support from the rest of the lab group, including Hanne Linda Nakkestad, Mette Haugen, Cecilie Totland, Kibret Mazengia, Margrethe Raspotnig, Sonia Gavasso, Liesbeth Kroondijk, Ida Herdlevær and Eirik Solheim, have been invaluable throughout the years. I also want to express my gratitude to Prof. Laurence A. Bindoff for proofreading of both article manuscripts and the thesis itself.

A huge thanks also to my mom, dad and sisters for their eternal support.

ABSTRACT

Background:

The pathogenesis of paraneoplastic cerebellar degeneration (PCD) with Yo-antibodies is unclear. The disease is generally accepted as immune-mediated, but whether the Yo antibodies themselves are pathogenic or if T cells are responsible for the neurodegeneration is not known. Yo antibodies are, nevertheless, good biomarkers for the disease.

The primary target of Yo antibodies was until recently thought to be CDR2. We showed, however, that these antibodies bind to CDR2L and not CDR2. CDR2L is present on both bound and free ribosomes in the cytoplasm of cerebellar Purkinje neurons as well as other cells types, but the cellular function and spatial conformation remains unknown.

Objective:

Paper I: To determine the major antigen of Yo antibodies in PCD patients.

Paper II: To define the subcellular location of both CDR2 and CDR2L and potential interaction partners.

Paper III: To generate a protocol for Purkinje neuron culture from both embryonic and postnatal rats that can be used for further characterization of PCD pathogenesis.

Methods:

Paper I: Patient samples (serum and CSF), cerebellar tissue (human and rat), cancer cell cultures (OvCar3 and HepG2), immunostaining, immunoprecipitation, fluorescent immunoblotting and recombinant DNA transfection.

Paper II: Patient samples (serum and CSF), cerebellar tissue (human), cancer cell cultures (OvCar3 and HepG2), Purkinje neuron cultures (rat), mass spectrometry-

based proteomics, immunostaining, proximity ligation assay, super-resolution microscopy and immunoprecipitation.

Paper III: Culturing of dissociated rat cerebellar tissue, immunostaining, Purkinje neuron counting, dendritic branch analysis, lentiviral transfection and micro-electrode array recordings.

Results:

Paper I: We demonstrated that CDR2L, and not CDR2, is the major antigen target of Yo antibodies. These antibodies do, however, bind recombinant CDR2.

Paper II: We found that CDR2L is predicted to interact with several ribosomal proteins and that it indeed does interact with the ribosomal protein rpS6. Interaction partners of CDR2 included the nuclear speckle proteins eIF4A3, SON and SRSF2.

Paper III: We found that a support layer, pH stability and co-factor supplements were essential to generate rat cerebellar cell cultures with high yield of mature Purkinje neurons.

Conclusions:

Paper I: The finding that Yo antibodies bind endogenous CDR2L, and not CDR2, allows us to rethink the mechanisms involved in Yo-mediated PCD. The binding of recombinant CDR2 suggests that these proteins have common epitopes which is not surprising considering their 45% amino acid sequence identity. Furthermore, test assays using CDR2L instead of CDR2 could be more sensitive, reducing the large amounts of false-positive results obtained today.

Paper II: Previous studies suggested that Yo antibodies bind a ribosomal target, but the locations of CDR2 and CDR2L were unknown. Our finding that CDR2L interacts specifically with ribosomal proteins, while CDR2 interacts with nuclear speckle proteins, adds further support for CDR2L being the primary Yo antibody target. Since

one of the interaction partners of CDR2, eIF4A3, translocates from the nucleus to the ribosome, where it interacts with rpS6, this also adds an indirect link between CDR2L and CDR2. Whether CDR2L and CDR2 have similar roles or are involved in related processes in protein transcription and translation remains to be resolved.

Paper III: We established a robust primary culture protocol that gave high yields of mature Purkinje neurons from both embryonic and postnatal rats. These cultures were well suited to high-throughput screening, genetic manipulation and electrophysiological recordings and will be useful for exploring both neurodegenerative and regenerative mechanisms.

LIST OF PUBLICATIONS

The thesis is based on the following papers:

- I. Krakenes T, Herdlevær I, Raspotnig M, Haugen M, Schubert M, Vedeler CA (2019): "CDR2L Is the Major Yo Antibody Target in Paraneoplastic Cerebellar Degeneration". ANN NEUROL 2019;86:316–321
- II. Herdlevær I, Krakenes T, Schubert M, Vedeler CA (2020): "Localization of CDR2L and CDR2 in Paraneoplastic Cerebellar Degeneration". Ann Clin Transl Neurol 2020 Oct 3. doi: 10.1002/acn3.51212. Online ahead of print
- III. Uggerud I, Kråkenes T, Vedeler CA, Schubert M (2020): "Development and optimization of a high-throughput 3D rat Purkinje neuron culture". Manuscript submitted, <https://www.biorxiv.org/content/10.1101/2020.05.20.105858v1.full>

Reprints were made with permission from Annals of Neurology and Annals of Clinical and Translational Neurology published by Wiley Periodicals LLC on behalf of American Neurological Association.

ABBREVIATIONS

APC	Antigen-presenting cell
CDR	Cerebellar degeneration-related
CSF	Cerebrospinal fluid
GABA	gamma-aminobutyric acid
HLA	Human leucocyte antigen
ICI	Immune checkpoint inhibitors
Ig	Immunoglobulin
ISF	Interstitial fluid
MHC	Major histocompatibility complex
NK cells	Natural killer cells
NA	Numerical aperture
PBS	Phosphate buffered saline
PCD	Paraneoplastic cerebellar degeneration
PCR	Polymerase chain reaction
PenStrep	Penicillin and streptomycin
PFA	Paraformaldehyde
PLA	Proximity ligation assay
PNS	Paraneoplastic neurological syndromes
STED	Stimulated emission depletion

1. INTRODUCTION

1.1 The Nervous System

1.1.1 Anatomy of the brain

The brain is divided into three major parts: the forebrain, the midbrain and the hindbrain. The forebrain includes thalamus, hypothalamus, subthalamus, epithalamus and the cerebrum with cerebral cortex, white matter and the basal ganglia. The midbrain connects the middle brain and brainstem while the hindbrain includes the medulla, pons and cerebellum. The main focus of this thesis will be cells in the cerebellum.

1.1.2 Cerebellum

The cerebellum plays an important role in motor control and may also be involved in some cognitive functions. In contrast to the irregular convolutions of the cerebral cortex, the cerebellar cortex has a highly regular arrangement, creating finely spaced parallel grooves. The cerebellum contains more neurons than the total from the rest of the brain, although it takes up only around 10% of the brain volume. Damage to the cells of the cerebellum produce disorders in fine movement, balance, posture and motor learning. The cerebellar cortex is commonly divided into three layers: the molecular layer, the Purkinje layer and the granular layer (Fig. 1).

1.1.2.1 *The molecular layer*

The molecular layer is the outermost layer of the cerebellar cortex and includes the dendritic trees of Purkinje neurons, a huge array of parallel fibers from the granule cells, as well as stellate and basket cells. Most of the parallel fibers synapse on Purkinje neurons¹ where they transmit excitatory signals using glutamate as neurotransmitter. Stellate and basket cells are interneurons that use the neurotransmitter GABA to inhibit the neuronal excitability of Purkinje neurons.

1.1.2.2 The Purkinje layer

The Purkinje layer includes the bodies of Bergman glial cells and Purkinje neurons. The latter are among the largest neurons in the brain: they receive more synaptic input than any other cell in the brain with estimates as high as 200,000 spines per Purkinje neuron². This synaptic input comes mainly from the parallel fibers of granule cells. Purkinje neurons are also GABAergic and thus forward inhibitory signals to their connections in the deep cerebellar nuclei.

1.1.2.3 The granule layer

Granule cells are among the smallest and most numerous neurons in the brain accounting for around 75% of the neurons in the brain³. These neurons use glutamate as neurotransmitter and thus exerts excitatory effects through their synaptic connections with Purkinje neurons.

1.1.2.4 Mossy and climbing fibers

In addition to the cells of the cerebellum, the excitatory mossy fibers and climbing fibers enter the cerebellum from outside and play a dominant role in cerebellar signaling. Both fibers continue through the cerebellar cortex and connect with the deep cerebellar nuclei, which are clusters of grey matter lying in the white matter at the core of the cerebellum. The deep nuclei are considered to be the main signaling output from the cerebellum.

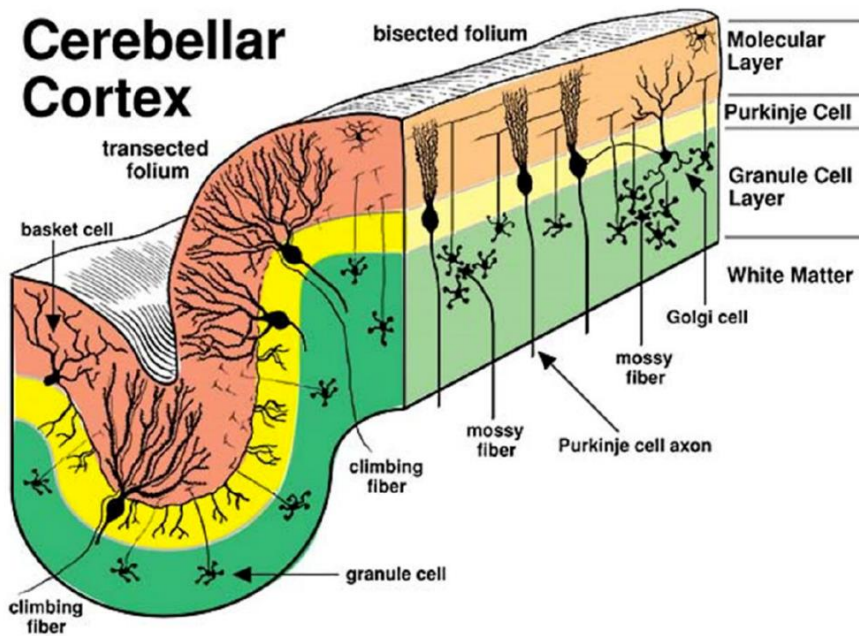


Figure 1: The layers of the cerebellar cortex, including the molecular layer, Purkinje cell layer and the granule cell layer. Reprinted by permission from Minnesota Veterinary Anatomy, University of Minnesota, <http://vanat.cvm.umn.edu/neurHistAtls/cataPages/cataCNS.html>.

1.2 Cells of the Nervous System

The major cells of the nervous system are neurons, glial cells and endothelial cells, with neurons being the most abundant. Although estimates vary⁴, it is thought that there are around 80-90 billion neurons in the brain⁵ and around 50 billion glial cells⁶.⁷ Endothelial cells, supporting blood supply, account for up to 20 billion cells present in the brain⁸, giving a ratio between neurons, glial cells and endothelial cells of approximately 5:3:1 and a total number of cells of around 150 billion.

1.2.1 Neurons

Neurons are conduits that receive electrical and chemical input through branched dendrites and relay the signal via the cell soma. The signal, called an action potential, travels through its axon to other cells. The surface of dendrites contains hundreds to

thousands of spines^{2, 9}, to which other cells can connect and make synapses to transmit their message. Purkinje cells are the neurons with most spines with estimates as high as 200,000 spines per cell. Most of these spines create synapses with parallel fibers from granule cells as well as a lower number of synapses with climbing fibers from the medulla².

Neurons are typically classified into three types: motor (efferent neurons), sensory (afferent neurons) and interneurons. The mechanism of neural signaling is mostly the same, with information received through dendrites and forwarded through axons, but neurons differ in both morphology, location and function.

Interneurons can be subdivided into local and relay interneurons. The former has short axons and are responsible for receiving and forwarding information within a small region. Relay interneurons, on the other hand, have long axons that connect different neural regions. Interneurons primarily use the inhibitory neurotransmitters GABA or glycine, although there are also excitatory ones using glutamate or acetylcholine. Interneurons create complex circuits needed for complex tasks.

Sensory neurons are located in the brainstem and spinal cord where they receive information from sensory organs and forward these signals to central structures of the brain. Sensory neurons have a single axon that splits into two: one part with dendrites in the end that connects to distant parts of the body to sense stimuli, and another part that forwards the information to the brain via the spinal cord. Sensory neurons are activated upon stimulation of our senses, either through physical or chemical stimuli and glutamate is present in all types of neurons in sensory ganglia.

Motor neurons are divided into upper and lower motor neurons. Upper motor neurons are located in the motor cortex of the cerebrum as well as in the brainstem and project their axons through the spinal cord where they connect to lower motor neurons either directly or through interneurons. Lower motor neurons are located in the brainstem and spinal cord and act as a link between upper motor neurons and muscles/glands. Upper motor neurons transmit their signals through glutamate, while lower motor neurons activate muscle through acetylcholine.

1.2.1.3 *Purkinje neurons*

The Purkinje neurons of the cerebellum are among the largest neurons in the brain and consist of a massive, planar dendritic tree extending into the molecular layer as well as an axon extending through the granule layer to the deep cerebellar nuclei. These neurons receive excitatory stimuli from the parallel fibers of granule cells as well as climbing and mossy fibers entering from outside of the cerebellum, while stellate and basket cells perform inhibitory stimuli. Purkinje neurons integrate all information available in the cerebellar cortex and forward inhibitory stimuli to the deep nuclei in the white matter of the cerebellum.

The somas of Purkinje neurons form a single-celled layer as illustrated in Figure 2. Their dendrites form a planar shape with minimal overlap, which is achieved through dynamic local branch growth behavior¹⁰. This dendritic shape allows each parallel fiber from granule cells to travel through and synapse with large numbers of Purkinje dendrites. Of the estimated 200,000 synapses on each Purkinje neuron, the vast majority synapse with parallel fibers. On average, parallel fibers form just under two synapses with each Purkinje neuron it travels through¹¹.

Being the sole output of the cerebellar cortex, any disturbance of Purkinje neuron signaling will cause severe symptoms¹²⁻¹⁴. This includes ataxia, which manifests in patients as reduced coordination that can affect balance and walking, speech and/or eye movement etc. Purkinje neuron disturbances can be triggered through genetic mutations (e.g. spinocerebellar ataxia), autoimmunity (e.g. gluten), toxic exposures (e.g. alcohol) or other neurodegenerative diseases (e.g. Creutzfeldt-Jakob disease)¹⁵⁻¹⁷. In these patients, cerebellar atrophy and Purkinje neuron loss can be seen post mortem.

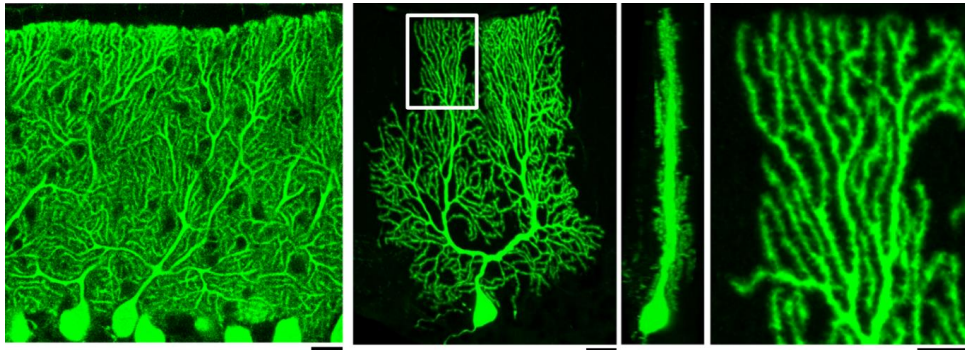


Figure 2: Purkinje neurons of the cerebellum displayed from different angles through calbindin staining. Reprinted by permission from Springer Nature, License #4967950299555: Springer Nature, *The Cerebellum, Dendritic Self-Avoidance and Morphological Development of Cerebellar Purkinje Cells*, Fujishima K et al. 2018¹⁰.

1.2.2 Glial cells

Glial cells (also called neuroglia or glia) are non-neural cells of the nervous system that support neurons structurally and metabolically. They have multiple functions including forming myelin around axons, providing nutrients, holding neurons in place and removing pathogens and dead neurons. In the central nervous system, these cells include oligodendrocytes, astrocytes, ependymal cells and microglia, while glial cells of the peripheral nervous system include Schwann cells and satellite cells.

Glial cells are essential for neural development and maintenance. Oligodendrocytes insulates neurons through myelin; astrocytes deliver nutrients, support the blood-brain barrier and assist in repair and regeneration of neurons¹⁸; microglia are phagocytes of the innate immune system that monitors the central nervous system and removes cellular debris, dead cells and pathogens as well as stimulating the adaptive immune system when needed; ependymal cells are involved in the production and regulation of cerebrospinal fluid.

The ratio of glial cells versus neurons varies between different regions of the nervous system. In the human spinal cord, there are estimated to be six times as many glial cells as neurons, while there are around equal amounts in the cerebral cortex. In the cerebellum however, there are around 20 times as many neurons as glial cells⁷,

mostly due to the enormous amount of cerebellar granule neurons, which alone are estimated to outnumber all other neurons in the nervous system combined¹⁹.

1.3. The Immune System

The immune system monitors the body and removes dead and damaged cells as well as substances that are found foreign and potentially harmful. The term *immunity* is derived from the Latin word *immunitas*, which referred to the protection from legal prosecutions offered to Roman senators during their tenure in office. This intricate system is divided into two parts: an *innate* part that provides an early and broad line of defense, and an *adaptive* part that generate a more powerful and specialized response. The immune system can also, unfortunately, target self molecules, in which the response is called autoimmune. The different cells of the immune system are displayed in Figure 3.

1.3.1 The innate immune system

The innate system is initiated immediately when required, and the main components of the system include (1) physical and chemical barriers, (2) specialized cells, (3) blood proteins and (4) cytokines. If foreign substances breach the epithelial barriers comprising skin, respiratory passages and the gastrointestinal tract, they will encounter the cells of the innate system stimulating the process of inflammation. Inflammation is driven by leukocytes and plasma proteins that are recruited to the breach site as a form of rapid defense. This immediate defense is mediated mainly through cytokines produced by a variety of immune cells. Cytokines are small signaling proteins that initiate the resistance to foreign substances such as microbes, viruses, toxins and cancer cells, with subsequent killing of infected cells by natural killer cells (NK cells). This initial defense further stimulates the adaptive system when needed for a more specific immune response.

1.3.2 The adaptive immune system

The adaptive system specifically targets foreign substances, and this requires time for initiation. Once established, this system has an ability to “remember” the substance and thus can generate a more vigorous response to repeated exposure. The main components of the adaptive system are cells, called *lymphocytes*, and *antibodies*. The latter are molecules produced by a subset of the lymphocytes. Substances targeted by the adaptive immune system are called *antigens*.

There are two types of adaptive immune response - humoral immunity and cell-mediated immunity. The former is mediated by antibodies produced by B lymphocytes (B cells) that tag foreign substances for removal. The latter is mediated by T lymphocytes (T cells) and targets substances such as bacteria and viruses that survive and proliferate inside host cells, where they are inaccessible to circulating antibodies. Both B and T cells are derived from hematopoietic stem cells in the bone marrow. The name B cell originate from their first detection in the bursa of Fabricius in birds and are matured in the bone marrow, while T cells got their name from their origin of maturation in the thymus.

1.3.2.1 T cells

Each T cell expresses specific antigen-binding receptors, called T cell receptors, on their cell membrane. When a T cell is presented with an antigen by antigen-presenting cells (APCs) such as dendritic cells, macrophages or B cells, they are activated and differentiate. This stimulation is mediated through major histocompatibility complex (MHC) molecules on the surface of the APCs. MHC molecules are present in all jawed vertebrates, and in humans they are called human leucocyte antigens (HLA). Class I MHC are found on most nucleated cells and present endogenous peptides, while class II MHC molecules, found on APCs, present exogenous peptides to T cells. This antigen-presentation occurs both in the blood stream and in the lymphatic system, often in lymph nodes where these immune cells accumulate.

Once activated, T cells differentiate into either cytotoxic T cells (CD8⁺ cells) or T helper (T_h) cells (CD4⁺). Cytotoxic T cells are responsible for the destruction of infected cells and tumor cells. Following resolution, most of the cytotoxic T cells are removed, but a small subset is kept as memory T cells that can be activated quickly on repeated exposure to the same antigen. T_h do not have cytotoxic or phagocytic properties, but are important for regulating the immune response. There are several subsets of T_h cells, with T_h1, T_h2 and T_h17 being the most frequent and the subset of T_h cells that are generated will depend on the antigen. T_h1 produce interferon gamma (IFN- γ) to stimulate removal of bacteria and viruses or other intracellular pathogens, as well as stimulating B cells. T_h2 cells release cytokines to stimulate removal of parasites and maturation of B cells. T_h17 cells release a different subset of cytokines and are particularly associated with chronic infections²⁰. As with cytotoxic T cells, a fraction of the T_h cells is kept as memory cells.

1.3.2.2 B cells

B cells have receptors that can recognize and bind pathogens directly without the need of APCs. These receptors are specific antibodies bound to the B cell's surface. Depending on the antigen that binds to these receptors, B cells can either clear the pathogen directly or ingest and present the antigen to T_h cells for further activation and differentiation. In both scenarios, the B cells differentiate into antibody-secreting plasma cells, while memory B cells are usually only seen in the latter scenario²¹.

Plasma cells are able to continuously release antibodies at an astounding rate of several thousand molecules per second²². These antibodies enter the circulation and tissues to provide protection against pathogens. When the antibodies bind to antigens, other immune cells are able to detect and destroy the pathogens. Once this is done, the plasma cells undergo apoptosis while the memory B cells persists in case of re-exposure.

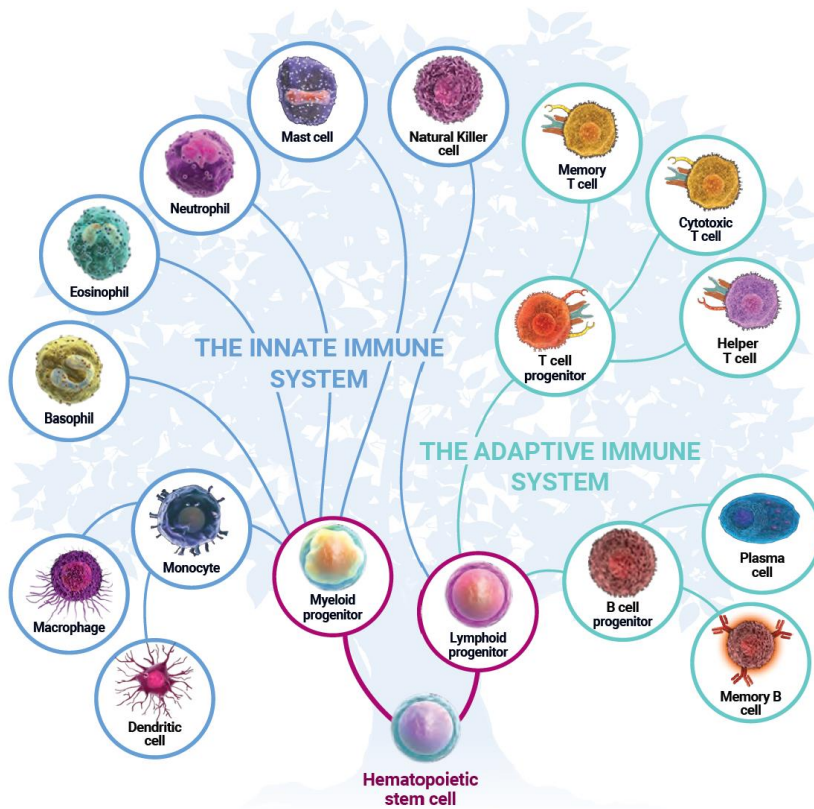


Figure 3: The different immune cells of the innate and adaptive immune system including their progenitors
Reprinted by permission from PeproTech Inc.

1.3.3 Autoimmunity

Under normal conditions, lymphocytes should not react against an individual's own molecules. Lymphocytes that do, are normally eliminated, inactivated or modified. This is managed through a process called *tolerance*. All humans are born with similar antigen receptor gene segments that recombine randomly to create a large and diverse repertoire before being expressed in lymphocytes. A lot of these receptors can recognize self-molecules and therefore needs to be removed. When the process of tolerance fails to remove self-reacting lymphocytes, autoimmunity can occur, causing tissue damage that is potentially lethal.

1.3.4 Autoantibodies

T cell receptors are bound to the cell itself, while B cells fill up their plasma membrane with receptors and subsequently release a lot of these as free-floating antibodies. Antibodies directed against self-molecules are called *autoantibodies*. These can be pathological at one site, causing disease, and simultaneously non-pathological at other sites as in the case of removing cancer cells, as will be discussed later.

1.3.5 Immune system and cancers

When a cancer develops in the body, cancer cells are usually eliminated by cytotoxic cells such as CD8⁺ T cells and NK cells²³. Sometimes, less immunogenic cancer cells are able to avoid the immune system, making them able to expand and travel to other tissues, a process called metastasis. Tumor growth and spread are not the only risks associated with cancer. Cancers can also trigger autoimmunity, a process that stimulates the immune system to kill otherwise healthy cells.

Treatment with immune checkpoint inhibitors (ICIs) has led to increased survival and long-term remission, even in patients with metastatic cancer²⁴. ICIs are monoclonal antibodies that target cytotoxic T-lymphocyte antigen 4 (CTLA4), programmed cell death 1 (PD-1) protein or its ligand PD-L1, ultimately inhibiting regulatory effects of T cell activation²⁵. However, when these checkpoints of the immune system are blocked, releasing the brakes of T cell activity, several side effects can occur including worsening of pre-existing and *de novo* development of autoimmune neurological diseases as paraneoplastic neurological syndromes^{26, 27}.

1.3.6 Immune system in the central nervous system

The brain, along with organs such as the eye, testes and placenta, is protected from many of the immune responses found in the rest of the body. These sites are so-called *immune-privileged sites*. In the brain, this protection is thought to be mediated by the blood-brain barrier consisting of vascular endothelium, the choroid plexus

epithelium, and the glia limitans that together cover the surface of the central nervous system and its blood vessels²⁸. The different brain barriers can be seen in Figure 4.

The brain is, however, connected to the peripheral immune system through an exchange system between the cerebrospinal fluid (CSF) and interstitial fluid (ISF), termed the glymphatic system²⁹. Lymphatic vessels are also found in the dura mater, indicating that ISF can drain to lymphoid tissues through subarachnoid CSF^{30, 31}. Since different parts of the brain differ in their communication with the immune system, the anatomy of the brain must be taken into consideration when considering the impact of immune-privilege.

Many neurodegenerative diseases are associated with a dysregulated immune response. Immune cells in the CNS are associated with various diseases such as multiple sclerosis and Alzheimer disease³²⁻³⁴. Paradoxically, the presence of immune cells in the CNS has been shown to decrease disease progression in some animal models: The lack of T cells in animal models of amyotrophic lateral sclerosis and Alzheimer disease resulted in a faster disease progression^{35, 36}. Thus, the different immune cells in the CNS associated with neurodegenerative diseases have to be thoroughly investigated to understand which cells are pathogenic and which have a protective role in the disease course.

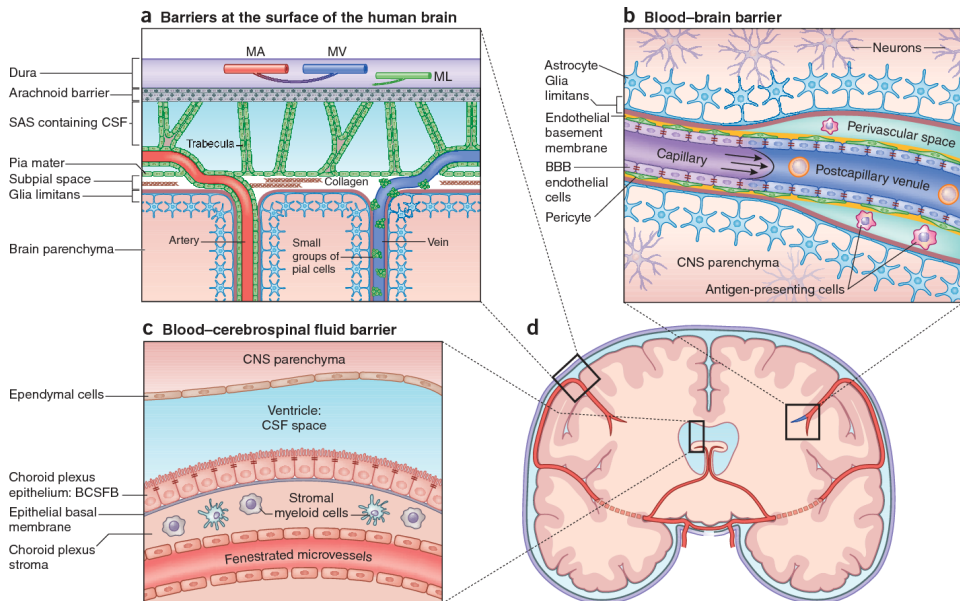


Figure 4: The barriers of the brain, including the meninges, astrocytes, endothelial and epithelial cells. Reprinted by permission from Springer Nature, License #4967960606352: Springer Nature, Neuroimmune Communication, The movers and shapers in immune privilege of the CNS, Engelhardt B et al. 2017²⁸.

1.4 Paraneoplastic Neurological Syndromes

The term *paraneoplastic syndrome* is used to describe symptoms or signs that result from damage to organs or tissues distant from the site of a malignant neoplasm or its metastasis³⁷. This damage can be caused either by molecules secreted by the tumor or by an immune response targeted at tumor molecules that also recognizes endogenously expressed proteins elsewhere in the body. In the latter scenario, the resulting autoimmunity can be disease causing and potentially lethal^{37, 38}.

Paraneoplastic syndromes affecting the nervous system are called paraneoplastic neurological syndromes (PNS)³⁹. Although the exact pathogenic mechanisms are unknown, the major steps are considered to be as follows: first, the immune system initiates an anti-tumor response; second, one or more of the antigens targeted by the immune system is also present and accessible in healthy cells of the nervous system; third, healthy cells are damaged and eventually killed by the immune system, either

through antibodies from plasma cells or through effector T cells (or both; Fig. 5)⁴⁰. It is not necessary that the tumor antigens are exactly the same as the molecules found in the normal cells: Each antibody and effector T cell only target parts of an antigen, thus self-molecules need only to contain parts resembling the tumor antigen to be targeted through molecular mimicry.

In PNS, neurological signs usually appear prior to identification of the cancer which is often too small to be discovered initially⁴¹⁻⁴³. The incidence of PNS varies from study to study⁴⁴, but paraneoplastic sensory neuronopathy seems to be the most abundant (0.7% of cancer diagnosis), followed by paraneoplastic encephalitis (0.3% of cancer diagnosis) and paraneoplastic cerebellar degeneration (0.2% of cancer diagnosis)⁴⁵. The most common cancers associated with PNS are small cell lung cancer, gynecological cancers, breast cancer and lymphoma²⁷ and the median age of onset in PNS patients has been reported to be in the early 60s^{38, 46}. The cancer is almost always diagnosed within five years after the onset of the PNS⁴⁷.

As pathogenesis of the neurological dysfunction is not well understood, the cornerstone of PNS therapy is early identification and treatment of the underlying tumor.

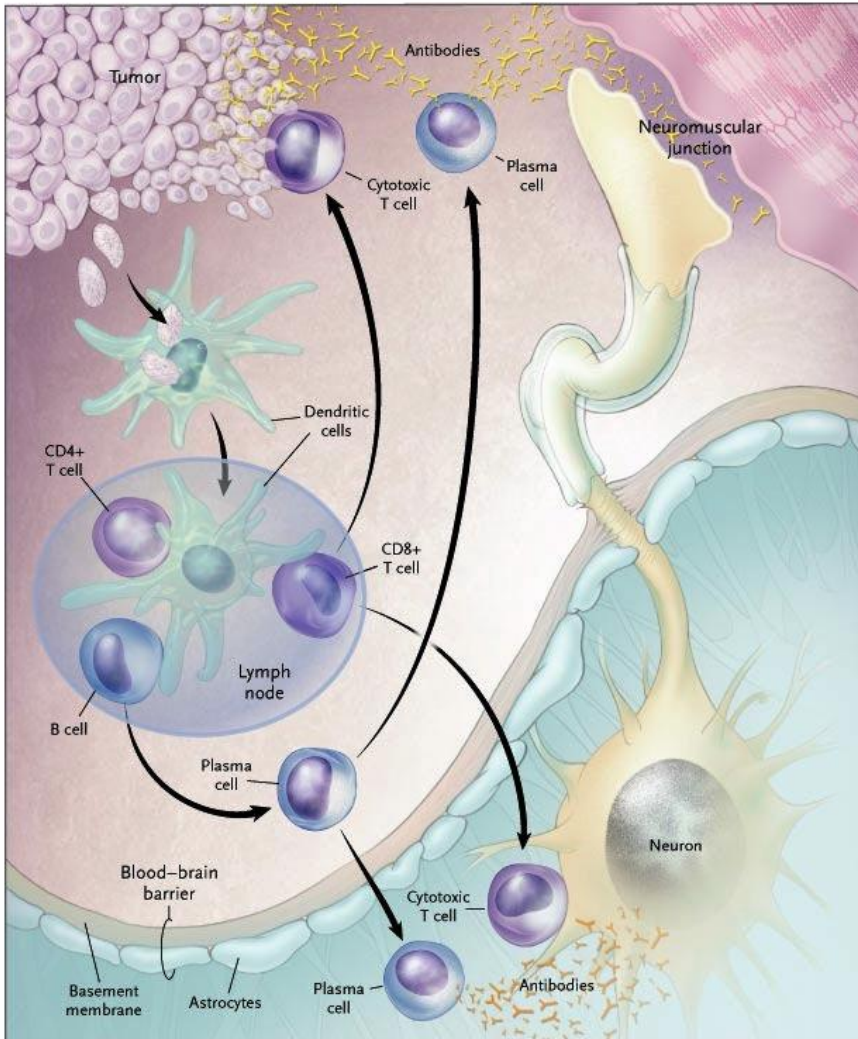


Figure 5: Proposed pathogenesis of PNS. Antigen-presenting cells, such as dendritic cells, present tumor antigens to CD4⁺ T cells, CD8⁺ T cells and B cells; CD8⁺ T cells and B cells mature into cytotoxic T cells and antibody-secreting plasma cells, respectively, with subsequent attack against both the nervous system (lower right), neuromuscular junctions (upper right) and the tumor cells (upper left) expressing the same antigen. Reproduced with permission from Damell and Posner (2003)³⁷, Copyright Massachusetts Medical Society.

1.4.1 Onconeural antibodies

Antibodies associated with tumors that also bind molecules in neural tissues are called onconeural antibodies⁴⁸. These antibodies can bind either intracellular or cell surface antigens. Most intracellular PNS antibodies are onconeural while cell surface PNS antibodies are not always related to a cancer²⁷. Cell surface autoantibodies are thought to have a direct pathogenic role⁴⁹, while intracellular autoantibodies are often referred to as T cell mediated^{50, 51}.

Detection of onconeural antibodies is used to define PNS and determine the underlying associated cancer. Table 1 shows the most important PNS-associated autoantibodies. The most well characterized ones are the Yo, Hu, Ri, CRMP5, Ma1/Ma2 and amphiphysin antibodies^{27, 47}. These antibodies have recognizable patterns when used to stain tissues of the nervous system, as well as specific detection of the associated proteins in recombinant assays such as line blots or cell-based assays. Both methods should be used to confirm a PNS diagnosis, as the methods separately can yield a high number of false positive results⁵²⁻⁵⁴.

Table 1: PNS autoantibodies, their targets and associated PNS and underlying associated cancers.

Antibody	Antigen	PNS	Cancer
Yo	CDR2L/CDR2, intracellular	PCD	Ovarian, breast and fallopian tube
Hu	HuD, intracellular	Encephalomyelitis, sensory neuronopathy	SCLC, NSCLC and extra-thoracic cancers
Ri	NOVA1/NOVA2, intracellular	Brainstem encephalitis and opsoclonus	Breast, lung and other cancers
Tr	DNER, intracellular	PCD	Hodkin lymphoma
Ma/Ma2	Ma1/Ma2, intracellular	Limbic encephalitis and brainstem encephalitis	Testicular, lung and other cancers
Amphiphysin	Amphiphysin, intracellular	SPS, encephalo-myelitis, sensorimotor neuropathy	SCLC, breast and other cancers
SOX1	SOX1, intracellular	LEMS and PCD	SCLC, NSCLC and extra-thoracic cancers
CRMP5	CRMP5, intracellular	Encephalomyelitis, sensorimotor neuropathy	SCLC, NSCLC, thymoma and extra-thoracic cancers
MAP1B	MAP1B, intracellular	Encephalomyelitis and/or sensorimotor neuropathy	SCLC, NSCLC and extra-thoracic cancers
NMDAR	GluN1, cell surface	Encephalitis	Teratoma
AMPA	GluA1/GluA2, cell surface	Limbic encephalitis and non-focal encephalitis	Lung, thymus, breast and other cancers
GABA_BR	B1 (GABA _B R), cell surface	Limbic encephalitis, cerebellar ataxia, opsoclonus myoclonus syndrome	SCLC
mGluR5	mGluR5, cell surface	Non-focal encephalitis	Hodgkin lymphoma
VGCC P/Q	VGCC P/Q, cell surface	LEMS, PCD	SCLC

Abbreviations: PCD, paraneoplastic cerebellar degeneration; SPS, stiff person syndrome; LEMS, Lambert-Eaton myasthenic syndrome; SCLC, small cell lung cancer; NSCLC, non-small cell lung cancer. Reprinted by permission from Springer Nature, License #4973870581810: Springer Nature, Nature Reviews Clinical Oncology, Paraneoplastic neurological syndromes in the era of immune-checkpoint inhibitors, Graus F et al²⁷.

1.4.2 Paraneoplastic cerebellar degeneration

Paraneoplastic cerebellar degeneration (PCD) is one of the most common PNS and comprises a heterogeneous group of disorders that are usually associated with gynaecological⁵⁵⁻⁶⁵, breast⁶⁶⁻⁷⁰ or lung cancer^{38, 71-74}. Association with other cancers such as esophageal cancers⁷⁵⁻⁷⁷, gastric cancers^{78, 79}, cholangiocarcinoma⁸⁰, uveal melanoma⁸¹ and prostatic adenocarcinoma⁸² have also been reported. The extensive loss of Purkinje neurons in these patients (Fig. 6) lead to a variety of cerebellar symptoms such as ataxia, dysarthria and nystagmus. Involvement of the neocortex, limbic system, basal ganglia, spinal cord and the peripheral nervous system have also been described⁸³.

Of the approximately 38 onconeural antibodies described in PCD patients, the most frequently detected are Yo antibodies followed by Hu, Tr and Ri antibodies⁸⁴. These four antibodies make up over 90% of the PCD cases⁸⁵. Despite the presence of these antibodies in sera and CSF of PCD patients, and the fact that they are good clinical diagnostic markers, their pathogenic relevance remains poorly understood.

Since antigen-specific cytotoxic T cells are found in peripheral blood of Yo-PCD patients⁸⁶ and CSF of Hu-PCD patients⁷³, some consider cytotoxic T cells to be the main effectors of neuronal loss. In the Yo-PCD study, cytotoxic T cells reacting with recombinant CDR2 peptides were found in the acute phase in one patient that had the class I MHC subtype HLA-A-*0201, but not in the chronic phase in three patients (two HLA-A*0201⁺ and one HLA-A*0201⁻). Memory T cells were found in both HLA-A*0201⁺ chronic patients, but not in the acute patient (HLA-A*0201⁺) or the chronic HLA-A*0201⁻ patient. Although the complex mechanisms are not yet understood, exploration of HLA alleles in PCD patients has identified genetic variants associated with protective or susceptible properties⁸⁷.

Since most relevant PCD antigens are intracellular, a first step in pathogenesis is thought to be the presentation of these antigens on the surface of cancer cells by class I MHC molecules to cytotoxic T cells. Under normal circumstances self antigens would not elicit an immune response. If, however, cytotoxic T cells are activated

against this self antigen in the tumor, these could potentially travel to the cerebellum and attack Purkinje neurons. This has been demonstrated in an animal model of PCD in which massive CD8⁺ T cell infiltration into the cerebellum, surrounding the Purkinje neuron soma and dendrites, appeared to be responsible for the neuronal loss⁵⁰. These authors hypothesized that MHC class I molecules present on Purkinje neurons⁸⁸ were upregulated by INF- γ secretion by the surrounding CD8⁺ T cells, rendering them susceptible to killing by the CD8⁺ T cells. Also observed in this model was microglia infiltration surrounding Purkinje neurons, similar to that demonstrated in patients⁸⁹.

In vitro studies have, however, demonstrated that Purkinje neurons are able to internalize both IgG and IgM⁹⁰. Antibody internalization occur in other neurons as well⁹¹. Purkinje neurons internalize both non-specific and specific antibodies, however, the non-specific ones were rapidly cleared, while specific antibodies were able to cause neuronal damage^{90, 92}. This is in line with in vitro studies of PCD pathogenesis: Yo antibodies cause neuronal loss in the absence of T cells^{93, 94}. Thus, greater knowledge is needed to understand the interplay between tumors, immune components and the neuronal damage in PCD patients.

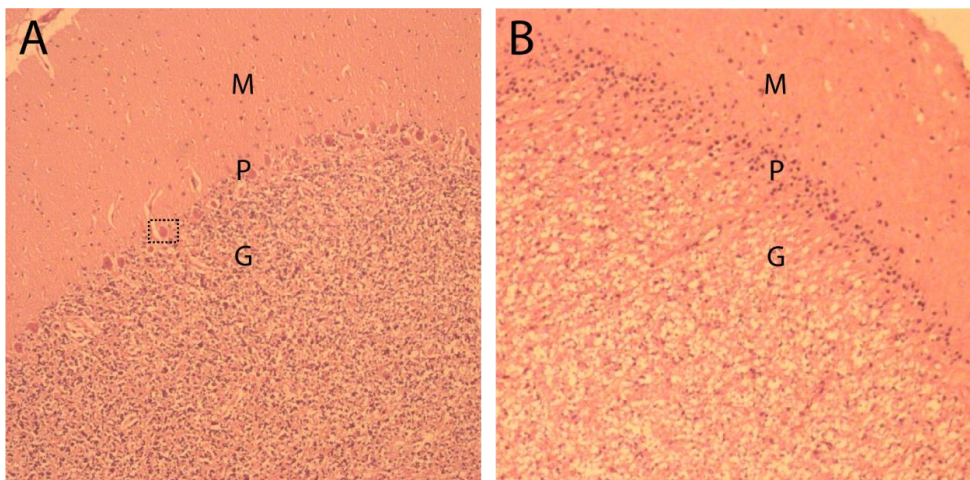


Figure 6: A) Cerebellar section from a control patient with Purkinje somas present (black box) and B) cerebellar section from a PCD patient where almost all Purkinje neurons are absent. M = molecular layer, P = Purkinje layer and G = granule layer; 20x objective.

1.4.3 Yo-associated PCD

Yo antibodies were first reported in patients with PCD almost four decades ago^{55, 95}. These antibodies react with cerebellar degeneration-related (CDR) proteins present in Purkinje neurons and are associated with Purkinje neuron death and severe cerebellar degeneration. Yo antibodies have been found to bind three different CDR proteins: CDR1, CDR2 and CDR2-Like (CDR2L)⁹⁶⁻¹⁰¹. However, CDR1 is no longer considered as a marker for Yo-PCD¹⁰², and CDR2L, rather than CDR2, is demonstrated to be the major Yo antigen¹⁰¹.

In Yo-associated PCD patients, the tumor diagnosis is usually established within a year of the onset of neurological signs^{103, 104}. However, in some cases the tumor diagnosis takes several years, and in some cases the cancer is first found postmortem¹⁰³. The long duration between onset of neurological symptoms and cancer detection seen in some of these patients could be due to an effective anti-tumor response, limiting its growth¹⁰⁴.

In normal cerebellar tissue, Yo antibodies bind Purkinje neurons as well as stellate and basket cells in humans, mice, rats and guinea pigs^{55, 58, 93, 95, 97, 105-116}. Yo antibodies also bind normal ovary tissue as well as cancerous tissue of the ovary^{114, 116}, cervix, lungs and colon¹¹⁷. These Yo antibodies are predominantly of IgG1 subclass, while IgG2, IgG3 and IgG4 are only found in some patients¹¹⁸.

There have been several attempts to produce an animal model of Yo-associated PCD using transfer of Yo antibodies or immunization with recombinant CDR2, all of which have been unsuccessful^{109, 119-121}. Possibly, our understanding of disease pathogenesis will remain limited until such a model is established. As CDR2L is now demonstrated to be the major antigen of Yo antibodies¹⁰¹, a model system using this protein as target could potentially be successful.

1.4.4 Cerebellar degeneration-related proteins

The amino acid sequence for all three CDR proteins is known and shows that CDR2L and CDR2 have 45% sequence identity, while the sequence identity with CDR1 is low. However, the information about the spatial structure and function of these proteins associated with Yo-PCD is limited.

CDR2 was considered the main Yo antigen for two decades^{86, 114, 115, 122}. This assumption was based primarily on the finding that only the CDR2 gene is expressed in tumors obtained from PCD patients¹¹⁴. However, in subsequent studies it has been demonstrated that both CDR2 and CDR2L are extensively expressed in normal as well as in malignant tissues^{116, 123} and that the CDR2L protein is highly expressed in PCD tumors, while CDR2 is not¹²⁴. Moreover, protein deposits of CDR2L were detected in germinal centers of all Yo-associated PCD tumors with tertiary lymphoid structures¹²⁴, suggesting an ongoing local immune response against CDR2L. Finally, we have recently demonstrated that Yo antibodies bind endogenous CDR2L, and not CDR2. The antibodies were, however, able to bind recombinant CDR2 proteins¹⁰¹.

1.4.4.1 CDR2

CDR2 (RefSeq NP_001793.1) was first described in 1991¹²⁵. The protein is 454 amino acids long, however, spatial structure and function are not fully understood. The mRNA and amino acid sequences, as well as the amino acid profile, can be seen in Appendix 9.1.

CDR2 protein was isolated by screening a human expression library with isolated cDNA clones showing epitopes that were recognized by sera from patients with PNS⁹⁸. The calculated molecular weight of the amino acid sequence is 51.9 kDa (Appendix 9.1.3) and reported molecular weights range from 52 to 62 kDa^{100, 108, 122}. Five human isoforms for CDR2 have been mapped computationally (The Uniprot Consortium), which could explain the different localizations found for CDR2 when using different antibodies^{101, 116}.

The protein contains a leucine zipper dimerization motif at amino acid 171-192, consisting of repeats of leucine residues forming an amphiphilic α -helix⁹⁹. It has been shown that CDR2 can homodimerize through this leucine zipper motif, and heterodimerize with other leucine zipper motif-containing molecules¹¹⁵.

In the cerebellum, CDR2 is expressed in the nuclei (strong) and cytoplasm (weak) of Purkinje neurons and stellate and basket cells^{100, 101, 116, 126}. The same localizations have been shown in both healthy and cancerous tissues^{101, 117, 126}.

1.4.4.2 CDR2L

CDR2L (RefSeq NP_055418.2) was first discovered in 1997 and is a 465 amino acid long protein sharing around 45% sequence identity with CDR2¹¹⁴. The mRNA and amino acid sequences, as well as the amino acid profile, can be seen in Appendix 9.2.

CDR2L has also been named CDR3 as it was the third CDR protein discovered. As for CDR2, the structure and function are not fully understood. The calculated molecular weight of the amino acid sequence is 53.0 kDa (Appendix 9.2.3), although molecular weights as high as 62 kDa have been reported in western blot analysis¹⁰⁰. No isoforms have yet been described for CDR2L.

CDR2L is present in the cytoplasm of Purkinje neurons and stellate and basket cells^{100, 101, 116, 126}. It is also present in both healthy and cancerous tissues of the ovary, mamma, prostate and testis¹¹⁶. Of note, recombinant CDR2L has been observed in the plasma membrane of transfected HeLa cells¹⁰⁰. Endogenous CDR2L has, however, so far only been observed intracellularly.

2. AIMS OF THE STUDY

The main aims of this thesis were to determine the major target of Yo antibodies and find the subcellular location of this antigen, and to create a Purkinje neuron culture suitable for the further characterization of the CDR proteins.

Objectives:

- a. Determine if CDR2 or CDR2L is the major antigen of Yo antibodies. (Paper I)
- b. Investigate the subcellular localization of CDR2 and CDR2L in both cancer cells and Purkinje neurons. (Paper II)
- c. Develop a Purkinje neuron culture from rats for further characterization of the CDR proteins. (Paper III)

3. METHODS

3.1 Patient Samples

Sex- and age-matched CSF and sera samples from patients with Yo antibodies (PCD patients) and without Yo antibodies and no neurological disease or underlying cancer (negative controls) were obtained from the Neurological Research Laboratory, Haukeland University Hospital (Regional Committees for Medical and Health Research Ethics (REK), #2013/1480).

3.2 Cerebellar Tissue

Cerebellar sections were cut from fresh frozen normal human tissue (REK, #2013/1503) or rat tissue (FOTS 20135149/20157494/20170001). Heat-induced epitope retrieval was performed prior to immunostaining.

3.3 Cell Culturing

OvCar3 (American Type Culture Collection (ATCC), #HTB-161) and HepG2 (ATCC, #HB-8065) cancer cell lines were maintained and subcultivated on poly-D-lysine-coated coverslips (Neuvitro, #GG-18-1.5-pdl) according to the manufacturer's protocol. Cells were washed twice with 0.1 M phosphate-buffered saline (PBS), fixed (4% paraformaldehyde in PBS, Thermo Fisher Scientific, #28908, 15 minutes), and quenched (50 mM NH₄Cl, Sigma-Aldrich, #254134, 5 minutes) prior to immunostaining.

3.4 Immunostaining

Fixed OvCar3 and HepG2 cells as well as cerebellar sections were permeabilized in 0.5% Triton X-100 (Sigma-Aldrich, #11332481001) in PBS for 5 minutes, washed in 0.5% gelatin (Sigma-Aldrich, #G7041) in PBS (3x 15 minutes), blocked in 10% SEABLOCK (Thermo Fisher Scientific, #37527) in PBS for 30 minutes, and

incubated with primary antibodies overnight at 4 °C. Following incubations, cells and sections were washed in gelatin-PBS, incubated with secondary antibodies for 2 hours at room temperature, and mounted using ProLong Diamond with DAPI (Thermo Fisher Scientific, #P36962). The following antibodies were used: rabbit anti-CDR2 (Sigma-Aldrich, #HPA018151), rabbit anti-CDR2L (Protein Technology, #14563-1-AP), mouse anti-rpS6 (Cell Signaling, #2317/Santa Cruz, #sc-74459), mouse anti-SON (Santa Cruz, #sc398508), mouse anti-eIF4A3 (Santa Cruz, #sc-365549), mouse anti-SRSF2 (Abcam, #ab11826), Alexa Fluor 488/594-labeled goat anti-human (Thermo Fisher Scientific, #A-11013/#A11014), Alexa Fluor 488/594-labeled goat anti-rabbit (Thermo Fisher Scientific, #R37116/#R37117), STAR580-labeled goat anti-mouse (Sigma-Aldrich, #52403), STAR635P-labeled goat anti-rabbit (Sigma-Aldrich, #53399), and Alexa Fluor 488/594-labeled goat anti-mouse (Thermo Fisher Scientific, #R37120/#R37121).

3.5 Fluorescent Immunoblotting

The cerebellar and cancer cell lysates were obtained using a Total Protein Extraction Kit (Millipore, Billerica, MA, #2140). Proteins were separated on a 10% TGX gel and transferred to a low-autofluorescence poly-vinylidene difluoride (PVDF) membrane. Antibodies consisted of rabbit anti-CDR2L, rabbit anti-CDR2, Yo-CSF, anti-rabbit Alexa Fluor 488, and anti-human Alexa Fluor 647 (Thermo Fisher Scientific, #A-21445). G:Box (Syngene, Frederick, MA) was employed for visualization.

3.6 Immunoprecipitation

OvCar3 and HepG2 cells were lysed in RIPA lysis buffer (Bioscience, #786-490) containing protease inhibitor cocktail (Sigma-Aldrich, #11873580001), 1 mM phenylmethylsulfonyl fluoride (PMSF, Sigma-Aldrich, #P7626), 1 mM sodium fluoride (NaF, Sigma-Aldrich #S6776) and 1 mM sodium orthovanadate (Na_3VO_4 , Sigma-Aldrich #450243). The lysate was centrifuged (22,000 g, 4 °C, 15 minutes) and the supernatant was collected.

Following the Bio-Rad SureBeads immunoprecipitation protocol, the proteins were immunoprecipitated from OvCar3 cell lysate by using Protein G Magnetic Beads (Bio-Rad Laboratories, Hercules, CA, #161-4023). Immunoprecipitated proteins were separated on a 10% TGX gel (Bio-Rad, #456-1035) and transferred to a PVDF membrane using the Trans-Blot Turbo Transfer kit (Bio-Rad, #170-4274). Western blot analysis was performed to detect the immunoprecipitated target proteins. The antibodies used were rabbit anti-CDR2L, mouse anti-CDR2, Yo-CSF, TidyBlot (Bio-Rad, #STAR209PA) and horseradish peroxidase anti-mouse IgG (Dako, Carpinteria, CA, #P0260).

3.7 Mass Spectrometry-based Proteomics

Proteins of interest were immunoprecipitated from HepG2 or OvCar3 cell lysates using the antibodies listed in Table 1 of Paper 2. A negative control consisting of beads and cancer cell lysate was also included. The samples were loaded on a 10% TGX gel and run approximately 1 cm into the resolving gel. Each lane was cut into cubes of approximately 1 mm² and hydrated in Milli-Q water (20 minutes, room temperature). The following paragraphs (including 3.7.1) describes the protocol used by the Proteomic Unit at University of Bergen to obtain the mass spectrometry-based data.

Detergents (i.e. sodium dodecyl sulfate) and salts were removed by washing the gel in 25 mM ammonium bicarbonate (Sigma-Aldrich, #09830-500G) and 50% acetonitrile (VWR, #34967-2.5L). Cysteine reduction and alkylation were accomplished with a 45-minute incubation in 10 mM dithiothreitol (Amersham Biosciences, #171318-02) at 56 °C followed by a 30-minute incubation in 55 mM iodoacetamide (VWR, #M216-30G) at room temperature in the dark. After washing in 25 mM ammonium bicarbonate and 50% acetonitrile, dried gel pieces were hydrated on ice for 20 minutes with a minimum volume of 6 ng/μL trypsin (sequencing-grade modified, Promega, #V511A) in digestion buffer (20 mM ammonium bicarbonate, 1 mM calcium chloride (Sigma-Aldrich, #C7902)), then covered with digestion buffer and incubated for 16 h at 37 °C. Trypsin activity was

quenched by acidification with trifluoroacetic acid (VWR, #1.08218.0050), and samples were desalted using StageTip C18 columns (Empore disk-C18, Agilent Life Sciences, #12145004) and the eluted peptides were dried and dissolved in 2% acetonitrile, 1% formic acid (VWR, #84865.260).

About 0.5 μg tryptic peptides were loaded onto an Ultimate 3000 RSLC system (Thermo Fisher Scientific) connected online to a Q-Exactive HF mass spectrometer (Thermo Fisher Scientific) equipped with EASY-spray nano-electrospray ion source (Thermo Fisher Scientific). All samples were loaded and desalted on a pre-column (Acclaim PepMap 100, 2 cm x 75 μm ID nanoViper column, packed with 3 μm C18 beads) at a flow rate of 5 $\mu\text{L}/\text{min}$ with 0.1% trifluoroacetic acid. Peptides were separated during a biphasic acetonitrile gradient (flow rate of 200 nL/minute) on a 50-cm analytical column (PepMap RSLC, 50 cm x 75 μm ID EASY-spray column, packed with 2 μm C18 beads). Solvent A and B were 0.1% formic acid in water and 100% acetonitrile, respectively. The gradient composition was 5% B during trapping (5 minutes) followed by 5–7% B over 0.5 minutes, 7–22% B for the next 59.5 minutes, 22–35% B over 22 minutes, and 35–80% B over 5 minutes. Elution of very hydrophobic peptides and conditioning of the column was performed during a 10-minute isocratic elution with 80% B and 15 minutes of isocratic conditioning with 5% B, respectively.

Charged peptides were analyzed by the Q-Exactive HF, operating in the data-dependent acquisition mode to automatically switch between full-scan MS and MS/MS acquisition. Mass spectra were acquired in the scan range 375–1500 m/z with a resolution of 60,000 at m/z 200 after an accumulation of 3,000,000 charges (maximum trap time set at 50 ms in the C-trap). The 12 peptides with the most intense signals above an intensity threshold of 50,000 counts and with charge states of 2 to 6 were sequentially isolated and accumulated to 100,000 charges (maximum trap time set at 110 ms) to a target value of 1×10^5 or a maximum trap time of 110 ms in the C-trap with isolation width maintained at 1.6 m/z (offset of 0.3 m/z) before fragmentation in the higher energy collision dissociation cell. Fragmentation was performed with a normalized collision energy of 32%, and fragments were detected

in the Q-Exactive at a resolution of 60,000 at m/z 200 with first mass fixed at m/z 110. One MS/MS spectrum of a precursor mass was allowed before dynamic exclusion for 30 seconds with “exclude isotopes” on. Accurate mass measurements in MS mode were accomplished by enabling the lock-mass internal calibration of the polydimethylcyclosiloxane ions generated in the electrospray process from ambient air (m/z 445.12003).

3.7.1 Database searching and criteria for protein identification

Tandem mass spectra data were extracted with Proteome Discoverer (version 2.3.0.523, Thermo Fisher Scientific) and were searched against human, reviewed protein sequences (SwissprotKB database, release 08-2018) with Sequest HT and MS Amanda search engines. The following search criteria were used: carbamidomethylation of cysteine (fixed modification), oxidation of methionine and acetyl of the protein N-terminus (variable modifications), a maximum of two missed trypsin cleavages, 0.02-Da fragment ion mass tolerance, and 10-ppm precursor ion tolerance. Search results from PD were loaded into Scaffold 4 (version 4.9.0, Proteome Software Inc.), and all spectra were searched with the X! Tandem search engine against identified proteins to identify nonspecific trypsin cleavages.

Peptide and protein identifications were filtered to achieve a false discovery rate < 1.0% (based on searching the reversed human database). Grouping of proteins sharing identical peptides was enabled. In order to evaluate the likelihood of the predicted interactions, the following criteria were established: (1) nonspecific bindings were removed based on the negative control (without primary antibodies); (2) the number of recognized peptides was set to at least two; (3) proteins that were identified by more than one of the antibodies to CDR2L or CDR2 were considered as more likely partners; (4) the likelihood of interaction was evaluated based on the predicted cellular location of each protein of interest. Protein-protein interactions were analyzed using the STRING database. STRING implements all publicly available sources of known and predicted protein-protein associations, together with computational analysis to evaluate potential connectivity networks.

3.8 Recombinant DNA and Transfection

Full-length CDR2 (OriGene Technologies, Rockville, MD, #RG204900) and CDR2L (OriGene Technologies, #RC206909) were ligated into a pCMV6-AC-GFP vector (OriGene Technologies, #PS100010). Following polymerase chain reaction, correct CDR2 and CDR2L vector sequences were confirmed using BioEdit v7.2.5. One Shot TOP10 Escherichia coli (Life Technologies, Carlsbad, CA, #C4040-10) were used for amplification, E.Z.N.A. Plasmid DNAKit (Omega Bio-Tek, Norcross, GA, #D6942) for purification, and Lipofectamine 3000 (Thermo Fisher Scientific, #L3000008) for transfection.

3.9 Super-Resolution Microscopy

A Leica TCS SP8 Stimulated Emission Depletion (STED) 3X confocal microscope equipped with a 93x glycerol objective (NA 1.3) and a 100x oil objective (NA 1.4) was used for imaging. The output of the adjustable white light excitation laser (up to 1.5 mW per line; pulsed) was kept between 1% and 20% and the STED laser (775 nm; up to 1.5 W) between 20% and 30%. Detection range for the emission: 410-470 nm for DAPI, 500-550 nm for Alexa Fluor 488, 605-625 nm for Alexa Fluor 594, 590-625 nm for STAR580 and 645-700 nm for STAR635P. Gating (between 1 and 6 ns) was applied for all channels as well as minimum three intensity averages. The lateral resolution was consistently measured to be between 40 and 50 nm. All experiments were run with negative controls, containing only secondary antibodies, simultaneously for laser intensity thresholding.

3.10 Proximity Ligation Assay

The proximity ligation assay was performed using the commercially available Duolink kit from Sigma-Aldrich (#DUO92101). Fixed OvCar3 cells were permeabilized for 5 minutes using 0.5% Triton X-100 diluted in PBS and blocked with 10% SEABLOCK in PBS. Primary antibodies against Hsp60 (EnCor Biotechnology, #CPCA-HSP60), CDR2, CDR2L, SON, and SRSF2 were applied for

1 hour (1:100 in blocking solution), followed by 3x 5-minute washes with Wash Buffer A supplied with the kit. Probes (+ and -) were diluted in blocking solution (1:5) and added to the cells for 1 hour (37 °C). The cells were washed 3x 5 minutes with Wash Buffer A and incubated with ligation buffer (1:5) and the ligase enzyme (1:40) for 30 minutes (37 °C). After 2x 5-minute washes with Wash Buffer A, amplification buffer (1:5) and the polymerase enzyme (1:80) were diluted in distilled water and applied to the cells for 100 minutes (37 °C, in the dark), followed by three 10-minute washes with Wash Buffer B (supplied with the kit). Prolong Diamond with DAPI was used to mount the coverslips (overnight, 4 °C). Mounted cells were stored at -20 °C.

3.11 Purkinje Neuron Culture

Neuronal culture preparation: All procedures were performed according to the National Institutes of Health Guidelines for the Care and Use of Laboratory Animals Norway (FOTS 20135149/20157494/20170001). Wistar Hannover GLAST rat pups (n = 328), embryonic day 18 (E18) to postnatal day 10 (P10), were used for neuronal culture preparation.

Following anaesthesia and decapitation, the brains were rapidly transferred into preparation solution (ice-cold EBSS solution (Gibco, #24010043) containing 0.5% glucose (Sigma, #G8769) and 10 mM HEPES (Gibco, #15630056)). The meninges and the medulla oblongata were carefully removed, and the cerebellum was separated from the pons and the midbrain. The cerebellum (and pons for the support layer) was transferred to a 15 mL tube containing 20 U/mL papain (Worthington, #LK003178) solved in preparation solution and warmed up to 36 °C. The tube was placed in the incubator for 15 minutes at 36°C with occasionally rotation to digest the tissue. The papain solution was removed with a fire polished Pasteur pipette and the digestion was stopped by adding pre-warmed stop media (advanced DMEM/F12 solution (Gibco, #12634010) containing 0.5% glucose (Sigma, #G8769) and 10% foetal bovine serum (FBS, Gibco, #10500064); 36 °C). After 5 minutes of deactivation, the stop media was removed and 250 µL growth media (containing 10% FBS) was added

per cerebellum. Finally, the tissue/media suspension was pipetted with a fire polished Pasteur pipette 100 times until the cells were separated.

Support layer: 375,000 cells/mL (from cerebellum and pons) were seeded on pre-coated coverslips from Neuvitro (#GG-12-1.5-PDL, 24 well, 500 μ L/well; #GG-18-1.5-PDL, 12 well, 1 mL/well; #GG-25-1.5-laminin, 6 well, 2 mL/well). The support layers were maintained in 6-, 12- or 24-well plates submerged in growth media (45% advanced DMEM/F12 solution (Gibco, #126340010), 45% NBM solution (Miltenyibiotec, #130-093-570), 1.5% B-27 serum-free supplement (Gibco, #17504044), 1.5% NB-21 serum-free supplement (Miltenyibiotec, #130-093-566), 1% NaPyruvate (Invitrogen, #11360088), 1% heat-inactivated FBS (Invitrogen, #10500064), 2% GLUTAMAX (Gibco, #35050038), 5 mg/mL D-glucose and 10 mM HEPES (Invitrogen, #15630056); 36°C). Half of the culture medium was replaced once a week.

Purkinje neuron layer (PN layer): E18 and P0 Purkinje neuron cultures: 500,000 cells/mL (from cerebellum) were seeded on support layers of different in vitro ages. P10 Purkinje neuron cultures: 750,000 cells/mL from the vermis of the cerebellum were seeded on support layers of different in vitro ages. The growth media was supplemented with insulin (Invitrogen, #12585014; 1:250, stock 4 mg/mL), progesterone (Sigma, #P8783; 1:2000, stock 80 mM), insulin-like growth factor 1 (IGF1; Promokine, #E-60840; 1:40000, stock 1 μ g/ μ L) and the protein kinase C inhibitor K252a (Alomone, #K-150; IC₅₀ 25 nM). In cultures that were maintained for more than 28 days in vitro the IGF1 and progesterone concentration were reduced to 10 ng/mL and 20 μ M, respectively. K252a was supplemented for 21 days before the washout process started; its optimal concentration was experimentally evaluated for each tested culture type. Half of the culture medium was replaced twice a week for cultures in 6 well plates and every second day for 12 and 24 well plates. The experiments done to investigate the culture parameters and their Purkinje neuron yield were performed randomly (three to six probes per experimental setting and five independently repeats for each group and condition).

Lentiviral gene editing: L7 promoter (full length 1005 bp) were cloned by SBI System Bioscience into the pCDH-L7-MCS-copGFP construct (#CS970S-1) and viral particle with a yield of 2.24×10^9 ifus/mL were produced. Lysed cerebellum of E18 or P0 rats (suspended in growth media without serum) were incubated for 10 minutes at 37 °C with 1.22×10^6 viral particles/mL and seeded onto a support layer (tested on both coverslips and live cell imaging dishes (35 mm, Ibidi, #80136)). Media was replaced after 3 days and transfection efficiency was evaluated by live cell imaging microscopy 24 hours post transfection, as well as daily until 21 DIV and weekly up to DIV 169 days. Lentiviral transfection of Purkinje neurons was also tested one day after feeding on 15 DIV and 29 DIV cultures (2.5×10^6 viral particles/mL). The neural morphology of GFP-expressing Purkinje neurons was done by capturing ten independent 3x3 tile scans (Zyla camera configuration; 2048x2048; CFI Plan Apochromat Lambda dry objective 10x (NA 0.45; pixel size 603 nm) or 20x (NA 0.75; pixel size 301 nm)) by the Andor Dragonfly microscope system (Oxford Instruments company). The viral transfection of the cultures was repeated three times.

Immunostaining: The Purkinje neuron cultures were washed with pre-warmed 0.1 M PBS (1xPBS; Gibco, #70013016) and fixed with 1.5-4% paraformaldehyde (PFA, pH 6-7.2; Thermo Scientific, #28908) containing 0.5% sucrose for 15 minutes at 36°C. Tris-based or citric acid-based heat induced antigen retrieval (pH 9 and pH 6; 45 minutes, 85 °C) were performed to enhance the staining of some of the markers. The cultures were quenched with 1xPBS containing 50 mM NH₄Cl (PBS_N), permeabilized with 0.2% Triton X-100 (Sigma, #T9284) in PBS_N (5 minutes, 36°C), washed with PBS_N containing 0.5% cold water fish gelatin (Sigma, #G7041; PBS_{NG}, 3x15 minutes), and incubated with primary antibodies overnight at 4 °C in PBS_{NG} containing 10% Sea Block (Thermo Scientific, #37527), 0.05% Triton X-100 and 100 μM glycine (Sigma, #G7126). The cultures were rinsed with PBS_{NG} (3x20 min) and incubated with secondary antibodies produced in donkeys conjugated to CF488/594/647 dyes (1:400; Biotium, #20014, #20115, #20046, #20015, #20152, #20047, #20074, #20075, #20169, #20170) for 2 hours at room temperature in PBS_{NG} containing 2.5% Sea Block. To remove unbound secondary antibodies, the cultures

were washed with PBS_N (3x 20 minutes) and MilliQ water before mounted to microscope glasses using Prolong Glass Antifade Reagent (Invitrogen, #P36981). The mounted cultures were kept two days in room temperature in the dark, followed by long term storage at 4°C.

Purkinje neuron count and imaging: Counting of Purkinje neurons was performed manually and blind by screening the coverslips with a Leitz Diaplan Fluorescence microscope (equipped with CoolLED pE-300white illuminator). Branch analysis of the dendritic trees and determination of maturity and synaptic interaction was done by taking 10 Z-stack images per coverslip (5 independent and randomized experiments) at 0.5-1 μm intervals (Zyla camera configuration; 2048x2048) at the Andor Dragonfly microscope system (CFI Plan Apochromat Lambda S LWD 40x NA 1.14 water objective (pixel size 151 nm); 60x NA 1.20 oil objective (pixel size 103 nm) or CFI SR HP Apo TIRF 100x NA 1.49 oil objective (pixel size 60 nm)). The images were superimposed with Fusion software (Oxford Instruments). 3D surface visualization of synapses was performed using IMARIS 9.3.1 (Oxford Instruments) and the filament tracer tool.

Dendritic tree branch analysis: The dendritic development (length and order) of the Purkinje neurons was evaluated by analyzing 10 Purkinje neurons per experiment in 10 independent experiments using the ImageJ plugin Simple_Neurit_Tracer (Neuroanatomy).

Micro-electrode array (MEA) recordings: E18 cultures at a concentration of 500,000 cells/mL were plated onto 24 well plates of the Multiwell-MEA-system precoated with PDL (Multi Channel System-MCS, Reutlingen, Germany). Each well contained 12 PEDOT-coated gold micro-electrodes (30 μm diameter, 300 μm space, 3x4 geometrical layout) on a glass base (#890850, 24W300/30G-288). The amplifier (24 bit; bandwidth: 0.1 Hz to 10 kHz, modifiable via software; default 1 Hz to 3.5 kHz; sampling frequency per channel: 50 kHz or lower, software controlled; input voltage range: ± 2500 mV), stimulator (current stimulation: max. ± 1 mA; voltage stimulation: max. ± 10 V; stimulation pattern: pulse or burst stimulation sites freely

selectable) and heating element (regulation: ± 0.1 °C) was integrated in the Multiwell-MEA head stage (driven by the MCS-Interface Board 3.0 Multiboot). The Multiwell recording platform was covered by a mini-incubator (5% CO₂ and balanced air). Electrophysiological signals were acquired at a sampling rate of 20 kHz (Multiwell-Screen software). Plates were tested every second day for spontaneous activity from 5 DIV. Raw voltage traces were recorded for 120 seconds (analyzed using offline MCS-Multiwell-Analyzer) to calculate spike rate and burst activity. Two experimental settings were tested: recording of spontaneous spike activity using (1) the Purkinje neuron culture media (up to 63 DIV) and (2) Purkinje neuron culture media until 28 DIV and then media change to organotypic brain slice culture media (30% advanced DMEM/F12 solution, 20% MEM solution (#41090028; Gibco), 25% EBSS solution (#24010043; Gibco), 25% heat-inactivated horse serum (#H1138; Sigma), 2% GLUTAMAX, 5 mg/ml D-glucose and 2% B-27 serum free supplement) for 45 days.

3.12 Methodological Considerations

A majority of the methods used in this thesis are dependent on commercial antibodies. Whereas the production and verification of antibodies has matured throughout the years to assure minimal cross-reactivity, there is still a possibility that a portion of the antibody binding is “unspecific” – that the antibodies bind other molecules with identical or similar epitopes to the primary target.

For the different CDR2 antibodies available, the binding patterns varied considerably. If this is due to cross-reactivity or different isoforms of CDR2 is not yet known. However, all CDR2 antibodies used were able to bind CDR2 and none of them displayed the same binding pattern as Yo antibodies. For the CDR2L antibody used, it was reassuring to see that the binding pattern was identical to that of Yo antibodies in all methods tested, i.e. that they indeed do target the same molecules.

4. RESULTS

4.1 Paper I

In sections of human and rat cerebellum, the CDR2L antibody bound to cytoplasmic structures in Purkinje neuron somas that overlapped completely with Yo antibody staining (taken from both CSF and serum). The CDR2L and Yo staining also overlapped in stellate and basket cells. However, staining of CDR2 was primarily found in the nuclei of these neurons, and did not colocalize with the CDR2L or Yo antibody staining. Performing immunofluorescence blots with lysed cerebellar tissue showed overlap between Yo and CDR2L at approximately 55 kDa, while CDR2 was only present at 62 kDa.

OvCar3 cells also express CDR2L and CDR2 endogenously. The same results were found in these cells: Yo and CDR2L colocalized in the cytoplasm, while no overlap was found with CDR2 (Fig. 7A). Immunofluorescence blots and co-IP of lysed OvCar3 cells confirmed the co-reactivity of Yo and CDR2L (Fig. 7B and C)

HepG2 cells were found to express high levels of CDR2, while CDR2L was absent. When recombinant CDR2L-GFP was transfected into the HepG2 cells, the Yo and CDR2L antibodies were able to bind, giving a complete fluorescent overlap with the GFP attached to the recombinant CDR2L. The CDR2 antibody did not bind the CDR2L-GFP protein. Upon transfection of CDR2-GFP however, both the Yo, CDR2L and CDR2 antibody were able to bind the recombinant protein. Similar results were obtained for all PCD samples tested.

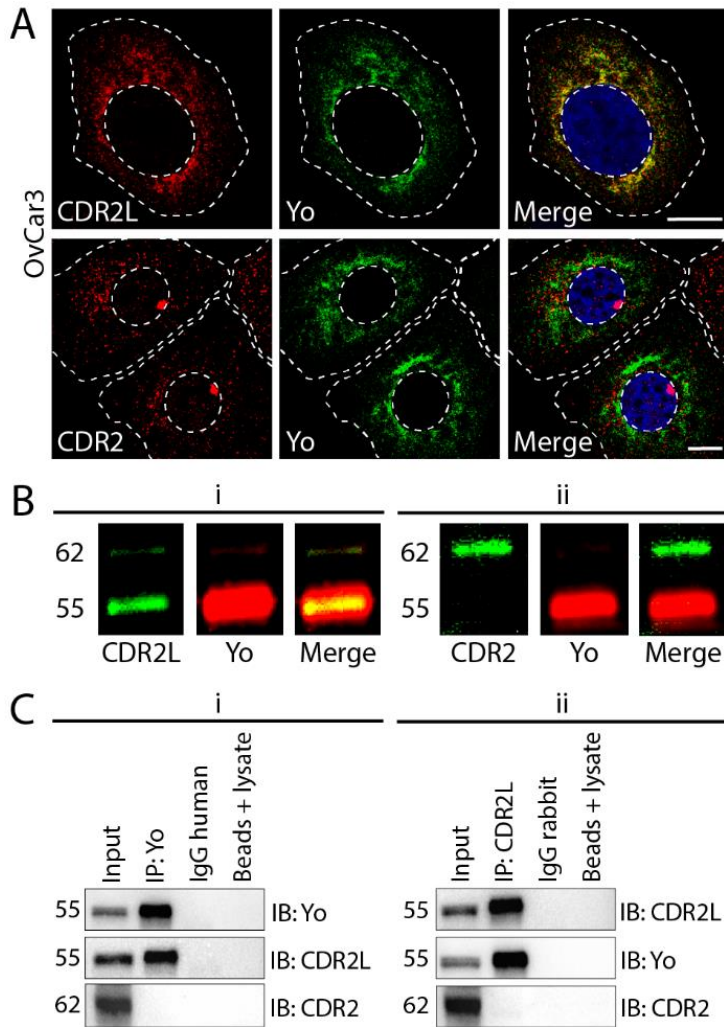


Figure 7: Yo antibodies bind to CDR2L, but not CDR2, in OvCar3 cells. Scale bars: 10 μm . **A)** Upper row: OvCar3 cells stained with Yo (CSF; green) and anti-CDR2L (red); Yo and CDR2L are colocalizing, giving the same granular, cytoplasmic staining pattern (seen as yellow in the merge image). Lower row: OvCar3 cells stained with Yo (CSF; green) and anti-CDR2 (red); Yo does not colocalize with CDR2. **B)** Fluorescent immunoblot of OvCar3 lysate. Anti-CDR2L and Yo (CSF) stain the same 55-kDa band; anti-CDR2 does not. Secondary antibody controls were negative. **C)** Western blot of proteins immunoprecipitated from the OvCar3 lysate by Yo (CSF) or CDR2L. The protein precipitated by Yo antibodies was recognized by the CDR2L antibody on western blot (i) and vice versa (ii); no relationship was observed between Yo or CDR2L and CDR2¹⁰¹.

4.2 Paper II

To ensure antibody specificity, CDR2L and CDR2 were immunoprecipitated from OvCar3 lysates and analyzed by mass spectrometry-based proteomics. The commercial antibodies raised against CDR2L and CDR2 were found to be specific. Yo antibodies bound CDR2L, but not CDR2, thus strengthening the conclusions in Paper I. The same experiments were performed in HepG2 cells: Yo antibodies were not able to bind CDR2.

The mass spectrometry-based proteomics also gave information about potential interaction partners of the two proteins. After applying the inclusion-criteria, CDR2L were predicted to interact with 50 ribosomal proteins that were tightly connected, while CDR2 was predicted to interact with the nuclear speckle proteins eIF4A3, SON and SRSF2 (Fig. 8).

Using super-resolution microscopy, CDR2L was found to colocalize with the ribosomal protein rpS6 in both OvCar3 cells, human cerebellum and in rat Purkinje neuron cultures. CDR2 colocalized with the nuclear speckle proteins SON, eIF4A3 and SRSF2. The same results were found through proximity ligation assay in OvCar3 cells. Co-immunoprecipitation of OvCar3 and HepG2 lysate showed that CDR2L indeed interacts with rpS6 and CDR2 with SON and eIF4A3.

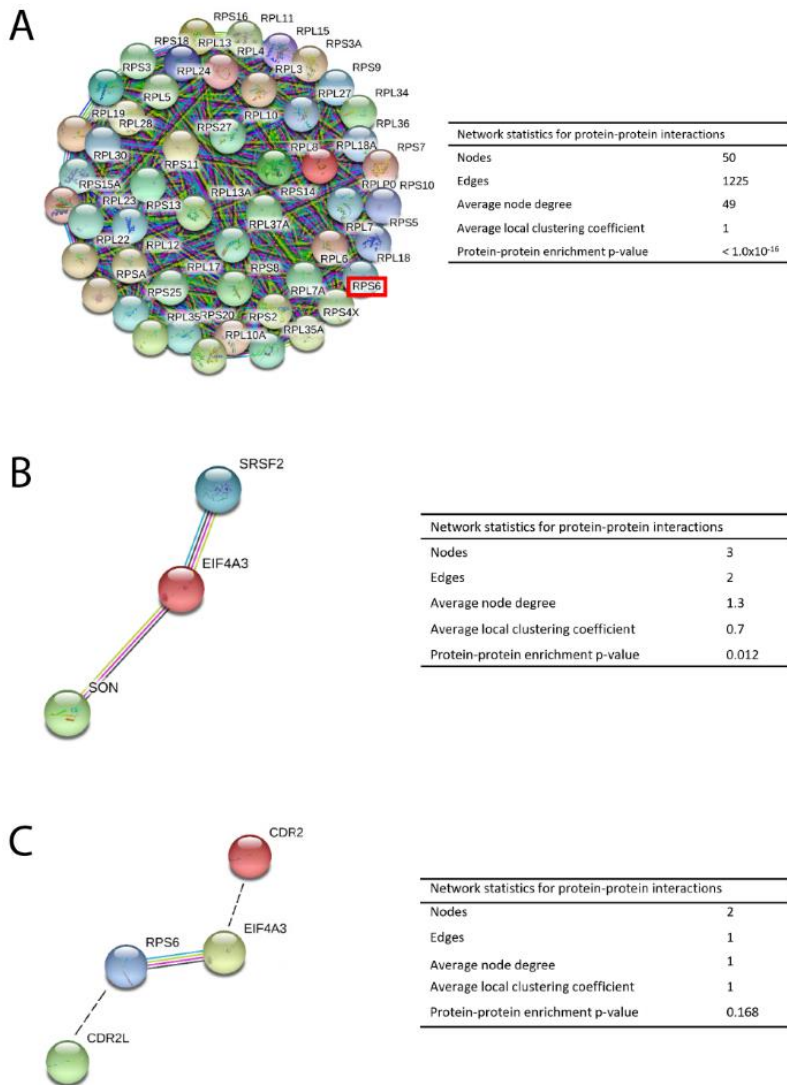


Figure 8: Protein-protein interaction networks visualized by STRING. **A)** CDR2L was predicted to interact with ribosomal proteins (rpS6, red box). The nodes indicate proteins, and the edges represent protein-protein associations. **B)** Protein-protein interaction network of nuclear speckles proteins, SON, eIF4A3, and SRSF2, predicted to interact with CDR2. eIF4A3 (red) directly interacts with SON (light green) and SRSF2 (blue). **C)** eIF4A3 (yellow) interacts with rpS6 (blue), indicated by colored edges. Predicted binding partners, CDR2L (green) and CDR2 (red), are manually gated (black, dotted lines). Color-coded edges; light blue: curated databases, dark blue: gene co-occurrence, pink: experimentally determined, green: text mining. Interactions with a medium score of 0.400 or more are shown¹²⁶.

4.3 Paper III

Growing rat cerebellar cells directly on pre-coated (poly-D-lysine or laminin) glass coverslips gave limited Purkinje neuron survival. Therefore, cerebellar cells (37,500 cells/mL) were plated and grown for one to six weeks to create a three-dimensional support layer before additional cerebellar cells (50,000-75,000 cells/mL) were added on top (Purkinje neuron layer; PN layer) and grown for an additional three to four weeks.

The age of the rats (embryonic day 18 to postnatal day 10; E18 to P10) when plating the support layer did not affect the survival of the Purkinje neurons in the PN layer. However, there was a strong correlation between the *in vitro* age of the support layer and the rat age of the PN layer: For E18 PN layers, the highest Purkinje neuron survival was found when plated onto a support layer of 14 days *in vitro* (DIV); for P0 PN layers when plated onto a support layer of 21 DIV; and for P10 PN layers when plated onto a support layer of 28 DIV (Fig. 9A). In conclusion, the older the rat age of the PN layer, the more mature the support layer should be to ensure high Purkinje neuron survival.

For the support layer, exchanging half of the growth medium with fresh medium once a week was sufficient to keep the pH stable. Due to the high number of cells after plating the PN layer, half of the media had to be exchanged twice a week for 6 well plates and every second day for 12 and 24 well plates. Media replacement once a week led to non-physiological pH fluctuations and cell death.

Adding the protein kinase C (PKC) inhibitor K252a to the growth media gave more well-developed Purkinje neuron dendrites in E18 and P0 PN layers; it did not affect the branching and maturation of dendrites in P10 PN layers (Fig. 9B). However, addition of K252a improved Purkinje neuron survival in P0 and P10 PN layers; no difference was observed for E18 PN layers (Fig. 9D). Six times as many Purkinje neurons survived when 10 nM K252a was added to P0 PN layers compared to cultures without K252a; for P10, 28 times as many Purkinje neurons survived when adding of 25 nM K252a to the media.

Furthermore, addition of 40 μ M progesterone to the growth medium gave increased dendritic branching in E18 PN layers (Fig. 9E); no difference was found for P0 and P10 PN layers. In cultures without both K252a and progesterone, adding insulin and insulin-like growth factor 1 (IGF1) was sufficient to maintain long-term growth of the other cerebellar cell types (Granule, Golgi, Lugaro, unipolar brush, stellate and basket cells).

The cultured neurons had active synapses as demonstrated by immunofluorescent staining using the synaptic markers voltage-gated calcium channels (VGCC), metabotropic glutamate receptor 1 (mGluR1), post-synaptic density protein 95 (PSD95), glutamate-decarboxylase 65 (GAD65), glycine transporter 2 (GlyT2), α -synuclein and bassoon (Fig. 9G).

Moreover, electrophysiological measurements of the E18 PN layers were performed (Fig. 9H). Using a 24 well multielectrode array, E18 PN layers gave spontaneous activity at 11 DIV (0.15 Hz) with spike frequency increasing until 21 DIV (2.56 Hz). This spike frequency was observed until 63 DIV, however the spike pattern became increasingly erratic after 28 DIV.

The cerebellar cultures were also well suited for genetic engineering. Lentiviral particles were used to express green fluorescent protein (GFP) in Purkinje neurons through implementation of the Purkinje neuron-specific L7 promoter (Fig. 9I). The virus particles were added at the day of seeding, and GFP could be seen after 3 DIV. At 14 DIV, over 60% of the Purkinje neurons were GFP positive, and the GFP signal were still present at 169 DIV. Transfection of the viral particles into Purkinje neurons at 14 DIV and 28 DIV were also successful, although the transfection rate declined the older the cultures were.

In summary, three main factors were found to be important for well-developed Purkinje neurons: (1) a three-dimensional support layer, (2) pH stability and (3) co-factor supplements.

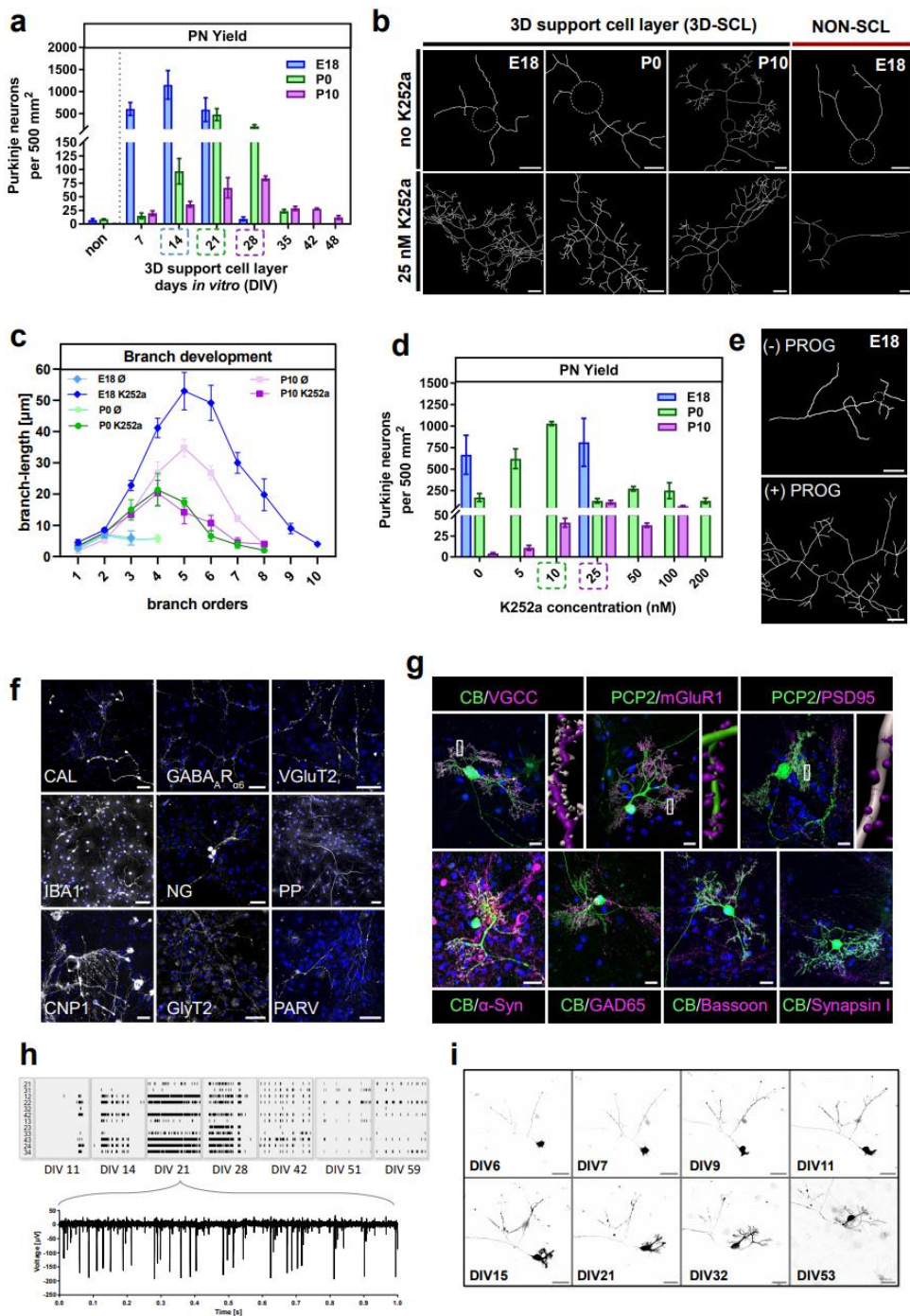


Figure 9: Evaluation of age-dependent rat Purkinje neuron culture. **(a)** Interdependent relationship of Purkinje neuron yield and in vitro age of the support cell layer (DIV 7 to 48) for E18, P0 and P10 derived-Purkinje neurons. **(b)** Representative Purkinje neuron skeletons depended on derived neuron age, support layer and protein kinase C (PKC) antagonist K252a. Scale bar: 20 μm . **(c)** Analysis of dendritic branch structure towards length and branch orders for Purkinje neurons derived from E18, P0 and P10 tissue without and with 25 μM K252a to modulate PKC activity. **(d)** Interdependent relationship of Purkinje neuron yield and concentration-dependent PKC activity modulation for E18, P0 and P10 derived Purkinje neurons. **(e)** Representative skeleton of an E18 derived-Purkinje neurons visualizing the effect of 40 μM progesterone on dendritic branching. Scale bar: 20 μm . **(f)** Immunohistochemical representation of the major cell types (white) forming the support layer: unipolar brush cells (CAL, calretinin), granule cells (GABAAR α 6), Golgi cells (NG, neurogranin; GlyT2), Lugaro cells (GlyT2), stellate and basket cells (PAV, parvalbumin), fibers such as mossy and climbing (VGluT2; PP, peripherin), oligodendrocytes (CNP1) as well as microglia (IBA1). Nuclei staining DAPI (blue). Scale bar: 50 μm . **(g)** Immunohistochemical representation of mature Purkinje neurons (green; CB, calbindin; PCP2, Purkinje cell specific protein 2) positive for post- and presynaptic biomarkers (magenta). Postsynaptic: VGCC, mGluR1, and PSD95 including 3D IMARIS reconstruction of the positive synapses of a chosen Purkinje neuron dendrite. Pre-synaptic: α -synuclein (α -syn; marker of glutamatergic synaptic terminals from granule cells/parallel fibres and unipolar brush cells), GAD65 (marker of axon terminals from stellate and basket cells), bassoon (marker of the active zone of mossy fiber terminals and parallel fiber terminals between Golgi cells and granule cells, and between basket cells and Purkinje neurons) and synapsin I (synaptic vesicle phosphoprotein of mature CNS synapses). Nuclei staining DAPI (blue). Scale bar: 20 μm . **(h)** MEA recorded spike patterns (10s) with a cut-out (1s) at day 21 in vitro following Purkinje neuron maturity. **(i)** Live-cell imaging of E18 derived Purkinje neuron expressing lentiviral-induced GFP from day of seeding (DIV0) up to 2 months (DIV53). Scale bar: 50 μm (Uggerud 2020, submitted).

5. DISCUSSION

5.1 Paper I

The three CDR antigens bound by Yo antibodies were identified in the late 80's and early 90's^{96, 99, 125}. For over two decades CDR2 was considered as the main antigen for the Yo antibodies present in PCD patients^{86, 114, 115, 122}. This assumption was based primarily on the finding that CDR2 mRNA was the only variant expressed in PCD-associated tumors¹¹⁴. In addition, CDR2 protein expression appeared restricted to the brain and testis. However, later studies showed that both CDR2 and CDR2L are present in several normal tissues, as well as cancerous tissue associated with PCD^{116, 124}.

In 2013, Yo antibodies were found to also bind CDR2L, and the coexistence of paratopes against both CDR2 and CDR2L was a strong indicator of PCD¹⁰⁰. In paper I, we showed that it is CDR2L, and not CDR2, that is the major target for Yo antibodies¹⁰¹. These antibodies do not bind endogenous CDR2, but do, however, bind recombinant CDR2. This led to the hypothesis that recombinant CDR2 shares one or several epitopes with CDR2L. This also explains why clinical tests can use recombinant CDR2 to verify a positive PCD result. However, as CDR2-based line blot assays give a high number of false-positive results (<10% specificity), it is believed that assays using CDR2L would be more sensitive⁵²⁻⁵⁴.

As most (if not all) Yo-associated PCD patients are recognized by the recombinant CDR2 assays, a paratope against a common epitope shared between CDR2L and CDR2 might be necessary to cause PCD (Fig. 10). This is in line with our finding that only patients with Yo antibodies towards both recombinant CDR2L and CDR2 have PCD, while patients with antibodies only binding one of the proteins do not^{54, 100}. Since Yo antibodies were not found to bind a common linear epitope between CDR2L and CDR2¹²⁷, the pathogenic epitope is likely conformational. Thus, the epitope can only be verified once the three-dimensional structures of these proteins are established.

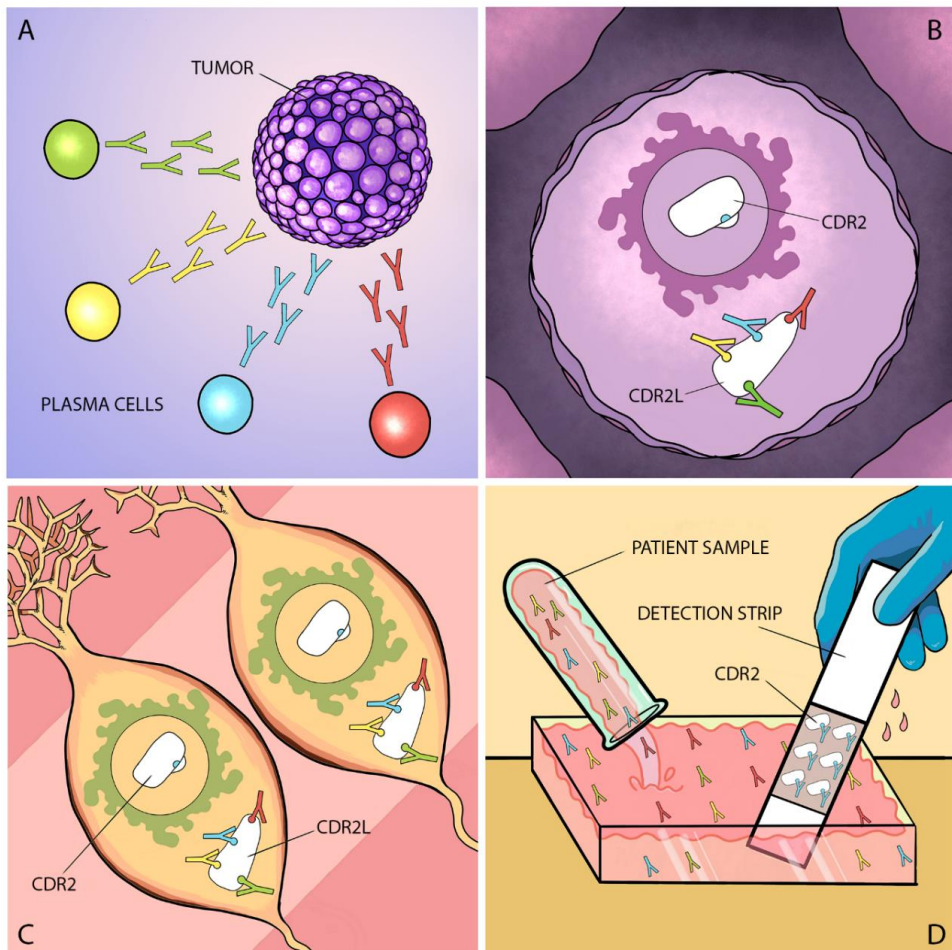


Figure 10: Proposed hypothesis of how Yo antibodies are able to bind both recombinant CDR2 and CDR2L, but only CDR2L under native conditions. **A)** Illustration of the initial, polyclonal response of Yo antibodies toward CDR2L in the tumors of PCD patients. **B)** A tumor cell with the polyclonal Yo antibodies targeting the CDR2L protein; CDR2 is unaffected as the epitope that is common to CDR2L (blue) is hidden by post-translational modifications or a partnering molecule (white fold covering the blue epitope). **C)** The Yo antibodies also bind to CDR2L in cerebellar Purkinje cells; however, they do not bind CDR2 as the common epitope (blue) is hidden here as well (by modifications or partnering molecules; white fold). **D)** When patient sera or CSF is applied to a line blot with recombinant CDR2 attached, binding of the common epitope (blue) is possible as it is not hidden by post-translational modifications or partnering molecules in the recombinant version¹⁰¹.

5.2 Paper II

Little is known about the pathogenesis of Yo-associated PCD, however a two-step hypothesis has been proposed: 1) production of anti-tumor immune components directed towards the Yo antigen (Yo antibodies and cytotoxic T cells targeting the same Yo epitopes) followed by 2) targeting of the Yo antigen in Purkinje neurons as a secondary effect. It has also been shown that Yo antibodies can induce Purkinje neuron loss in cerebellar slice cultures in the absence of T cells^{93, 94, 128}.

To elucidate the mechanism causing Purkinje neuron death in Yo-associated PCD, the localization and function of the target proteins must be established. Yo antibodies are known to bind to clusters of ribosomes as well as vesicles within the trans face of the Golgi^{107, 111}, but no studies have used specific antibodies against CDR2L and CDR2 to determine their subcellular localization.

There are several commercial antibodies against both CDR2L and CDR2, each with different localization patterns. Binding pattern varies particularly with CDR2 antibodies, possibly reflecting the five different predicted isoforms for this protein (The UniProt Consortium). In paper II, we showed that the CDR2L and CDR2 antibodies bound their predicted targets without cross-reactivity to other CDR proteins. Furthermore, Yo antibodies were found to only bind CDR2L, thus confirming the results in paper I.

In addition to confirming antibody specificity, the mass spectrometry analysis revealed several ribosomal proteins as potential interaction partners of CDR2L, and various nuclear speckle proteins as potential partners for CDR2. Through super-resolution microscopy, proximity ligation assay and co-immunoprecipitation, we found that CDR2L colocalized with rpS6 and CDR2 colocalized with SON and eIF4A3. This corresponds well with a previous study which showed that the Yo antigen interacts with c-Myc¹¹⁵, a regulator of ribosome biogenesis and protein synthesis¹²⁹, and that CDR2 interacts with nuclear proteins such as PKN, MRGX, MRG15¹³⁰⁻¹³².

Although CDR2L and CDR2 share 45% sequence homology, they are not necessarily associated with the same functions in the cell. However, eIF4A3, one of the partners found for CDR2, is known to translocate from the nucleus to the ribosome where it interacts with rps6, the interaction partner of CDR2L^{133, 134}, thus establishing an indirect connection between CDR2 and CDR2L (Fig. 11). The potential role of CDR2L and CDR2 in this pathway will have to be further analyzed.

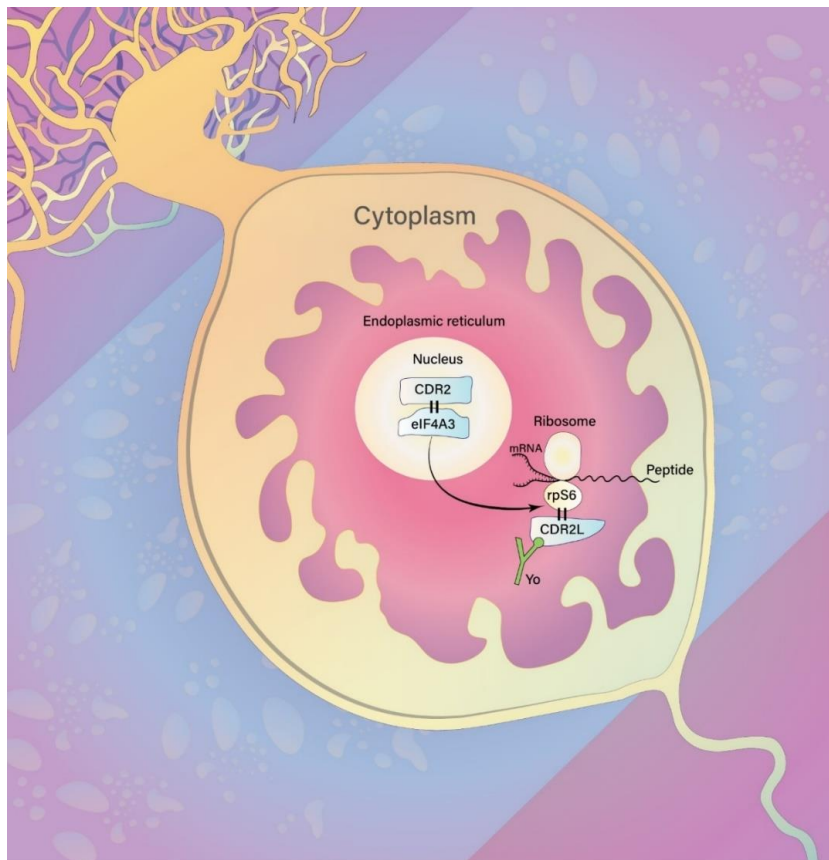


Figure 11: Hypothesis of CDR2L and CDR2 involvement in protein synthesis in Purkinje neurons. CDR2 localizes to the nucleus and directly interacts with nuclear speckle protein eIF4A3. eIF4A3, in conjunction with other cytoplasmic initiation factors, facilitates mRNA binding to the 40S ribosomal subunit. This event is important for mRNA maturation and translation, ultimately resulting in the synthesis of new proteins. CDR2L interacts with ribosomal subunit protein rps6; therefore, we propose that CDR2L and CDR2 are both involved in the process of protein synthesis. Furthermore, Yo antibody (green) binding to CDR2L in Purkinje neurons of PCD patients may, therefore, interfere with the function of the ribosomal machinery, resulting in disrupted mRNA translation and/or protein synthesis¹²⁶.

5.3 Paper III

To investigate the mechanisms causing PCD, and other neurodegenerative disorders, good model systems are vital. Rat and mouse models are commonly used in biomedical research, and several protocols for generating cerebellar cultures from mice, including some with healthy Purkinje neurons, have been published¹³⁵⁻¹³⁹. Rats are, however, more physiologically, genetically and morphologically similar to humans, and mimic many of the human neurodegenerative disease mechanisms better than mice models do¹⁴⁰⁻¹⁵⁰. In addition to being more comparable to humans in many aspects, rats are around ten times heavier than mice and are less easily stressed by human contact¹⁵¹, making rats easier to handle as well as being easier to dissect.

Protocols for rat cerebellar cell cultures are, however, limited. These either report poor Purkinje neuron survival and dendritic development or do not demonstrate neuronal activity^{152, 153}. Furthermore, no other protocol has demonstrated high yields of Purkinje neurons by the use of postnatal rat pups. This led us to explore ways of creating a more robust rat cerebellar culture protocol with high yield of mature and synaptically active Purkinje neurons that could be generated from both embryonic and postnatal rat pups.

The main factors found to be important for well-developed Purkinje neurons were (1) a support layer, (2) pH stability and (3) co-factor supplements (Fig. 12). The support layer provides cell-to-cell communication in the form of juxtacrine as well as paracrine factors that can help Purkinje neurons, and other cells of the cerebellum, to grow and mature. Fluctuations in pH, visible by the shift of media color (by using Phenol red; yellow indicating acidic pH, orange neutral and pink basic), caused extensive cell death and decreased Purkinje neuron survival. By changing the media more often, pH was stabilized and cell death minimized.

As for co-factor supplements, the PKC inhibitor K252a¹⁵⁴ was found to be important for both dendritic length and branch orders of E18 and P0 PN layers. It did, however, cause decreased dendrite length when applied to P10 PN layers although it did not affect the branch orders. Inclusion of K252a in the media also led to increased

numbers of surviving Purkinje neurons in P0 and P10 PN layers, while no changes were seen for E18 PN layers. In addition to K252a, progesterone also led to more mature dendrites in E18 PN layers; no difference was observed for P0 and P10 PN layers.

The neurons in the cultures were positive for all tested synaptic markers, as well as being both electrically active and possible to genetically manipulate at all stages of maturation. This demonstrates that the protocol is robust and versatile and can thus be used in a wide variety of cerebellar studies.

To summarize, three elements were essential for high yield of active Purkinje neurons: (1) a support layer, (2) pH stability (media should be prepared fresh on the day of use and the support layers should be fed 24 hours prior to the plating of a PN layer), and (3) co-factor supplements (repeated thaw-freeze cycles should be avoided).

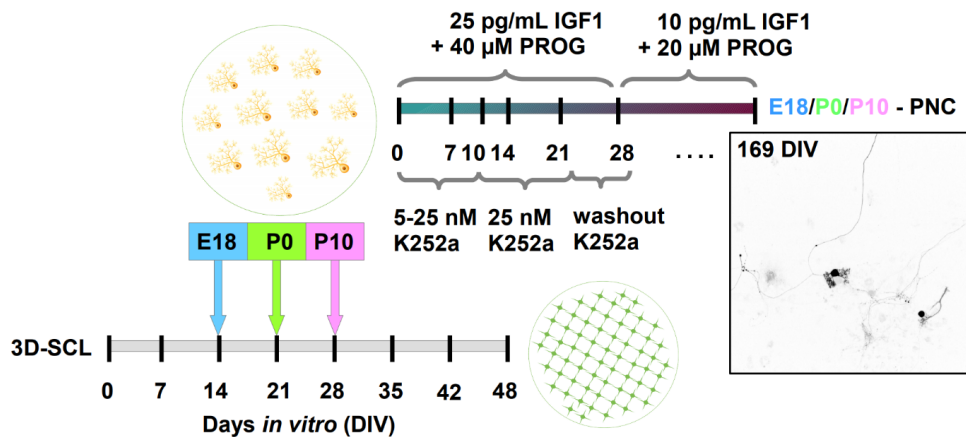


Figure 12: Optimized rat Purkinje neuron culture protocol. Each tested culture desired different conditions of support and activity independent of the starting tissue age. Whereas the supplementation of insulin-like growth factor 1 (IGF1) and progesterone (PROG) induced a stable environment to obtain high survival rates of Purkinje neurons, PKC mainly shaped the dendritic tree development (exception: P10 derived neurons where the survival was highly dependent on the inhibition of PKC but not their dendritic tree development). The optimized protocol for all tested tissues relied on the time point of placing the Purkinje neuron (PN) layer and the inclusion of IGF1, progesterone and K252a. The K252a concentration was adjusted as follows: DIV 1-10:

E18 - 5 nM, P0 - 10 nM, P10 - 25 nM; DIV 10-22: 25 nM; DIV 22-28: washout phase (DIV 22-24: 12.5 nM; DIV 24-26: 6.75 nM; DIV 26-28: 3.35 nM). At DIV 28 the IGF1 and progesterone concentration was reduced to proceed to long term culture conditions. The protocol allows to grow a stable Purkinje neuron culture for up to 6 months (DIV 163) in a 6 to 24 well format (Uggerud 2020, submitted).

6. ADVANCES AND FUTURE ASPECTS

With CDR2L now established as the major antigen target of Yo antibodies, we can reexamine the neurodegenerative mechanisms involved in PCD. Where earlier models focusing on CDR2 did not elicit PCD symptoms^{112, 120, 121, 155}, it is now possible to try and create an animal model of Yo-mediated PCD driven by CDR2L. Moreover, many neurodegenerative diseases have immune-related aspects and exploration of the immune mechanisms involved in PCD will be beneficial for these diseases as well.

As the specific immune mechanism causing Purkinje neuron loss in PCD is unresolved, it will be vital to investigate further the cellular functions of CDR2 and CDR2L. We will need to elucidate how the binding of these proteins by internalized Yo antibodies causes neurodegeneration, while the presence of other antibodies does not⁹²⁻⁹⁴. CDR2L could be directly involved in the cellular biosynthesis through an effect on ribosomes, resulting in disruption of protein synthesis and subsequent cell death. Alternatively, or perhaps additionally, CDR2L binding by Yo antibodies may cause disturbances in calcium homeostasis in Purkinje neurons^{92, 93} with subsequent disruption of protein synthesis¹⁵⁶.

Investigation of whether CDR2L is present in the plasma membrane, as has been shown for recombinant CDR2L in HeLa cells¹⁰⁰, will also be important. The presence of CDR2L in the plasma membrane, making it accessible to the environment, could contribute both to increased antibody internalization and targeting by cytotoxic immune cells. Furthermore, dysregulated regulatory immune cells are likely involved in the pathogenesis, where CDR2L is recognized in the tumor as non-self. The activation of B and T cells in the tumor and how they execute the neuronal damage needs to be further explored, as well as which of the immune components that perform the final effector role. As it has been demonstrated *in vitro* that both antibodies and T cells can be responsible for PCD-associated neurodegeneration^{50, 93, 94}, one could speculate that both components can be involved simultaneously, with

the antibodies causing internal disturbances and T cells releasing cytotoxic granules on the outside.

The protocol we derived for cerebellar cultures giving viable Purkinje neurons has already been used in the exploration of Yo-associated PCD¹²⁶. These cultures can be used in combination with Yo antibodies conjugated to fluorescent dyes to study the internalization process, binding patterns and possible functional role in living Purkinje neurons. Additionally, as PCD can be used as a model system for autoimmune diseases, the cultures can also be used to resolve other neuronal mechanisms. In our laboratory these cultures are already being used to model demyelination and to investigate if stem cells are able to remyelinate the affected axons.

7. CONCLUSIONS

Paper I: The finding that Yo antibodies bind endogenous CDR2L, and not CDR2, allows us to rethink the mechanisms involved in Yo-mediated PCD. The binding of recombinant CDR2 suggests that these proteins have common epitopes which is not surprising considering their 45% amino acid sequence identity. Furthermore, test assays using CDR2L instead of CDR2 could be more sensitive, reducing the large amounts of false-positive results obtained today.

Paper II: Previous studies suggested that Yo antibodies bind a ribosomal target, but the locations of CDR2 and CDR2L were unknown. Our finding that CDR2L interacts specifically with ribosomal proteins, while CDR2 interacts with nuclear speckle proteins, adds further support for CDR2L being the primary Yo antibody target. Since one of the interaction partners of CDR2, eIF4A3, translocates from the nucleus to the ribosome, where it interacts with rpS6, this also adds an indirect link between CDR2L and CDR2. Whether CDR2L and CDR2 have similar roles or are involved in related processes in protein transcription and translation remains to be resolved.

Paper III: We established a robust primary culture protocol that gave high yields of mature Purkinje neurons from both embryonic and postnatal rats. These cultures were well suited to high-throughput screening, genetic manipulation and electrophysiological recordings and will be useful for exploring both neurodegenerative and regenerative mechanisms.

8. SOURCE OF DATA

1. Albus, J.S., *A Theory of Cerebellar Function*. Mathematical Biosciences 1971. **10**: p. 25-61.
2. Eccles, J.C., M. Ito, and J.n. Szentágothai, *The cerebellum as a neuronal machine*. 1967, Berlin, New York etc.: Springer-Verlag. 335 p.
3. Llinas, R.R., K.D. Walton, and E.J. Lang, *Ch. 7 Cerebellum*. The Synaptic Organization of the Brain 2004.
4. Von Bartheld, C.S., *Myths and truths about the cellular composition of the human brain: A review of influential concepts*. Journal of Chemical Neuroanatomy, 2018. **93**: p. 2-15.
5. Williams, R.W. and K. Herrup, *The Control of Neuron Number*. 1988. **11**(1): p. 423-453.
6. Haug, H., *History of neuromorphometry*. Journal of Neuroscience Methods, 1986. **18**(1-2): p. 1-17.
7. Bahney, J. and C.S. Von Bartheld, *The Cellular Composition and Glia-Neuron Ratio in the Spinal Cord of a Human and a Nonhuman Primate: Comparison With Other Species and Brain Regions*. The Anatomical Record, 2018. **301**(4): p. 697-710.
8. Bahney, J. and C.S. Von Bartheld, *Validation of the isotropic fractionator: Comparison with unbiased stereology and DNA extraction for quantification of glial cells*. 2014. **222**: p. 165-174.
9. Fox, C.A., et al., *The primate cerebellar cortex: a Golgi and electron microscopic study*. Prog Brain Res, 1967. **25**: p. 174-225.
10. Fujishima, K., K. Kawabata Galbraith, and M. Kengaku, *Dendritic Self-Avoidance and Morphological Development of Cerebellar Purkinje Cells*. The Cerebellum, 2018.
11. Napper, R.M.A. and R.J. Harvey, *Number of parallel fiber synapses on an individual Purkinje cell in the cerebellum of the rat*. 1988. **274**(2): p. 168-177.
12. Jarius, S. and B. Wildemann, *'Medusa head ataxia': the expanding spectrum of Purkinje cell antibodies in autoimmune cerebellar ataxia. Part 3: Anti-Yo/CDR2, anti-Nb/AP3B2, PCA-2, anti-Tr/DNER, other antibodies, diagnostic pitfalls, summary and outlook*. J Neuroinflammation, 2015. **12**: p. 168.
13. Jarius, S. and B. Wildemann, *'Medusa head ataxia': the expanding spectrum of Purkinje cell antibodies in autoimmune cerebellar ataxia. Part 2: Anti-PKC-gamma, anti-GluR-delta2, anti-Ca/ARHGAP26 and anti-VGCC*. J Neuroinflammation, 2015. **12**: p. 167.
14. Jarius, S. and B. Wildemann, *'Medusa-head ataxia': the expanding spectrum of Purkinje cell antibodies in autoimmune cerebellar ataxia. Part 1: Anti-mGluR1, anti-Homer-3, anti-Sj/ITPR1 and anti-CARP VIII*. J Neuroinflammation, 2015. **12**: p. 166.
15. Mitoma, H., M. Hadjivassiliou, and J. Honnorat, *Guidelines for treatment of immune-mediated cerebellar ataxias*. Cerebellum Ataxias, 2015. **2**: p. 14.
16. Koeppen, A.H., *The neuropathology of the adult cerebellum*. 2018, Elsevier. p. 129-149.

17. Fernández, M., T. Sierra-Arregui, and O. Peñagarikano, *The Cerebellum and Autism: More than Motor Control*. 2019, IntechOpen.
18. Anderson, M.A., et al., *Astrocyte scar formation aids central nervous system axon regeneration*. *Nature*, 2016. **532**(7598): p. 195-200.
19. Andersen, B.B., L. Korbo, and B. Pakkenberg, *A quantitative study of the human cerebellum with unbiased stereological techniques*. *The Journal of Comparative Neurology*, 1992. **326**(4): p. 549-560.
20. Marshall, J.S., et al., *An introduction to immunology and immunopathology*. Allergy, Asthma & Clinical Immunology, 2018. **14**(S2).
21. Chaplin, D.D., *Overview of the immune response*. *Journal of Allergy and Clinical Immunology*, 2010. **125**(2): p. S3-S23.
22. Alberts, B., *Molecular biology of the cell*. 5th ed. 2008, New York: Garland Science.
23. Teng, M.W.L., et al., *From mice to humans: developments in cancer immunoediting*. *Journal of Clinical Investigation*, 2015. **125**(9): p. 3338-3346.
24. Ribas, A. and J.D. Wolchok, *Cancer immunotherapy using checkpoint blockade*. *Science*, 2018. **359**(6382): p. 1350-1355.
25. Dubey, D., et al., *Varied phenotypes and management of immune checkpoint inhibitor-associated neuropathies*. *Neurology*, 2019. **93**(11): p. e1093-e1103.
26. Williams, T.J., et al., *Association of Autoimmune Encephalitis With Combined Immune Checkpoint Inhibitor Treatment for Metastatic Cancer*. *JAMA Neurology*, 2016. **73**(8): p. 928.
27. Graus, F. and J. Dalmau, *Paraneoplastic neurological syndromes in the era of immune-checkpoint inhibitors*. *Nature Reviews. Clinical Oncology*, 2019. **16**(9): p. 535-548.
28. Engelhardt, B., P. Vajkoczy, and R.O. Weller, *The movers and shapers in immune privilege of the CNS*. *Nat Immunol*, 2017. **18**(2): p. 123-131.
29. Asgari, M., D. de Zélicourt, and V. Kurtcuoglu, *Glymphatic solute transport does not require bulk flow*. *Sci Rep*, 2016. **6**: p. 38635.
30. Louveau, A., T.H. Harris, and J. Kipnis, *Revisiting the Mechanisms of CNS Immune Privilege*. *Trends Immunol*, 2015. **36**(10): p. 569-577.
31. Aspelund, A., et al., *A dural lymphatic vascular system that drains brain interstitial fluid and macromolecules*. *J Exp Med*, 2015. **212**(7): p. 991-9.
32. Croxford, A.L., S. Spath, and B. Becher, *GM-CSF in Neuroinflammation: Licensing Myeloid Cells for Tissue Damage*. *Trends Immunol*, 2015. **36**(10): p. 651-662.
33. Kipnis, J., *Multifaceted interactions between adaptive immunity and the central nervous system*. *Science*, 2016. **353**(6301): p. 766-771.
34. Pavelek, Z., et al., *Innate Immune System and Multiple Sclerosis. Granulocyte Numbers Are Reduced in Patients Affected by Relapsing-Remitting Multiple Sclerosis during the Remission Phase*. *J Clin Med*, 2020. **9**(5).
35. Beers, D.R., et al., *CD4+ T cells support glial neuroprotection, slow disease progression, and modify glial morphology in an animal model of inherited ALS*. 2008. **105**(40): p. 15558-15563.
36. Marsh, S.E., et al., *The adaptive immune system restrains Alzheimer's disease pathogenesis by modulating microglial function*. 2016: p. 201525466.

37. Darnell, R.B. and J.B. Posner, *Paraneoplastic syndromes involving the nervous system*. N Engl J Med, 2003. **349**(16): p. 1543-54.
38. Graus, F., et al., *Anti-Hu-associated paraneoplastic encephalomyelitis: analysis of 200 patients*. Brain, 2001. **124**(Pt 6): p. 1138-48.
39. Anderson, N.E., J.M. Cunningham, and J.B. Posner, *Autoimmune pathogenesis of paraneoplastic neurological syndromes*. Crit Rev Neurobiol, 1987. **3**(3): p. 245-99.
40. Dalmau, J.O. and J.B. Posner, *Paraneoplastic Syndromes*. Archives of Neurology, 1999. **56**(4): p. 405.
41. Dalmau, J. and J.B. Posner, *Neurological paraneoplastic syndromes*. Springer Seminars in Immunopathology, 1996. **18**(1): p. 85-95.
42. Bolla, L. and R.M. Palmer, *Paraneoplastic cerebellar degeneration. Case report and literature review*. Arch Intern Med, 1997. **157**(11): p. 1258-62.
43. Ances, B.M., et al., *Treatment-responsive limbic encephalitis identified by neuropil antibodies: MRI and PET correlates*. Brain, 2005. **128**(Pt 8): p. 1764-77.
44. Braik, T., et al., *Paraneoplastic neurological syndromes: unusual presentations of cancer. A practical review*. Am J Med Sci, 2010. **340**(4): p. 301-8.
45. Nath, U. and R. Grant, *Neurological paraneoplastic syndromes*. J Clin Pathol, 1997. **50**(12): p. 975-80.
46. Candler, P.M., et al., *A follow up study of patients with paraneoplastic neurological disease in the United Kingdom*. J Neurol Neurosurg Psychiatry, 2004. **75**(10): p. 1411-5.
47. Graus, F., et al., *Recommended diagnostic criteria for paraneoplastic neurological syndromes*. J Neurol Neurosurg Psychiatry, 2004. **75**(8): p. 1135-40.
48. Seeger, R.C., P.M. Zeltzer, and S.A. Rayner, *Onco-neural antigen: a new neural differentiation antigen expressed by neuroblastoma, oat cell carcinoma, Wilms' tumor, and sarcoma cells*. J Immunol, 1979. **122**(4): p. 1548-55.
49. Mitoma, H., et al., *Consensus Paper: Neuroimmune Mechanisms of Cerebellar Ataxias*. The Cerebellum, 2016. **15**(2): p. 213-232.
50. Yshii, L.M., et al., *CTLA4 blockade elicits paraneoplastic neurological disease in a mouse model*. Brain, 2016. **139**(11): p. 2923-2934.
51. Dalmau, J., C. Geis, and F. Graus, *Autoantibodies to Synaptic Receptors and Neuronal Cell Surface Proteins in Autoimmune Diseases of the Central Nervous System*. Physiological Reviews, 2017. **97**(2): p. 839-887.
52. Ruiz-García, R., et al., *The Diagnostic Value of Onconeural Antibodies Depends on How They Are Tested*. Frontiers in Immunology, 2020. **11**(1482).
53. Dechelotte, B., et al., *Diagnostic yield of commercial immunodots to diagnose paraneoplastic neurologic syndromes*. Neurol Neuroimmunol Neuroinflamm, 2020. **7**(3).
54. Herdlevær, I., et al., *Paraneoplastic cerebellar degeneration: the importance of including CDR2L as a diagnostic marker*. Neurology: Neuroimmunology & Neuroinflammation, 2020, in press.

55. Greenlee, J.E. and H.R. Brashear, *Antibodies to cerebellar Purkinje cells in patients with paraneoplastic cerebellar degeneration and ovarian carcinoma*. *Ann Neurol*, 1983. **14**(6): p. 609-13.
56. Drlicek, M., et al., *Antibodies of the anti-Yo and anti-Ri type in the absence of paraneoplastic neurological syndromes: a long-term survey of ovarian cancer patients*. 1997. **244**(2): p. 85-89.
57. Matsushita, H., et al., *Paraneoplastic cerebellar degeneration with anti-Purkinje cell antibody associated with primary tubal cancer*. *Gynecol Obstet Invest*, 1998. **45**(2): p. 140-3.
58. Peterson, K., et al., *Paraneoplastic cerebellar degeneration. I. A clinical analysis of 55 anti-Yo antibody-positive patients*. *Neurology*, 1992. **42**(10): p. 1931-7.
59. Cao, Y., et al., *Anti-Yo Positive Paraneoplastic Cerebellar Degeneration Associated with Ovarian Carcinoma: Case Report and Review of the Literature*. 1999. **75**(1): p. 178-183.
60. McKeon, A., *Purkinje Cell Cytoplasmic Autoantibody Type 1 Accompaniments*. *Archives of Neurology*, 2011. **68**(10): p. 1282.
61. Zaborowski, M.P., et al., *Paraneoplastic neurological syndromes associated with ovarian tumors*. *Journal of Cancer Research and Clinical Oncology*, 2015. **141**(1): p. 99-108.
62. Venkatraman, A. and P. Opal, *Paraneoplastic cerebellar degeneration with anti-Yo antibodies - a review*. *Ann Clin Transl Neurol*, 2016. **3**(8): p. 655-63.
63. Rana, A.Q., A.N. Rana, and A. Adlul, *Acute ataxia due to anti-Yo antibody paraneoplastic cerebellar degeneration 4 months prior to diagnosis of uterine carcinoma*. 2012. **112**(3): p. 303-304.
64. Panegyres, P.K. and A. Graves, *Anti-Yo and anti-glutamic acid decarboxylase antibodies presenting in carcinoma of the uterus with paraneoplastic cerebellar degeneration: a case report*. *Journal of Medical Case Reports*, 2012. **6**(1): p. 155.
65. Brock, S., et al., *Anti-Yo Antibody-Positive Cerebellar Degeneration Associated with Endometrial Carcinoma: Case Report and Review of the Literature*. 2001. **13**(6): p. 476-479.
66. Dorn, C., et al., *Paraneoplastic neurological syndrome: patient with anti-Yo antibody and breast cancer: a case report*. 2003. **269**(1): p. 62-65.
67. Ogita, S., et al., *Paraneoplastic Cerebellar Degeneration with Anti-Yo Antibody in a Patient with HER2neu Overexpressing Breast Cancer: A Case Report with a Current Literature Review*. 2008. **14**(4): p. 382-384.
68. Plantone, D., et al., *Brainstem and spinal cord involvement in a paraneoplastic syndrome associated with anti-Yo antibody and breast cancer*. 2011. **258**(5): p. 921-922.
69. Rojas-Marcos, I., et al., *Human epidermal growth factor receptor 2 overexpression in breast cancer of patients with anti-Yo-associated paraneoplastic cerebellar degeneration*. 2012. **14**(4): p. 506-510.
70. Tanriverdi, O., et al., *Anti-Yo Antibody-mediated Paraneoplastic Cerebellar Degeneration in a Female Patient with Pleural Malignant Mesothelioma*. *Japanese Journal of Clinical Oncology*, 2013. **43**(5): p. 563-568.

71. Dalmau, J., et al., *Detection of the anti-Hu antibody in the serum of patients with small cell lung cancer? A quantitative western blot analysis*. 1990. **27**(5): p. 544-552.
72. Graus, F., et al., *Anti-Hu antibodies in patients with small-cell lung cancer: association with complete response to therapy and improved survival*. *J Clin Oncol*, 1997. **15**(8): p. 2866-72.
73. Roberts, W.K., et al., *Patients with lung cancer and paraneoplastic Hu syndrome harbor HuD-specific type 2 CD8+ T cells*. *Journal of Clinical Investigation*, 2009.
74. Hasadsri, L., et al., *Anti-Yo Associated Paraneoplastic Cerebellar Degeneration in a Man with Large Cell Cancer of the Lung*. *Case Reports in Neurological Medicine*, 2013. **2013**: p. 1-5.
75. Sutton, I.J., et al., *Anti-Yo antibodies and cerebellar degeneration in a man with adenocarcinoma of the esophagus*. 2001. **49**(2): p. 253-257.
76. Xia, K., J.R. Saltzman, and D.L. Carr-Locke, *Anti-Yo antibody-mediated paraneoplastic cerebellar degeneration in a man with esophageal adenocarcinoma*. *MedGenMed*, 2003. **5**(3): p. 18.
77. Debes, J.D., et al., *Anti-Yo-Associated Paraneoplastic Cerebellar Degeneration in a Man with Adenocarcinoma of the Gastroesophageal Junction*. 2007. **24**(5): p. 395-397.
78. Meglič, B., F. Graus, and A. Grad, *Anti-Yo-associated paraneoplastic cerebellar degeneration in a man with gastric adenocarcinoma*. 2001. **185**(2): p. 135-138.
79. Goto, A., et al., *[Anti-Yo antibody associated paraneoplastic cerebellar degeneration with gastric adenocarcinoma in a male patient: a case report]*. *Rinsho Shinkeigaku*, 2006. **46**(2): p. 144-7.
80. Bruhnding, A., D. Notch, and A. Beard, *Anti-Yo positive paraneoplastic cerebellar degeneration in the setting of cholangiocarcinoma*. *J Clin Neurosci*, 2017. **36**: p. 71-72.
81. Valpione, S., et al., *Paraneoplastic cerebellar degeneration with anti-Yo antibodies associated with metastatic uveal melanoma*. *J Neurol Sci*, 2013. **335**(1-2): p. 210-2.
82. Matschke, J., et al., *Paraneoplastic cerebellar degeneration and anti-Yo antibodies in a man with prostatic adenocarcinoma*. *Journal of Neurology, Neurosurgery & Psychiatry*, 2006. **78**(7): p. 775-777.
83. Joubert, B., K. Rostasy, and J. Honnorat, *Immune-mediated ataxias*. *Handb Clin Neurol*, 2018. **155**: p. 313-332.
84. Yshii, L., C. Bost, and R. Liblau, *Immunological Bases of Paraneoplastic Cerebellar Degeneration and Therapeutic Implications*. *Frontiers in Immunology*, 2020. **11**(991).
85. Shams'ili, S., et al., *Paraneoplastic cerebellar degeneration associated with antineuronal antibodies: analysis of 50 patients*. *Brain*, 2003. **126**(Pt 6): p. 1409-18.
86. Albert, M.L., et al., *Tumor-specific killer cells in paraneoplastic cerebellar degeneration*. *Nat Med*, 1998. **4**(11): p. 1321-4.

87. Hillary, R.P., et al., *Complex HLA association in paraneoplastic cerebellar ataxia with anti-Yo antibodies*. J Neuroimmunol, 2018. **315**: p. 28-32.
88. McConnell, M.J., et al., *H2-Kb and H2-Db regulate cerebellar long-term depression and limit motor learning*. Proceedings of the National Academy of Sciences, 2009. **106**(16): p. 6784-6789.
89. Storstein, A., B.K. Krossnes, and C.A. Vedeler, *Morphological and immunohistochemical characterization of paraneoplastic cerebellar degeneration associated with Yo antibodies*. Acta Neurol Scand, 2009. **120**(1): p. 64-7.
90. Hill, K.E., et al., *Cerebellar Purkinje cells incorporate immunoglobulins and immunotoxins in vitro: implications for human neurological disease and immunotherapeutics*. 2009. **6**(1): p. 31.
91. Geis, C., et al., *Stiff person syndrome-associated autoantibodies to amphiphysin mediate reduced GABAergic inhibition*. 2010. **133**(11): p. 3166-3180.
92. Panja, D., C.A. Vedeler, and M. Schubert, *Paraneoplastic cerebellar degeneration: Yo antibody alters mitochondrial calcium buffering capacity*. Neuropathol Appl Neurobiol, 2018.
93. Schubert, M., et al., *Paraneoplastic CDR2 and CDR2L antibodies affect Purkinje cell calcium homeostasis*. Acta Neuropathol, 2014. **128**(6): p. 835-52.
94. Greenlee, J.E., et al., *Anti-Yo antibody uptake and interaction with its intracellular target antigen causes Purkinje cell death in rat cerebellar slice cultures: a possible mechanism for paraneoplastic cerebellar degeneration in humans with gynecological or breast cancers*. PLoS One, 2015. **10**(4): p. e0123446.
95. Jaeckle, K.A., et al., *Autoimmune response of patients with paraneoplastic cerebellar degeneration to a Purkinje cell cytoplasmic protein antigen*. Ann Neurol, 1985. **18**(5): p. 592-600.
96. Dropcho, E.J., et al., *Cloning of a brain protein identified by autoantibodies from a patient with paraneoplastic cerebellar degeneration*. Proc Natl Acad Sci U S A, 1987. **84**(13): p. 4552-6.
97. Furneaux, H.M., et al., *Characterization of a cDNA encoding a 34-kDa Purkinje neuron protein recognized by sera from patients with paraneoplastic cerebellar degeneration*. Proc Natl Acad Sci U S A, 1989. **86**(8): p. 2873-7.
98. Sakai, K., et al., *Isolation of a complementary DNA clone encoding an autoantigen recognized by an anti-neuronal cell antibody from a patient with paraneoplastic cerebellar degeneration*. Ann Neurol, 1990. **28**(5): p. 692-8.
99. Fathallah-Shaykh, H., et al., *Cloning of a leucine-zipper protein recognized by the sera of patients with antibody-associated paraneoplastic cerebellar degeneration*. Proc Natl Acad Sci U S A, 1991. **88**(8): p. 3451-4.
100. Eichler, T.W., et al., *CDR2L Antibodies: A New Player in Paraneoplastic Cerebellar Degeneration*. PLoS One, 2013. **8**(6): p. e66002.
101. Krakenes, T., et al., *CDR2L Is the Major Yo Antibody Target in Paraneoplastic Cerebellar Degeneration*. Ann Neurol, 2019. **86**(2): p. 316-321.

-
102. Totland, C., et al., *Expression of the onconeural protein CDR1 in cerebellum and ovarian cancer*. *Oncotarget*, 2018. **9**(35): p. 23975-23986.
 103. Rojas-Marcos, I., et al., *Spectrum of paraneoplastic neurologic disorders in women with breast and gynecologic cancer*. *Medicine (Baltimore)*, 2003. **82**(3): p. 216-23.
 104. Greenlee, J.E., *Anti-Yo autoimmunity; dangerous for the brain but not the tumor?* *Journal of the Neurological Sciences*, 2006. **250**(1-2): p. 1-2.
 105. Greenlee, J.E. and H.L. Lipton, *Anticerebellar antibodies in serum and cerebrospinal fluid of a patient with oat cell carcinoma of the lung and paraneoplastic cerebellar degeneration*. *Ann Neurol*, 1986. **19**(1): p. 82-5.
 106. Anderson, N.E., M.K. Rosenblum, and J.B. Posner, *Paraneoplastic cerebellar degeneration: clinical-immunological correlations*. *Ann Neurol*, 1988. **24**(4): p. 559-67.
 107. Rodriguez, M., et al., *Autoimmune paraneoplastic cerebellar degeneration: ultrastructural localization of antibody-binding sites in Purkinje cells*. *Neurology*, 1988. **38**(9): p. 1380-6.
 108. Furneaux, H.M., et al., *Selective expression of Purkinje-cell antigens in tumor tissue from patients with paraneoplastic cerebellar degeneration*. *N Engl J Med*, 1990. **322**(26): p. 1844-51.
 109. Graus, F., et al., *Effect of intraventricular injection of an anti-Purkinje cell antibody (anti-Yo) in a guinea pig model*. *J Neurol Sci*, 1991. **106**(1): p. 82-7.
 110. Tomimoto, H., J.M. Brengman, and T. Yanagihara, *Paraneoplastic cerebellar degeneration with a circulating antibody against neurons and non-neuronal cells*. *Acta Neuropathol*, 1993. **86**(2): p. 206-11.
 111. Hida, C., et al., *Ultrastructural localization of anti-Purkinje cell antibody-binding sites in paraneoplastic cerebellar degeneration*. *Arch Neurol*, 1994. **51**(6): p. 555-8.
 112. Tanaka, K., et al., *Passive transfer and active immunization with the recombinant leucine-zipper (Yo) protein as an attempt to establish an animal model of paraneoplastic cerebellar degeneration*. *J Neurol Sci*, 1994. **127**(2): p. 153-8.
 113. O'Brien, T.J., et al., *Anti-Yo positive paraneoplastic cerebellar degeneration: a report of three cases and review of the literature*. *J Clin Neurosci*, 1995. **2**(4): p. 316-20.
 114. Corradi, J.P., et al., *A post-transcriptional regulatory mechanism restricts expression of the paraneoplastic cerebellar degeneration antigen cdr2 to immune privileged tissues*. *J Neurosci*, 1997. **17**(4): p. 1406-15.
 115. Okano, H.J., et al., *The cytoplasmic Purkinje onconeural antigen cdr2 down-regulates c-Myc function: implications for neuronal and tumor cell survival*. *Genes Dev*, 1999. **13**(16): p. 2087-97.
 116. Raspotnig, M., et al., *Cerebellar degeneration-related proteins 2 and 2-like are present in ovarian cancer in patients with and without Yo antibodies*. *Cancer Immunol Immunother*, 2017. **66**(11): p. 1463-1471.
 117. Totland, C., et al., *CDR2 antigen and Yo antibodies*. *Cancer Immunol Immunother*, 2011. **60**(2): p. 283-9.

118. Greenlee, J.E., et al., *Antibody types and IgG subclasses in paraneoplastic neurological syndromes*. J Neurol Sci, 2001. **184**(2): p. 131-7.
119. Sakai, K., et al., *Induction of anti-Purkinje cell antibodies in vivo by immunizing with a recombinant 52-kDa paraneoplastic cerebellar degeneration-associated protein*. Journal of Neuroimmunology, 1995. **60**(1-2): p. 135-141.
120. Tanaka, M., et al., *Trial to establish an animal model of paraneoplastic cerebellar degeneration with anti-Yo antibody. 1. Mouse strains bearing different MHC molecules produce antibodies on immunization with recombinant Yo protein, but do not cause Purkinje cell loss*. Clin Neurol Neurosurg, 1995. **97**(1): p. 95-100.
121. Tanaka, K., et al., *Trial to establish an animal model of paraneoplastic cerebellar degeneration with anti-Yo antibody. 2. Passive transfer of murine mononuclear cells activated with recombinant Yo protein to paraneoplastic cerebellar degeneration lymphocytes in severe combined immunodeficiency mice*. Clin Neurol Neurosurg, 1995. **97**(1): p. 101-5.
122. Darnell, J.C., M.L. Albert, and R.B. Darnell, *Cdr2, a target antigen of naturally occurring human tumor immunity, is widely expressed in gynecological tumors*. Cancer Res, 2000. **60**(8): p. 2136-9.
123. Totland, C., et al., *Avidity of onconeural antibodies is of clinical relevance*. Cancer Immunol Immunother, 2013. **62**(8): p. 1393-6.
124. Small, M., et al., *Genetic alterations and tumor immune attack in Yo paraneoplastic cerebellar degeneration*. Acta Neuropathol, 2018. **135**(4): p. 569-579.
125. Sakai, K., et al., *Isolation of a complementary DNA clone encoding an autoantigen recognized by an anti-neuronal cell antibody from a patient with paraneoplastic cerebellar degeneration*. Ann Neurol, 1991. **30**(5): p. 738.
126. Herdlevær, I., et al., *Localization of CDR2L and CDR2 in paraneoplastic cerebellar degeneration*. Annals of Clinical and Translational Neurology, 2020.
127. O'Donovan, B., et al., *High-resolution epitope mapping of anti-Hu and anti-Yo autoimmunity by programmable phage display*. Brain Communications, 2020. **2**(2).
128. Greenlee, J.E., et al., *Purkinje cell death after uptake of anti-Yo antibodies in cerebellar slice cultures*. J Neuropathol Exp Neurol, 2010. **69**(10): p. 997-1007.
129. van Riggelen, J., A. Yetil, and D.W. Felsher, *MYC as a regulator of ribosome biogenesis and protein synthesis*. Nat Rev Cancer, 2010. **10**(4): p. 301-9.
130. Takanaga, H., et al., *PKN interacts with a paraneoplastic cerebellar degeneration-associated antigen, which is a potential transcription factor*. Exp Cell Res, 1998. **241**(2): p. 363-72.
131. Sakai, K., et al., *Interaction of a paraneoplastic cerebellar degeneration-associated neuronal protein with the nuclear helix-loop-helix leucine zipper protein MRG X*. Mol Cell Neurosci, 2002. **19**(4): p. 477-84.

-
132. Sakai, K., et al., *Effect of a paraneoplastic cerebellar degeneration-associated neural protein on B-myb promoter activity*. Neurobiol Dis, 2004. **15**(3): p. 529-33.
 133. Chan, C.C., et al., *eIF4A3 is a novel component of the exon junction complex*. Rna, 2004. **10**(2): p. 200-9.
 134. Singh, G., et al., *The cellular EJC interactome reveals higher-order mRNP structure and an EJC-SR protein nexus*. Cell, 2012. **151**(4): p. 750-764.
 135. Fischer, G., *Cultivation of mouse cerebellar cells in serum free, hormonally defined media: Survival of neurons*. Neuroscience Letters, 1982. **28**(3): p. 325-329.
 136. Weber, A. and M. Schachner, *Maintenance of immunocytologically identified Purkinje cells from mouse cerebellum in monolayer culture*. 1984. **311**(1): p. 119-130.
 137. Baptista, C.A., et al., *Cell-cell interactions influence survival and differentiation of purified purkinje cells in vitro*. 1994. **12**(2): p. 243-260.
 138. Tabata, T., et al., *A reliable method for culture of dissociated mouse cerebellar cells enriched for Purkinje neurons*. J Neurosci Methods, 2000. **104**(1): p. 45-53.
 139. Shabanipour, S., et al., *Primary Culture of Neurons Isolated from Embryonic Mouse Cerebellum*. J Vis Exp, 2019(152).
 140. Von Horsten, S., et al., *Transgenic rat model of Huntington's disease*. Human Molecular Genetics, 2003. **12**(6): p. 617-624.
 141. Gibbs RA, W.G., Metzker ML, Muzny DM, Sodergren EJ, Scherer S, Scott G, Steffen D, Worley KC, Burch PE, Okwuonu G, Hines S, Lewis L, DeRamo C, Delgado O, Dugan-Rocha S, Miner G, Morgan M, Hawes A, Gill R, Celera Holt RA, Adams MD, Amanatides PG, Baden-Tillson H, Barnstead M, Chin S, Evans CA, Ferriera S, Fosler C, et al, *Genome sequence of the Brown Norway rat yields insights into mammalian evolution*. Nature, 2004. **428**(6982): p. 493-521.
 142. Nuber, S., et al., *A progressive dopaminergic phenotype associated with neurotoxic conversion of α -synuclein in BAC-transgenic rats*. Brain, 2013. **136**(2): p. 412-432.
 143. Do Carmo, S. and A. Cuello, *Modeling Alzheimer's disease in transgenic rats*. Molecular Neurodegeneration, 2013. **8**(1): p. 37.
 144. Parker, C.C., et al., *Rats are the smart choice: Rationale for a renewed focus on rats in behavioral genetics*. Neuropharmacology, 2014. **76**: p. 250-258.
 145. Oakly, A.C., et al., *A genetic deletion of the serotonin transporter greatly enhances the reinforcing properties of MDMA in rats*. Molecular Psychiatry, 2014. **19**(5): p. 534-535.
 146. Vengeliene, V., A. Bilbao, and R. Spanagel, *The alcohol deprivation effect model for studying relapse behavior: A comparison between rats and mice*. Alcohol, 2014. **48**(3): p. 313-320.
 147. Ellenbroek, B. and J. Youn, *Rodent models in neuroscience research: is it a rat race?* Disease Models & Mechanisms, 2016. **9**(10): p. 1079-1087.
 148. Drummond, E. and T. Wisniewski, *Alzheimer's disease: experimental models and reality*. Acta Neuropathologica, 2017. **133**(2): p. 155-175.

149. Dawson, T.M., T.E. Golde, and C. Lagier-Tourenne, *Animal models of neurodegenerative diseases*. Nature Neuroscience, 2018. **21**(10): p. 1370-1379.
150. Jacob, H.J. and A.E. Kwitek, *Rat genetics: attaching physiology and pharmacology to the genome*. Nat Rev Genet, 2002. **3**(1): p. 33-42.
151. Meijer, M.K., et al., *Influence of environmental enrichment and handling on the acute stress response in individually housed mice*. Laboratory Animals, 2007. **41**(2): p. 161-173.
152. Furuya, S., A. Makino, and Y. Hirabayashi, *An improved method for culturing cerebellar Purkinje cells with differentiated dendrites under a mixed monolayer setting*. Brain Res Brain Res Protoc, 1998. **3**(2): p. 192-8.
153. Bilimoria, P.M. and A. Bonni, *Cultures of cerebellar granule neurons*. CSH Protoc, 2008. **2008**: p. pdb prot5107.
154. Kase, H., et al., *K-252 compounds, novel and potent inhibitors of protein kinase C and cyclic nucleotide-dependent protein kinases*. Biochem Biophys Res Commun, 1987. **142**(2): p. 436-40.
155. Santomaso, B.D., et al., *A T-cell receptor associated with naturally occurring human tumor immunity*. Proc Natl Acad Sci U S A, 2007. **104**(48): p. 19073-8.
156. Doutheil, J., et al., *Relation of neuronal endoplasmic reticulum calcium homeostasis to ribosomal aggregation and protein synthesis: implications for stress-induced suppression of protein synthesis*. Brain Res, 1997. **775**(1-2): p. 43-51.

9. APPENDIX

9.1 CDR2

9.1.1 CDR2 mRNA sequence

1 gccaaaagtgc cacgttgggc cggcggcggc cgtgaagact ggcggctgcg tgagactccg
61 gctccaggcg ttcgaccct aatgccggc cgttggggcc gtcggtaggc gcgagggcag
121 tcgaggcagc cggccggtcg gcggccgccg gcgggaacgg ggctgaggcg gcgcagcggg
181 gcttggggcg cggcgcgtcc cggccgaggc cggctctggc tgagggcgga gggggccggg
241 aagagcccgg ggcagcggct gaggcgggac ggcggcgggg gccgctgcc ctagaagacc
301 cagccgagat gctggcggaa aacctgtag aggagttag gatgaaggag gacgagccgt
361 ggtacgacca ccaggacctc cagcaagatc ttaacttgc tgctgagctt ggaagacat
421 tactggatcg gaacacagag ttggaggact ctgtcagca gatgtataca accaatcagg
481 agcagttaca gaaattgag tatctgacga agcaagtga acttctacgg cagatgaac
541 aacaacatgc aaagtttat gaacaattag acgtcacagc aagggaactg gaagaacaa
601 atcaaaagct agttgctgac agcaaggcct cacagcaaaa gattctgagc ctgactgaaa
661 cgattgaatg cctgcaaac aacattgac acctccagag ccaagtggag gagctgaagt
721 catctggcca agggagaagg agcccgggaa agtgtgacca ggagaaaccg gcaccagct
781 ttgcatgtct gaaggagctg tatgacctcc gccaacactt cgtgtatgat catgtgttcg
841 ctgagaagat cacttccttg caaggtcagc caagccctga tgaagaggaa aatgagcact
901 tgaaaaaac agtgacaatg ttgcaggccc agctgagcct ggagcggcag aagcgggtga
961 ctatggagga ggaatatggg ctctgttaa aggagaacag tgaactggag cagcagctgg
1021 gggccacagg tcctaccga gcacgggcgc tggaactaga ggccgaggtg gcagagatgc
1081 gacagatgtt gcagtcagag catccattg tgaatggagt tgagaagctg gtgccagact
1141 ctctgtatgt tctttcaaa gagcccagcc agagcctgct ggaagagatg ttctgactg
1201 tgccggaatc acatagaaag cctctcaagc gcagcagcag tgagacgac ctcagcagct
1261 tggcagggag tgacatcgtg aaggccacg aggagacctg catcaggagg gccaaaggct
1321 tgaacagag gggcatctcc ctctgcacg aagtggacac gcagtacagc gccctgaagg
1381 tgaagtatga agagttgctg aagaagtcc aagaggaaca ggactccctg tcacacaagg
1441 ctgtgcagac ctccagggct gcagccaagg acctgactgg agtgaacgcc cagtctgagc

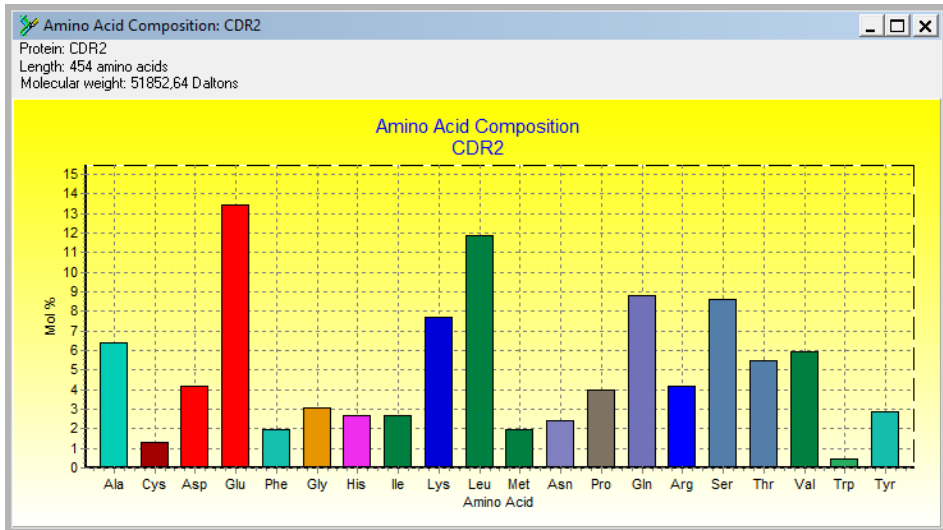
1501 ctgttgccag cggctgggaa ctggcctctg tcaaccaga gccctgagt tccctacaa
1561 cacctccaga atacaaagcg ttgttaagg agatcttag ttgcatcaag aaaactaagc
1621 aggaaataga tgaacagaga acaaaatacc gatcactctc ctctcattct taattgaacc
1681 tctagctcta ctactaattt gctattgcc tctgctctc ctctccatt cagacaagtg
1741 ttgtagact ctgaagccta atgttactca tgacgttgc ctctattgctt tgctattta
1801 gcaaatgcat acaacgagga aaggagggtgg ctagtggat cagtctctg atccactcc
1861 atttaagctc ccaggaat cccatgacaa actggcctct ggctggcgcg ctgattagac
1921 ttcagttctc gaaaaggacc agtggagggga agagctatac ttctggagaa gtaggcctgg
1981 agttactaca gtatggggga aaagggtcga gttagaacaa agctaaaggca attcctattg
2041 cttccttgcg caacttctca aaacgatgaa agtcagaagg ctgtcaaact caatatctt
2101 tgcaaacagt ttgaactgtg tgaattcatt acgaagaatg ttcgagagaa agcaggggtc
2161 taatccaaaa gaaatgcat taaccaatac tccaagtctc tgagtttgt tatactgaa
2221 ctagtgaac tgtgactgac aggtaatcct aatatacca aatccaactg aataccaaat
2281 tgagatggca aatftttgtt tgatataagt tagcttgta gcatatgcc tagaggcct
2341 ccatccctgt attctaagt tttactcaa agctctagcc ttaggatag gtgaatatgt
2401 aaatcttta tcaattctc aaattcaaac taaaggggaa agatcaaacc cctccctc
2461 ctacctgtt tctgagctgg ctgactgcc agccacaagc tgctcttga gagtctta
2521 cattcctgta aatgtttga ctgttgcag aaattcctat ctactttatt aagcagtatt
2581 gatctgactg tggaacatc ctctcacttg cattcttta acttaaaact atttaagaac
2641 tgatgttccg attattgtat atattttct aaaaaccaa taaagctacc tatgaaaatg
2701 aa (RefSeq: NM_001802.1)

9.1.2 CDR2 amino acid sequence

MLAENLVEEFEMKEDEPWYDHQDLQQDLQLAAELGKTLDRNTELEDSVQ
QMYTTNQEQLQEIEYLTKQVELLRQMNEQHAKVYEQLDVTARELEETNQKL
VADSKASQKILSLTETIECLQTNIDHLQSQVEELKSSGQGRSPGKCDQEKP
APSFACKELYDLRQHFVYDHFVFAEKITSLQGQPSPEEENEHLKKTVTMLQ
AQLSLERQKRVTMEEYGLVLKENSELEQLGATGAYRARALELEAEVAEM
RQMLQSEHPFVNGVEKLPDSLYVPFKEPSQSLLEEMFLTPESHKPLKRSS
SETILSSLAGSDIVKGHEETCIRRAKAVKQRGISLLHEVDTQYSALKVKEYEELL

KKCQEEQDSLHKAVQTSRAAAKDLTGVNAQSEPVASGWELASVNPEPVSS
PTTPPEYKALFKEIFSCIKKTKQEIDEQRTKYRSLSSHS (RefSeq: NP_001793.1)

9.1.3 CDR2 amino acid profile



9.2 CDR2L

9.2.1 CDR2L mRNA sequence

```

1 aagatgcagc ggcggctccg gttgtcggc ggcggggccag gacgagcggc gacccgagcc
61 gggcaggggg cgcccggcac ggcaccggcg cgtcctagc gcccagacc cgctgegg
121 cccgatcct cttgccaact gtcccaccg cgtccctgc cactccacc tttgtgtgc
181 cgcagcccg tgccccggc tctcggggac cccggccggg ccggaccctg gcaaagcgcc
241 aggccccgcg tgggtcccc gcgagcgggt gatggcgagg ggcgcggcg cgggctctgt
301 agcccagtt cccgacgtg gaggccccg ccgcctcagc cgattgtcc cgggccggc
361 gcaccggccc tgagtgcgc cgccgcagca cccggccgc gcccggggg ccatgcggag
421 agccggggg atggaggact tctccggga ggaagaggag tctgtgtac accagcagga
481 cctggagcag gacttgacc tagctcgga gctggggaag actctgtgg agaggaacaa
541 ggagctggag gggtcctgc agcagatga ctccacaaat gaggaacagg tgcaggagat
601 cgagtaccta accaagcagc tggacacgt gcggcacgtg aacgagcagc acgccaagt

```

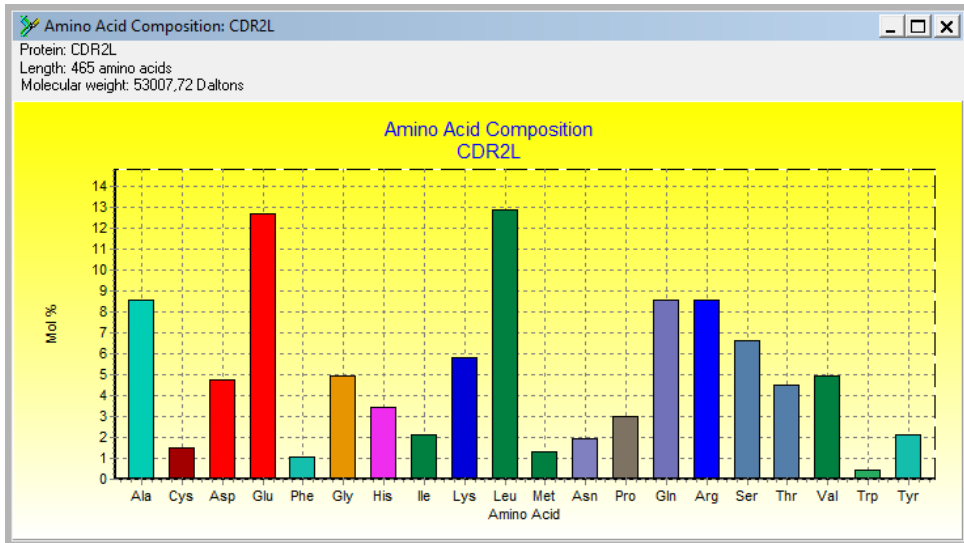
661 ctatgagcag ctggacctga cagccccgga cctggagctg accaaccaca ggctggtgct
721 ggagagtaag gctgccccagc agaagatcca tgggctgacg gagaccattg agcgcctcca
781 ggctcagggtg gaggagctgc aggccaggt ggagcaactg agaggcctgg aacagctgcg
841 agtctccgg gagaagcggg aacgcaggcg taccatccac acctcccct gcctcaagga
901 gctgtgcacc agccccggg gcaaggatgc ttccgcta cacagttct cctggagct
961 gggccccggg ccctgggagc aggagaacga gggctgcag acctgggagg gggcgtgcg
1021 ctcccagggtg agccaggagc ggcagcgcaa ggagcgggagc gagcgcgagt acaccgggtg
1081 gctgcaggag tactcgggagc tggagcgcca gctgtgcgag atggaggcct gtcgctgag
1141 tgtgcaggag ctggaggcgg agctgctgga gctgcagcag atgaagcagg ccaagaccta
1201 cctactgggt cggagcacc acctggcca ggcctgctc gaccctca cgcaggcccc
1261 tgaggccgac gatccccagc ccggccggg ggacgacttg ggcgcccagg acggggtctc
1321 ctcaccggca gcctctccag gccacgtgtg gcgcaagagc tgcagcgaca ctgcgtcaa
1381 cgccatctg gccaaagacc cagccagccg gcacgcgggc aacctcacac tgcagccaa
1441 cagcgtgcgc aagcggggca tgtccatct cggggagggtg gacgagcagt accacgcgt
1501 gctggagaag tacgaggagc tgctgagcaa gtgccggcag cacggggccg gagtgcggca
1561 cgccggcgtg cagacctgc gcccatctc ccgggacagc tcgtggaggg acctgcgagg
1621 gggtgaggag ggccagggtg aggtcaaggc aggagagaag agcctgagcc agcacgtgga
1681 ggccgtggac aagcggctgg aacagagcca gcccagtagc aaggcgctct tcaaagagat
1741 ctctccagg atccagaaga ccaaggctga catcaacgcc accaaagtca agacgcacag
1801 cagcaagtga ccctctccg gcctgcagcc tccccaggg tggaagcctg ggggtccctc
1861 aggcctgggc ggtgcagctt ccagagagcg agcgccttt agcggcctgc caccacagca
1921 cgcggcctcc tgatccgga gacgcagca tgtccctgc tgagcggagg cagcccact
1981 gtcctgcctc ccaggagccc ttggccact cgcgccagcc caaaggcgca gctctgagtt
2041 caaagcaaaa tgtcccact acccaggga tccccagct ccccagccc ctggcttct
2101 gacctgcgc ctcacctca gactggtgac caggcttctg aaagccattc tggatcagtt
2161 ggctttttt ttttttgg ttaagttgt ttttctaag agattgcaa tgcaaggtc
2221 cctgacccc ttgccacaac tgaaacct tgaaagggga cccagggcc agctgttca
2281 ggggttctc ggaccacca ctgcttcc ccaacctga tgcgtgaca ttcccttag
2341 accagctgc ccacctccag ggtcctgacc aggtcagaga tctcccctgc catgcagagc
2401 aggaagcctc agctgggctt ggagtgctcc tgctccagcc ctgccaggga caggttctc
2461 cctgatact ctggcccc cgcagatctg tagccagtca gaggaggagg agaaggagcc

2521 cctcagcaga gtggtgcagt ttcgctcaga gcttgtctcc ttggcttcca accccagaaa
 2581 tgcctgtctgg gccttaagct ttccaggggc cggggcagtg gggagcccc atccctcac
 2641 accgccacca actaaccaag ctggcctct gactcccgtc tctgtgcttg cccccatctc
 2701 agggaccatg atgtctcagt cactccacgc tccccacagg ccaaccctgg cacaggctat
 2761 gtctgcagcc cccagaatgt tctggacatg caccaccage cggtggtccc aatgtccacc
 2821 cctgcctccc ctctactggg gactgggggt ttgccccat gctgcatcgt gttgtattgg
 2881 gatgggctg aggaacatgc tccctccctc cctcccataa aatgctctct ctctactcc
 2941 cacctttgtg gggggctttt gaggaccag ctgcgtcagg agttttgctt caagatgta
 3001 gaaagtcaag ttcagctaag agacaccag gtccccagct tgcctgagc agccctcag
 3061 ggcttetggt tcctctgcc gccctctctg agacctaga aaccagaaga gccatacagt
 3121 cagtggaagg cgggggggcc ctggcctctg caccgggac ccagtgggaa cctctatgcc
 3181 ttatttattt ctaatgggta aaggggtttt ctaccaagc atccctgacc tcttgagac
 3241 accacctgct ttccggcgg cactgtgatg ggagctggtg gcgactgagt cctctgtac
 3301 gtcaactgg gaaactttg tcctttgagg ctaggcagct cctgccctc cgtgtgtgc
 3361 tgttatctgg gggagaggag tgtggaaggg ttgggggaag agctccagcc tgtctgctc
 3421 ccagctctgt agtggcagac cagcgtcacc ttgaagat acgtgagaga aatatatta
 3481 caaatgcttt atctctctt ttaataaaaa atgcaccagt attctaaaag caaaaaaaaa
 3541 aaaaa (RefSeq: NM_014603.2)

9.2.2 CDR2L amino acid sequence




MRRAAGMEDFSAAAAESWYDQQDLEQDLHLAAELGKTLERNKELEGLQQ
 MYSTNEEQVQEIEYLTKQLDTRLHVNEQHAKVYEQLDLTARDLELTNHRLV
 LESKAAQQKIHLTETIERLQAQVEELQAQVEQLRGLQLRVLREKRERRRTI
 HTFPCLKELCTSPRCKDAFRLHSSSLELGPRPLEQENERLQTLVGALRSQVSQ
 ERQRKERAEREYTAVLQEYSELERQLCEMEACRLRVQELEAELELQQMKQ
 AKTYLLGPDDHLAEALLAPLTQAPEADDPQPGRGDDLGAQDGVSSPAASPG
 HVVRKSCSDTALNAIVAKDPASRHAGNLTlhANSVRKRGMSILREVDEQYH
 ALLEKYEELLSKCRQHAGVVRHAGVQTSRPISRDSSWRDLRGGEEGQGEVK
 AGEKSLSQHVEAVDKRLEQSQPEYKALFKEIFSRIQKTKADINATKVKTHSSK
 (RefSeq: NP_055418.2)

9.2.3 CDR2L amino acid profile



10. ORIGINAL PUBLICATIONS

CDR2L Is the Major Yo Antibody Target in Paraneoplastic Cerebellar Degeneration

Torbjørn Kråkenes, MSc ¹
 Ida Herdlevær, MSc,^{1,2}
 Margrethe Raspotnig, MD,¹
 Mette Haugen, BSc,²
 Manja Schubert, ScD ² and
 Christian A. Vedeler, MD, PhD ^{1,2,3}

The pathogenesis of Yo-mediated paraneoplastic cerebellar degeneration (PCD) is unclear. We applied cerebrospinal fluid and serum from PCD patients as well as CDR2 and CDR2L antibodies to neuronal tissue, cancer cell lines, and cells transfected with recombinant CDR2 and CDR2L to elucidate which is the major antigen of Yo antibodies. We found that Yo antibodies bound endogenous CDR2L, but not endogenous CDR2. However, Yo antibodies can bind the recombinant CDR2 protein used in routine clinical testing for these antibodies. Because Yo antibodies only bind endogenous CDR2L, we conclude that CDR2L is the major antigen of Yo antibodies in PCD.

ANN NEUROL 2019;86:316–321

Paraneoplastic cerebellar degeneration (PCD) is one of the most common paraneoplastic neurological syndromes.¹ In PCD patients, the immune system targets a tumor antigen that is also expressed endogenously in the nervous system.² Among the most frequently detected onconeural antibodies in PCD patients are Yo antibodies.³ Yo reactivity with cerebellar degeneration-related (CDR) proteins present in Purkinje cells is associated with Purkinje cell death⁴ and severe cerebellar degeneration.⁵

Yo antibodies react with 2 proteins, CDR2 (RefSeq NP_001793.1) and CDR2-like (CDR2L; RefSeq NP_055418.2), that have 45% sequence identity.⁶ CDR2 has previously been considered as the main Yo antigen.^{6–9} This assumption is based in part on the finding that only the *CDR2* gene is expressed in tumors obtained from PCD patients.⁶ However, recent studies have demonstrated that both CDR2 and CDR2L are widely expressed in normal as well as in malignant tissues^{10,11} and that the CDR2L protein, but not CDR2, is highly expressed in PCD tumors.¹² Furthermore, CDR2L protein deposits are detected in germinal centers of all Yo-mediated PCD

tumors with tertiary lymphoid structures,¹² suggesting an ongoing local immune response against CDR2L. In line with this, we have shown that preabsorption with CDR2L abolishes Yo antibody staining of human Purkinje cells completely, whereas preabsorption with CDR2 does not.¹³

To determine which onconeural antigen is the major target of Yo antibodies, we studied the reactivity of Yo antibodies toward both native and recombinant CDR2 and CDR2L proteins. Our findings show that Yo antibodies react only to native CDR2L, and not to CDR2, suggesting that CDR2L is the major target of these antibodies in vivo.

Materials and Methods

Patient Samples

Five sex- and age-matched cerebrospinal fluid (CSF)/serum patient samples with Yo antibodies (PCD patients) and 5 without Yo antibodies (controls) were obtained from the Neurological Research Laboratory, Haukeland University Hospital (Regional Committees for Medical and Health Research Ethics (REK), #2013/1480).¹⁰

Cerebellar Tissue

Cerebellar sections were cut from fresh frozen normal human tissue (REK, #2013/1503) or paraformaldehyde (PFA)-perfused rat brains (The Norwegian regulation of the use of animals in research, #20157494) that required additional heat-induced epitope retrieval prior to immunostaining.¹⁴

Cell Cultures

The OvCar3 (American Type Culture Collection [ATCC], #HTB-161) and the HepG2 (ATCC, #HB-8065) cancer cell lines were maintained and subcultivated on poly-D-lysine-coated coverslips (Neuvitro, Vancouver, WA; #GG-18-1.5-pdl) according to the manufacturer's protocol. Cells were washed (2 × 0.1M phosphate-buffered saline [PBS]), fixed (15 minutes, 4% PFA-PBS; Thermo Fisher Scientific, Waltham, MA; #28908), and quenched (5 minutes, 50mM NH₄Cl; Sigma-Aldrich, St Louis, MO; #254134) prior to immunostaining.

From the ¹Department of Clinical Medicine, University of Bergen, Bergen, Norway; ²Department of Neurology, Haukeland University Hospital, Bergen, Norway; and ³Neuro-SysMed - Centre of Excellence for Experimental Therapy in Neurology, Departments of Neurology and Clinical Medicine, Bergen, Norway

Address correspondence to Kråkenes, Department of Clinical Medicine, Faculty of Medicine, University of Bergen, Jonas Lies vei 87, Bergen, 5021, Norway. E-mail: torbjornkrakenes@gmail.com

Received Nov 26, 2018, and in revised form May 9, 2019. Accepted for publication May 27, 2019.

View this article online at wileyonlinelibrary.com. DOI: 10.1002/ana.25511.

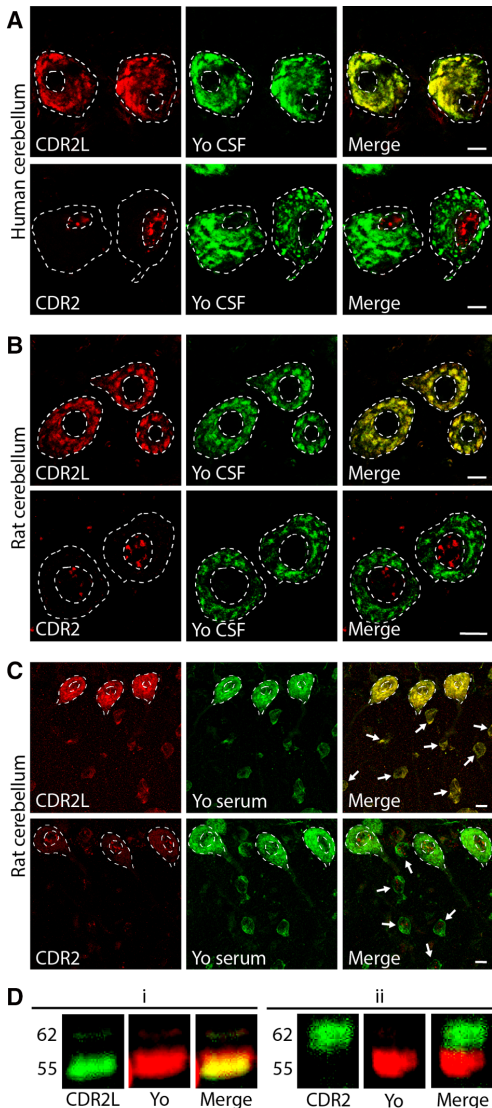


FIGURE 1: Yo antibodies bind to CDR2L, but not CDR2, in cerebellar Purkinje cells. Scale bars = 10µm. (A) Sections of fresh frozen human cerebellum. Upper row: Section stained with Yo (cerebrospinal fluid [CSF]; green) and anti-CDR2L (red); the antibodies colocalize in the cytoplasm (seen as yellow in the merge image). Lower row: Section stained with Yo (CSF; green) and anti-CDR2 (red); no colocalization is seen between Yo and CDR2. (B) Sections of paraformaldehyde (PFA)-perfused rat cerebellum. Upper row: Section stained with Yo (CSF; green) and anti-CDR2L (red); CDR2L colocalize with Yo. Lower row: Section stained with Yo (CSF; green) anti-CDR2 (red); no colocalization is seen. (C) Sections of PFA-perfused rat cerebellum. Upper row: Section stained with Yo (serum; green) and anti-CDR2L (red); Yo and CDR2L colocalize in the Purkinje cells (outlined) as well as in the stellate and basket cells (arrows). Lower

Immunocytochemistry

Cancer cells and cerebellar sections were permeabilized (5 minutes, 0.5% Triton X-100-PBS; Sigma-Aldrich, #11332481001), washed (3×15 minutes, 0.5% gelatin-PBS; Sigma-Aldrich, #G7041), blocked (30 minutes, 10% SEABLOCK; Thermo Fisher, #37527), incubated with primary antibodies (overnight, 4°C), washed, incubated with secondary antibodies (2 hours, room temperature), and mounted (ProLong Diamond with DAPI; Thermo Fisher Scientific, #P36962). Antibodies consisted of rabbit anti-CDR2 (AA270-392; Sigma-Aldrich, #HPA018151; cerebellar sections and HepG2 cells), mouse anti-CDR2 (full-length; LSBio, Seattle, WA; #C181958; OvCar3 cells), rabbit anti-CDR2L (AA116-465; Protein Technology, Wuhan, Hubei, P.R.C #14563-1-AP), antihuman Alexa Fluor 488/594 (Thermo Fisher Scientific, #A-11013/#A-11014), antirabbit Alexa Fluor 488/594 (Thermo Fisher Scientific, #R37116/#R37117), antirabbit STAR635P (Sigma-Aldrich, #53399-500UG), and antimouse Alexa Fluor 488/594 (Thermo Fisher Scientific, #R37120/#R37121). A Leica (Wetzlar, Germany) SP8 STED 3X confocal microscope equipped with a $\times 100$ 1.4 numerical aperture oil objective was used for imaging.

Immunoprecipitation

Following the Bio-Rad SureBeads immunoprecipitation protocol, the proteins were immunoprecipitated from OvCar3 cell lysate by using Protein G Magnetic Beads (Bio-Rad Laboratories, Hercules, CA; #161-4023). Immunoprecipitated proteins were separated on a 10% TGX gel (Bio-Rad, #456-1035) and transferred to a polyvinylidene difluoride (PVDF) membrane using the Trans-Blot Turbo Transfer kit (Bio-Rad, #170-4274). Western blot analysis was performed to detect the immunoprecipitated target proteins. Antibodies consisted of rabbit anti-CDR2L, mouse anti-CDR2, Yo-CSF, TidyBlot (Bio-Rad, #STAR209PA), and horseradish peroxidase antimouse IgG (Dako, Carpinteria, CA; #P0260).

Fluorescent Immunoblotting

The cerebellar and cancer cell lysates were obtained using a Total Protein Extraction Kit (Millipore, Billerica, MA; #2140). Proteins were separated on a 10% TGX gel and transferred to a low-autofluorescence PVDF membrane. Antibodies consisted of rabbit anti-CDR2L, rabbit anti-CDR2, Yo-CSF, antirabbit Alexa Fluor 488, and antihuman Alexa Fluor 647 (Thermo Fisher Scientific, #A-21445). G:Box (Syngene, Frederick, MA) was employed for visualization.

Recombinant DNA and Transfection

Full-length CDR2 (OriGene Technologies, Rockville, MD; #RG204900) and CDR2L (OriGene Technologies, #RC206909) were ligated into a pCMV6-AC-GFP vector (OriGene Technologies,

row: Section stained with Yo (serum; green) and anti-CDR2 (red); no colocalization is seen between Yo and CDR2. These images are a z-stack merge, as not all stellate/basket cells were in the same focal plane as the Purkinje cells; thus, the cytoplasmic staining found over or under the nuclei may appear nuclear although it is not (eg, the Yo serum staining is not nuclear). (D) Fluorescent immunoblot of rat cerebellar lysate. Anti-CDR2L and Yo (CSF) stain the same band at 55kDa; anti-CDR2 does not. Secondary antibody controls were negative.

#PS100010). Following polymerase chain reaction, correct CDR2 and CDR2L vector sequences were confirmed using BioEdit v7.2.5. One Shot TOP10 *Escherichia coli* (Life Technologies, Carlsbad, CA; #C4040-10) were used for amplification, E.Z.N.A. Plasmid DNA Kit (Omega Bio-Tek, Norcross, GA, #D6942) for purification, and Lipofectamine 3000 (Thermo Fisher Scientific, #L3000008) for transfection.

Results

CDR2L and Yo Staining Overlap

In sections of human and rat cerebellum, CDR2L showed a cytoplasmic staining pattern in Purkinje cell somas that overlapped completely with the Yo antibody staining from both CSF and serum (Fig 1). CDR2L and Yo also colocalized in the stellate and basket cells. In contrast, CDR2 primarily

stained the nuclei of these neurons and gave no overlap with the Yo antibodies. Under denaturing conditions, immunofluorescence blots of rat cerebellar lysate showed that CDR2L and Yo were recognized at 55kDa, whereas CDR2 was only visible at 62kDa.

CDR2L and Yo Colocalize in Ovarian Cancer Cells

In OvCar3 cells, which express both CDR2 and CDR2L endogenously, we found that CDR2L and Yo colocalized in the cytoplasm, whereas CDR2 showed no colocalization with Yo (Fig 2A). The coreactivity of the CDR2L and Yo

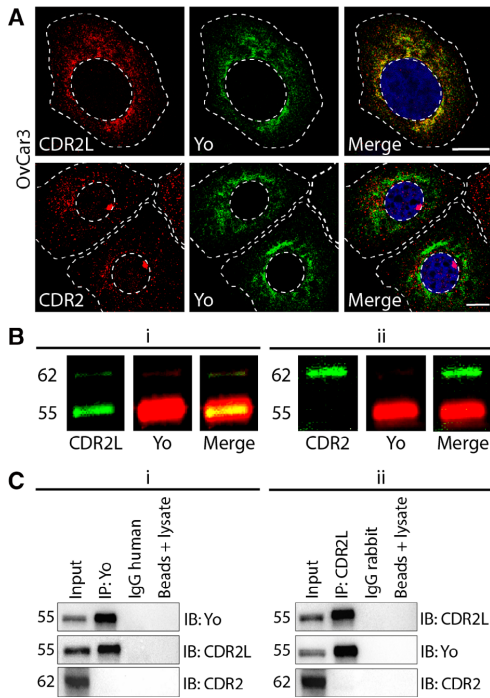


FIGURE 2: Yo antibodies bind to CDR2L, but not CDR2, in OvCar3 cells. Scale bars = 10µm. (A) Upper row: OvCar3 cells stained with Yo (cerebrospinal fluid [CSF]; green) and anti-CDR2L (red); Yo and CDR2L colocalize, giving the same granular, cytoplasmic staining pattern (seen as yellow in the merge image). Lower row: OvCar3 cells stained with Yo (CSF; green) and anti-CDR2 (red); Yo does not colocalize with CDR2. (B) Fluorescent immunoblot (IB) of OvCar3 lysate. Anti-CDR2L and Yo (CSF) stain the same 55kDa band; anti-CDR2 does not. Secondary antibody controls were negative. (C) Immunoblot of proteins immunoprecipitated (IP) from the OvCar3 lysate by Yo (CSF) or CDR2L. The protein precipitated by Yo antibodies was recognized by the CDR2L antibody on Western blot (i) and vice versa (ii); no relationship was observed between Yo or CDR2L and CDR2.

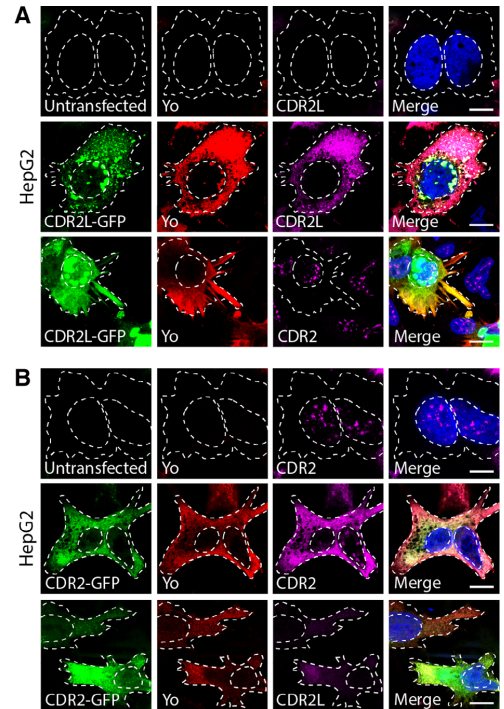


FIGURE 3: HepG2 cells, with a high endogenous level of CDR2, are not stained by Yo antibodies. However, Yo antibodies are able to bind recombinant CDR2. Scale bars = 10µm. (A) Untransfected HepG2 cells (first row) and HepG2 cells transfected with a vector expressing recombinant CDR2L-GFP (second and third row; green) were incubated with Yo (cerebrospinal fluid [CSF]; red), anti-CDR2L (first and second row; magenta), and anti-CDR2 (third row; magenta). Nuclei were stained with DAPI. Only upon expression of recombinant CDR2L was Yo and CDR2L antibody staining observed. The CDR2 antibody did not bind the recombinant CDR2L protein. (B) Untransfected HepG2 cells (first row) and HepG2 cells transfected with a vector expressing CDR2-GFP (second and third row; green) were incubated with Yo (CSF; red), anti-CDR2 (first and second row; magenta), and anti-CDR2L (third row; magenta). Native CDR2 is present in untransfected HepG2 cells, but no Yo staining was found. When recombinant CDR2-GFP was present, both the Yo and CDR2L antibody were able to bind.

antibodies was confirmed by both fluorescent Western blotting and immunoprecipitation (see Fig 2B, C).

Yo Antibodies Detect Recombinant CDR2 and CDR2L

Yo and CDR2L staining was absent in untransfected HepG2 cells, whereas CDR2 was present in the nuclei of these cells (Fig 3). In HepG2 cells transfected with recombinant CDR2

or CDR2L linked to green fluorescent protein (CDR2-GFP and CDR2L-GFP), however, Yo antibodies colocalized with both CDR2L-GFP and CDR2-GFP. Similar results were obtained for all PCD samples tested.

Discussion

We demonstrate that Yo antibodies in the CSF and serum of PCD patients consistently react with CDR2L in human

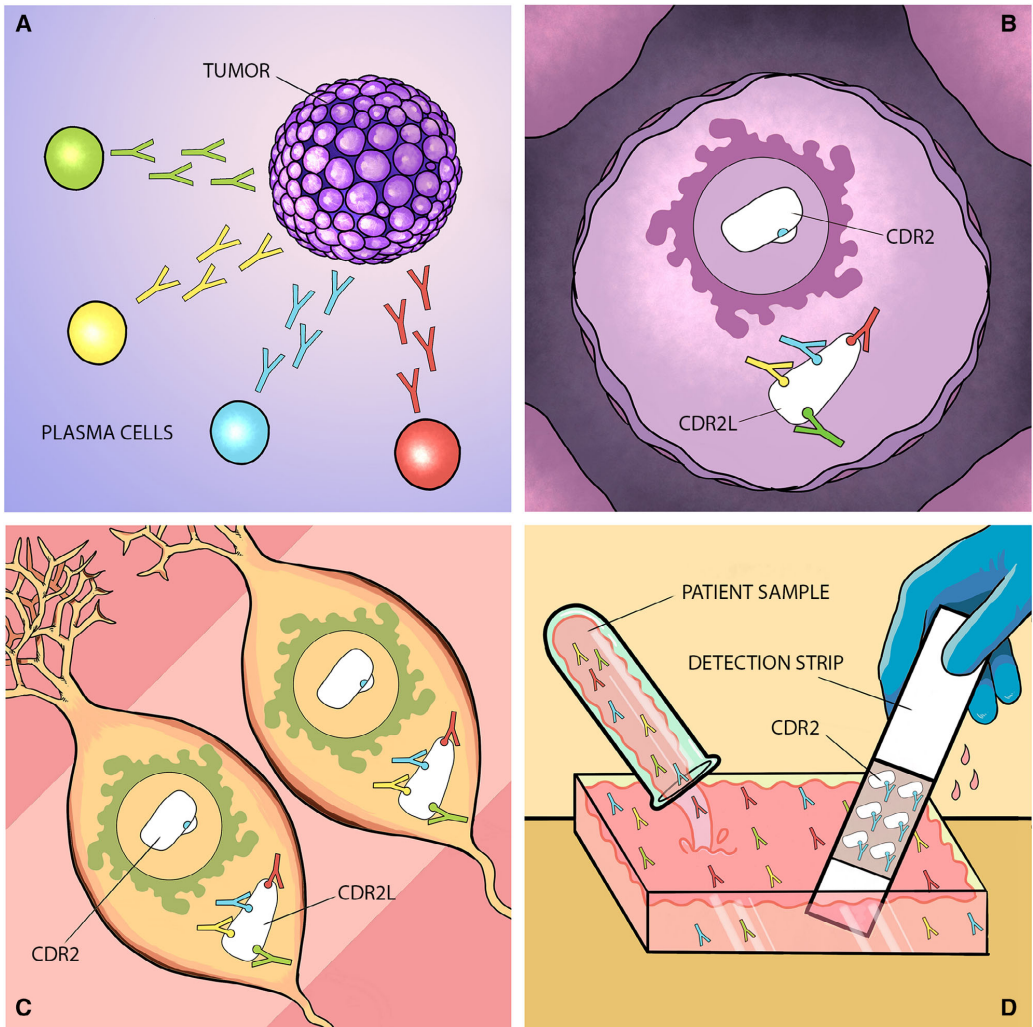


FIGURE 4: Proposed hypothesis of how Yo antibodies are able to bind both recombinant CDR2 and CDR2L, but only CDR2L under native conditions. (A) Illustration of the initial, polyclonal response of Yo antibodies toward CDR2L in the tumors of paraneoplastic cerebellar degeneration patients. (B) A tumor cell with the polyclonal Yo antibodies targeting the CDR2L protein; CDR2 is unaffected, as the epitope that is common to CDR2L (blue) is hidden by post-translational modifications or a partnering molecule (white fold covering the blue epitope). (C) The Yo antibodies also bind to CDR2L in cerebellar Purkinje cells; however, they do not bind CDR2, as the common epitope (blue) is hidden here as well (by modifications or partnering molecules; white fold). (D) When patient sera or cerebrospinal fluid is applied to a line blot with recombinant CDR2 attached, binding of the common epitope (blue) is possible, as it is not hidden by post-translational modifications or partnering molecules in the recombinant version.

and rat brain tissue as well as in cultured cancer cells. Despite sequence homology between CDR2 and CDR2L, Yo antibodies did not cross-react with endogenously expressed CDR2. These findings were confirmed by using HepG2 cells that express CDR2 endogenously, but not CDR2L; Yo antibodies were not able to bind the endogenous CDR2 in these cells either. We therefore conclude that CDR2L is the major antigen of Yo antibodies under native conditions. This result indicates that previous research on Yo-mediated PCD has focused on a protein that is not the major antigenic target of Yo antibodies.

CDR2L and Yo antibodies gave a granular, cytoplasmic staining pattern that colocalized in both human and rat Purkinje cells, as well as in stellate and basket cells. In contrast, CDR2 reactivity primarily occurred in the nuclei of these neuronal cells, where Yo antibody staining was absent. In the human cancer cell lines OvCar3 and HepG2, we found strong staining of CDR2 in the nuclei, as well as some cytoplasmic staining. Similar CDR2 staining has also been found in other cancer cell lines and tissues.¹⁵

We found that none of our PCD patient samples cross-reacted with endogenous CDR2. Thus, CDR2L-exclusive epitopes appear to be the major targets of Yo antibodies under native conditions. Furthermore, we observed competitive binding between the CDR2L and the Yo antibodies, whereas the CDR2 antibody staining was not affected by high Yo antibody concentrations (data not shown). This is in line with our previous results showing that the reactivity of Yo antibodies in the Purkinje cells disappears completely when preabsorbed with recombinant CDR2L protein, but only partially with recombinant CDR2.¹³

In routine clinical testing for onconeural antibodies, line blots and cell-based assays use recombinant CDR2 as the antigen target for Yo antibodies (Euroimmun, www.euroimmun.com; ravo Diagnostika, www.ravo.de). Because we did not find any reactivity of Yo antibodies toward native CDR2, we investigated this further by transfecting HepG2 cells with CDR2 and CDR2L linked to green fluorescent protein. Our results showed that Yo antibodies did bind recombinant CDR2, meaning that the protein can still be used for clinical diagnostic purposes. However, line blot and cell-based assays using CDR2L may be more sensitive for detecting Yo antibodies.

Whereas Yo antibodies are able to bind recombinant CDR2, they appear unable to access this epitope on endogenous CDR2, likely because it is hidden by post-translational modifications or by partnering molecules (Fig 4). A recent study did not find any common linear epitopes detected by Yo antibodies for CDR2 and CDR2L.¹⁶ This suggests that any common epitope is likely conformational, a feature that can be elucidated once the 3-dimensional structures of these proteins are established.

Our present results strengthen the hypothesis that CDR2L is the major target of Yo antibodies. This is in line with the recent findings that CDR2L expression was detected in all samples of ovarian cancers from PCD patients, whereas CDR2 was only weakly expressed in 40% of the tumors.¹² Furthermore, CDR2L deposits were found in germinal centers of all Yo-mediated PCD tumors with tertiary lymphoid structures, suggesting a humoral immune response against CDR2L.¹² Thus, Yo antibodies targeting CDR2L in tumor cells, with binding of CDR2L in Purkinje cells as an unfortunate side effect, likely contributes to the development of PCD. CDR2L should therefore be included in future research into the pathogenesis of Yo-mediated PCD.

Acknowledgment

This work was supported by grants from Helse Vest, the Torbjørng Hauges Legacy, and the University of Bergen (PhD stipend #2016/7580-RAKA). The confocal imaging was performed at the Molecular Imaging Center and was thus supported by the Department of Biomedicine and the Faculty of Medicine at the University of Bergen and its partners.

We thank Dr L. Bindoff for valuable discussion of our paper.

Author Contributions

T.K., M.S., and C.A.V. contributed to the conception and design of the study; T.K., I.H., M.R., and M.H. contributed to the acquisition and analysis of data; T.K., M.S., and C.A.V. contributed to drafting the text and preparing figures.

Potential Conflicts of Interest

Nothing to report.

References

1. Rees JH. Paraneoplastic syndromes: when to suspect, how to confirm, and how to manage. *J Neurol Neurosurg Psychiatry* 2004;75(suppl 2):ii43–ii50.
2. Darnell RB, Posner JB. Paraneoplastic syndromes involving the nervous system. *N Engl J Med* 2003;349:1543–1554.
3. Storstein A, Monstad SE, Haugen M, et al. Onconeural antibodies: improved detection and clinical correlations. *J Neuroimmunol* 2011; 232:166–170.
4. Storstein A, Krossnes BK, Vedeler CA. Morphological and immunohistochemical characterization of paraneoplastic cerebellar degeneration associated with Yo antibodies. *Acta Neurol Scand* 2009; 120:64–67.
5. Greenlee JE, Brashear HR. Antibodies to cerebellar Purkinje cells in patients with paraneoplastic cerebellar degeneration and ovarian carcinoma. *Ann Neurol* 1983;14:609–613.
6. Corradi JP, Yang C, Darnell JC, et al. A post-transcriptional regulatory mechanism restricts expression of the paraneoplastic cerebellar degeneration antigen cdr2 to immune privileged tissues. *J Neurosci* 1997;17:1406–1415.

7. Darnell JC, Albert ML, Darnell RB. Cdr2, a target antigen of naturally occurring human tumor immunity, is widely expressed in gynecological tumors. *Cancer Res* 2000;60:2136–2139.
8. Okano HJ, Park WY, Corradi JP, Darnell RB. The cytoplasmic Purkinje onconeural antigen cdr2 down-regulates c-Myc function: implications for neuronal and tumor cell survival. *Genes Dev* 1999;13:2087–2097.
9. Albert ML, Darnell JC, Bender A, et al. Tumor-specific killer cells in paraneoplastic cerebellar degeneration. *Nat Med* 1998;4:1321–1324.
10. Raspotnig M, Haugen M, Thorsteinsdottir M, et al. Cerebellar degeneration-related proteins 2 and 2-like are present in ovarian cancer in patients with and without Yo antibodies. *Cancer Immunol Immunother* 2017;66:1463–1471.
11. Totland C, Ying M, Haugen M, et al. Avidity of onconeural antibodies is of clinical relevance. *Cancer Immunol Immunother* 2013;62:1393–1396.
12. Small M, Treilleux I, Couillault C, et al. Genetic alterations and tumor immune attack in Yo paraneoplastic cerebellar degeneration. *Acta Neuropathol* 2018;135:569–579.
13. Eichler TW, Totland C, Haugen M, et al. CDR2L antibodies: a new player in paraneoplastic cerebellar degeneration. *PLoS One* 2013;8:e66002.
14. Schubert M, Panja D, Haugen M, et al. Paraneoplastic CDR2 and CDR2L antibodies affect Purkinje cell calcium homeostasis. *Acta Neuropathol* 2014;128:835–852.
15. Totland C, Aarskog NK, Eichler TW, et al. CDR2 antigen and Yo antibodies. *Cancer Immunol Immunother* 2011;60:283–289.
16. O'Donovan BD, Mandel-Brehm C, Vazquez SE, et al. Exploration of anti-Yo and anti-Hu paraneoplastic neurological disorders by PhIP-Seq reveals a highly restricted pattern of antibody epitopes. *bioRxiv* 2018;502187.

RESEARCH ARTICLE

Localization of CDR2L and CDR2 in paraneoplastic cerebellar degeneration

Ida Herdlevær^{1,2,a} , Torbjørn Kråkenes^{1,a} , Manja Schubert²  & Christian A. Vedeler^{1,2,3} ¹Department of Clinical Medicine, University of Bergen, Bergen, Norway²Department of Neurology, Haukeland University Hospital, Bergen, Norway³Departments of Neurology and Clinical Medicine, Neuro-SysMed - Centre of Excellence for Experimental Therapy in Neurology, Bergen, Norway

Correspondence

Ida Herdlevær, Department of Neurology, Haukeland University Hospital, Jonas Lies vei 65, 5021 Bergen, Norway. Tel: +47 48 05 68 97; Fax: +47 55 97 51 64; E-mail: idaherd@gmail.com

Torbjørn Kråkenes, Department of Clinical Medicine, Faculty of Medicine, University of Bergen, Jonas Lies vei 87, 5021 Bergen, Norway. Tel: +47 99 26 79 85; Fax: +47 55 97 51 64; E-mail: torbjornkrakenes@gmail.com

Funding Information

This work was supported by grants from Helse Vest, the University of Bergen, and Torbjørn Hauges Legacy. The confocal imaging was performed at the Molecular Imaging Center and was supported by the Department of Biomedicine and the Faculty of Medicine, University of Bergen, and its partners.

Received: 26 June 2020; Revised: 7 August 2020; Accepted: 11 September 2020

Annals of Clinical and Translational Neurology 2020; 7(11): 2231–2242

doi: 10.1002/acn3.51212

^aThese authors contributed equally to this work.

Introduction

Paraneoplastic neurological syndromes are rare autoimmune-mediated diseases^{1,2} characterized by the production of antibodies that target antigens expressed both by the tumor and endogenously in the central nervous system.^{3,4} One of the most common forms of paraneoplastic neurological syndromes is paraneoplastic cerebellar degeneration (PCD).⁵ In patients with PCD and breast or ovarian cancer,

Abstract

Objective: Identify the subcellular location and potential binding partners of two cerebellar degeneration-related proteins, CDR2L and CDR2, associated with anti-Yo-mediated paraneoplastic cerebellar degeneration. **Methods:** Cancer cells, rat Purkinje neuron cultures, and human cerebellar sections were exposed to cerebrospinal fluid and serum from patients with paraneoplastic cerebellar degeneration with Yo antibodies and with several antibodies against CDR2L and CDR2. We used mass spectrometry-based proteomics, super-resolution microscopy, proximity ligation assay, and co-immunoprecipitation to verify the antibodies and to identify potential binding partners. **Results:** We confirmed the CDR2L specificity of Yo antibodies by mass spectrometry-based proteomics and found that CDR2L localized to the cytoplasm and CDR2 to the nucleus. CDR2L co-localized with the 40S ribosomal protein S6, while CDR2 co-localized with the nuclear speckle proteins SON, eukaryotic initiation factor 4A-III, and serine/arginine-rich splicing factor 2. **Interpretation:** We showed that Yo antibodies specifically bind to CDR2L in Purkinje neurons of PCD patients where they potentially interfere with the function of the ribosomal machinery resulting in disrupted mRNA translation and/or protein synthesis. Our findings demonstrating that CDR2L interacts with ribosomal proteins and CDR2 with nuclear speckle proteins is an important step toward understanding PCD pathogenesis.

the dominant onconeural antibody, anti-Yo, is detected in both serum and cerebrospinal fluid (CSF).⁶ Anti-Yo antibodies are directed against two proteins, cerebellar degeneration-related protein 2 (CDR2) and CDR2-like (CDR2L), which are endogenously expressed in Purkinje neurons of the cerebellum.⁷ The interaction between anti-Yo and CDR proteins is thought to mediate Purkinje neuron dysfunction and death.⁵ A two-step process has been proposed, with the internalization of Yo antibodies as the primary event,

followed by the subsequent activation of cytotoxic T cells.^{8,9} However, it has also been demonstrated that Yo antibodies can induce Purkinje neuron death in the absence of T lymphocytes.^{8,10}

Previously we showed that CDR2L is the major Yo antibody target in PCD.⁷ However, we cannot exclude a functional role for CDR2 in anti-Yo-mediated PCD pathogenesis. These proteins display a high degree of homology with approximately 45% sequence identity,^{11,12} and both are widely expressed in normal as well as malignant tissues.^{3,13} Ovarian malignancy is the most frequent cancer type found in Yo-mediated PCD, and both CDR2L and CDR2 are highly expressed in this type of cancer.^{3,14}

Earlier studies have suggested that CDR2L and CDR2 are cytoplasmic proteins.^{3,13} However, detailed subcellular localization using antigen-specific antibodies has not been performed. Current knowledge concerning the biologic function of CDR2L is limited. CDR2 has leucine zipper and zinc-finger DNA binding domains, characteristic of transcriptional regulatory proteins^{11,15,16} and occurrence of these domains in the predicted open reading frame suggests that CDR2 has a role in regulating gene expression.^{11,17} CDR2 interacts with the serine/threonine protein kinase PKN and cell cycle-related proteins MRG15 and MRGX; all involved in signal transduction or gene transcription.^{15,18,19}

In this study, we examined the subcellular locations of CDR2L and CDR2 and their protein-protein interactions. Our findings suggest that CDR2L and CDR2 have different roles: CDR2L interacts with cytosolic ribosomes and appears to function in protein synthesis, while CDR2 associates with nuclear speckle proteins and appears to be involved in mRNA maturation.

Materials and Methods

Patient samples

Five sex- and age-matched CSF samples from patients with Yo antibodies (PCD patients) and five without Yo antibodies and no neurological disease or underlying cancer (negative controls) were obtained from the Neurological Research Laboratory, Haukeland University Hospital (Regional Committees for Medical and Health Research Ethics, 2013/1480).

Cell culture

OvCar3 (American Type Culture Collection (ATCC), #HTB-161) and HepG2 (ATCC, #HB-8065) cancer cell lines were maintained and subcultivated on poly-D-lysine-coated coverslips (Neuvitro, #GG-18-1.5-pdl) according to the manufacturer's protocol. Cells were washed twice with 0.1 M phosphate-buffered saline (PBS), fixed (15 min, 4%

paraformaldehyde in PBS, Thermo Fisher Scientific, #28908), and quenched (5 min, 50 mmol/L NH₄Cl, Sigma-Aldrich, #254134) prior to immunostaining.

Cerebellar tissue preparation

Cerebellar sections were cut from fresh frozen normal human tissue (REK, #2013/1503). Heat-induced epitope retrieval was performed prior to immunostaining.

Rat Purkinje neuron cultures

All procedures were performed according to the National Institutes of Health Guidelines for the Care and Use of Laboratory Animals Norway (FOTS 20135149/20157494/20170001). Embryonic day 18 Wistar Hannover GLAST rat pups were used for neuronal culture preparation. The protocol has recently been described.²⁰

Immunochemistry

Fixed OvCar3 cells and cerebellar sections were permeabilized in 0.5% Triton X-100-PBS (Sigma-Aldrich, #11332481001) for 5 min, washed in 0.5% gelatin-PBS (Sigma-Aldrich, #G7041) three times with 15 min each wash, blocked in 10% SEABLOCK (Thermo Fisher Scientific, #37527) in PBS for 30 min, and incubated with primary antibodies overnight at 4 °C. Following incubations, cells and sections were washed in gelatin-PBS, incubated with secondary antibodies for 2 h at room temperature, and mounted using ProLong Diamond with DAPI (Thermo Fisher Scientific, #P36962). The following antibodies were used: rabbit anti-CDR2 (Sigma-Aldrich, #HPA018151), rabbit anti-CDR2L (Protein Technology, #14563-1-AP), mouse anti-rpS6 (Cell Signaling, #2317/Santa Cruz #sc-74459), mouse anti-SON (Santa Cruz, #sc398508), mouse anti-eIF4A3 (Santa Cruz, #sc-365549), mouse anti-SRSF2 (Abcam, #ab11826), Alexa Fluor 488/594-labeled goat anti-human (Thermo Fisher Scientific, #A-11013/#A11014), Alexa Fluor 488/594-labeled goat anti-rabbit (Thermo Fisher Scientific, #R37116/#R37117), rabbit anti-STAR635P (Sigma-Aldrich, #53399-500UG), and Alexa Fluor 488/594-labeled goat anti-mouse (Thermo Fisher Scientific, #R37120/#R37121).

Super-resolution microscopy

A Leica TCS SP8 Stimulated Emission Depletion (STED) 3X confocal microscope equipped with a 100x oil objective with a numerical aperture of 1.4 was used for imaging. The output of the excitation laser (up to 1.5 mW per line; pulsed) was kept between 1% and 20% and the STED laser (775 nm; up to 1.5 W) between 20% and 30%. Gating (between 1 and

6 ns) was applied for all channels as well as a minimum of three intensity averages. The lateral resolution was consistently measured to be between 40 and 50 nm.

Immunoprecipitation

OvCar3 and HepG2 cells were lysed in RIPA lysis buffer (Bioscience #786-490) containing protease inhibitor cocktail (Sigma-Aldrich #11873580001), 1 mmol/L phenylmethylsulfonyl fluoride (PMSF, Sigma-Aldrich #P7626), 1 mmol/L sodium fluoride (NaF, Sigma-Aldrich #S6776), and 1 mmol/L sodium orthovanadate (Na_3VO_4 , Sigma-Aldrich #450243). The lysate was centrifuged (22,000g, 4°C, 15 min) and the supernatant was collected.

Following the Bio-Rad SureBeads immunoprecipitation protocol, the proteins were immunoprecipitated from OvCar3 and HepG2 cell lysates using Protein G Magnetic Beads (Dynabeads, Thermo Fischer Scientific, #1004D). Immunoprecipitated proteins were separated on a 10% TGX gel (Bio-Rad, #456-1035) and transferred to a polyvinylidene difluoride (PVDF) membrane using the Trans-Blot Turbo Transfer kit (Bio-Rad, #170-4274). Western blot analysis was performed to detect proteins of interest using the following primary antibodies: rabbit anti-CDR2L (Proteintech, #14563-1-AP), mouse anti-rpS6 (Santa Cruz #sc-74459), rabbit anti-CDR2 (Sigma-Aldrich, #018151), mouse anti-CDR2 (Santa Cruz, #sc100320) mouse anti-SON, mouse and rabbit anti-eIF4A3 (Abcam, #ab32485). The secondary antibodies used were TidyBlot (Bio-Rad, #STAR209PA) and horseradish peroxidase anti-mouse IgG and anti-rabbit IgG (Dako, #P0260 and #P0217). A negative control consisting of beads and cancer cell lysate was also included.

Proximity ligation assay

The proximity ligation assay was performed using the commercially available Duolink kit from Sigma-Aldrich

(#DUO92101). Fixed OvCar3 cells were permeabilized for 5 min using 0.5% Triton X-100 diluted in PBS and blocked with 10% SEABLOCK in PBS. Primary antibodies against Hsp60 (EnCor Biotechnology, #CPCA-HSP60), CDR2 (Sigma-Aldrich, #018151), CDR2L (Proteintech, #14563-1-AP), SON, and SRSF2 were applied for 1 h (1:100 in blocking solution), followed by 3x 5-minute washes with Wash Buffer A supplied with the kit. Probes (+ and -) were diluted in blocking solution (1:5) and added to the cells for 1 h (37 °C). The cells were washed 3x for 5 min each with Wash Buffer A and incubated with ligation buffer (1:5) and ligase enzyme (1:40) for 30 min (37°C). After 2x 5-minute washes with Wash Buffer A amplification buffer (1:5) and the polymerase enzyme (1:80) were diluted in distilled water and applied to the cells for 100 min (37 °C, in the dark), followed by three 10-minute washes with Wash Buffer B (supplied with the kit). Prolong Diamond with DAPI was used to mount the coverslips (overnight, 4 °C). Mounted cells were stored at -20 °C.

Mass spectrometry-based proteomics analysis

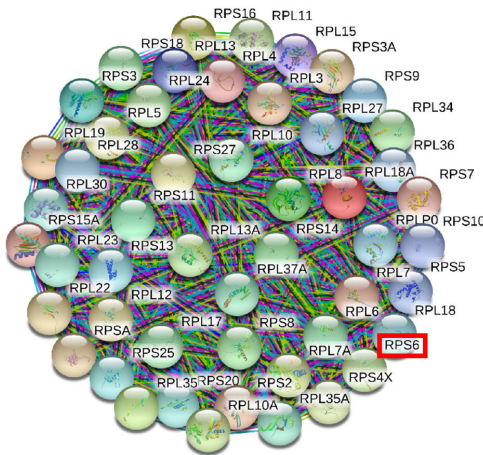
Proteins of interest were immunoprecipitated from HepG2 or OvCar3 cell lysates using the antibodies listed in Table 1. A negative control consisting of beads and cancer cell lysate was also included. The samples were loaded on a 10% TGX gel and run approximately 1 cm into the resolving gel. Each lane was cut into cubes of approximately 1 mm² and hydrated in Milli-Q water (20 min, room temperature). Detergents (i.e. sodium dodecyl sulfate) and salts were removed by washing the gel in 25 mmol/L ammonium bicarbonate (Sigma-Aldrich, #09830-500G) and 50% acetonitrile (VWR, #34967-2.5L). Cysteine reduction and alkylation were accomplished with a 45-minute incubation in 10 mmol/L dithiothreitol (Amersham Biosciences, #171318-02) at 56

Table 1. Antibody specificities determined by mass spectrometry analysis of CDR2L and CDR2 proteins immunoprecipitated from OvCar3 and HepG2 cell lysates.

Target	Source/Supplier	Cat. no.	AA seq.	Cell line	#Peptides	Interaction
Yo	Yo positive CSF			OvCar3	54	CDR2L
Yo	Yo positive CSF			HepG2	-	-
CDR2L	Sigma- Aldrich	HPA022015	395-464	OvCar3	56	CDR2L
CDR2L	Proteintech	14563-1-AP	116-465	OvCar3	68	CDR2L
CDR2L	Proteintech	66791-1-Ig	116-465	OvCar3	69	CDR2L
CDR2	Sigma-Aldrich	HPA018151	270-392	HepG2	49	CDR2
CDR2	Sigma-Aldrich	HPA023870	112-234	HepG2	41	CDR2
CDR2	Santa Cruz	Sc-100320	296-405	HepG2	57	CDR2
CDR2	LS Bio	C181958	Full length	HepG2	51	CDR2

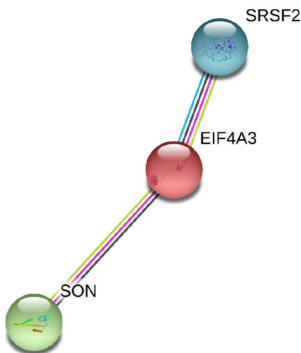
AA seq., amino acid sequence.

A



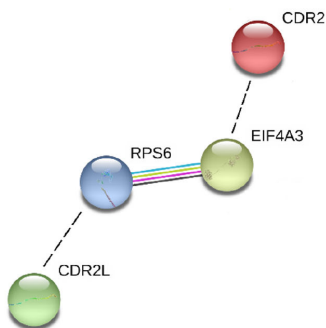
Network statistics for protein-protein interactions	
Nodes	50
Edges	1225
Average node degree	49
Average local clustering coefficient	1
Protein-protein enrichment p-value	< 1.0x10 ⁻¹⁶

B



Network statistics for protein-protein interactions	
Nodes	3
Edges	2
Average node degree	1.3
Average local clustering coefficient	0.7
Protein-protein enrichment p-value	0.012

C



Network statistics for protein-protein interactions	
Nodes	2
Edges	1
Average node degree	1
Average local clustering coefficient	1
Protein-protein enrichment p-value	0.168

Figure 1. Protein-protein interaction networks visualized by STRING. (A) CDR2L was predicted to interact with ribosomal proteins (rpS6, red box). The nodes indicate proteins, and the edges represent protein-protein associations. (B) Protein-protein interaction network of nuclear speckles proteins, SON, eIF4A3, and SRSF2, predicted to interact with CDR2. eIF4A3 (red) directly interacts with SON (light green) and SRSF2 (blue). (C) eIF4A3 (yellow) interacts with rpS6 (blue), indicated by colored edges. Predicted binding partners, CDR2L (green) and CDR2 (red), are manually gated (black, dotted lines). Color-coded edges; light blue: curated databases, dark blue: gene co-occurrence, pink: experimentally determined, green: text mining. Interactions with a medium score of 0.400 or more are shown.

°C followed by a 30-minute incubation in 55 mmol/L iodoacetamide (VWR, #M216-30G) at room temperature in the dark. After washing in 25 mmol/L ammonium bicarbonate and 50% acetonitrile, dried gel pieces were hydrated on ice for 20 min with a minimum volume of 6 ng/μL trypsin (sequencing-grade modified, Promega, #V511A) in digestion buffer (20 mmol/L ammonium bicarbonate, 1 mmol/L calcium chloride (Sigma-Aldrich, #C7902)), then covered with digestion buffer and incubated for 16 h at 37°C. Trypsin activity was quenched by acidification with trifluoroacetic acid (VWR, #1.08218.0050), and samples were desalted using StageTip C18 columns (Empore disk-C18, Agilent Life Sciences, #12145004) and the eluted peptides were dried and dissolved in 2% acetonitrile, 1% formic acid (VWR, #84865.260).²¹

About 0.5 μg tryptic peptides were loaded onto an Ultimate 3000 RSLC system (Thermo Fisher Scientific) connected online to a Q-Exactive HF mass spectrometer (Thermo Fisher Scientific) equipped with EASY-spray nano-electrospray ion source (Thermo Fisher Scientific). All samples were loaded and desalted on a pre-column (Acclaim PepMap 100, 2 cm x 75 μm ID nanoViper column, packed with 3 μm C18 beads) at a flow rate of 5 μL/min with 0.1% trifluoroacetic acid. Peptides were separated during a biphasic acetonitrile gradient (flow rate of 200 nL/minute) on a 50-cm analytical column (PepMap RSLC, 50 cm x 75 μm ID EASY-spray column, packed with 2 μm C18 beads). Solvent A and B were 0.1% formic acid in water and 100% acetonitrile, respectively. The gradient composition was 5% B during trapping (5 min) followed by 5–7% B over 0.5 min, 7–22% B for the next 59.5 min, 22–35% B over 22 min, and 35–80% B over 5 min. Elution of very hydrophobic peptides and conditioning of the column was performed during a 10-minute isocratic elution with 80% B and 15 min of isocratic conditioning with 5% B, respectively.

Charged peptides were analyzed by the Q-Exactive HF, operating in the data-dependent acquisition mode to automatically switch between full-scan MS and MS/MS acquisition. Mass spectra were acquired in the scan range 375–1500 m/z with a resolution of 60,000 at m/z 200 after an accumulation of 3,000,000 charges (maximum trap time set at 50 ms in the C-trap). The 12 peptides with the most intense signals above an intensity threshold of 50,000 counts and with charge states of 2 to 6

were sequentially isolated and accumulated to 100,000 charges (maximum trap time set at 110 ms) to a target value of 1×10^5 or a maximum trap time of 110 ms in the C-trap with isolation width maintained at 1.6 m/z (offset of 0.3 m/z) before fragmentation in the higher energy collision dissociation cell. Fragmentation was performed with a normalized collision energy of 32%, and fragments were detected in the Q-Exactive at a resolution of 60,000 at m/z 200 with first mass fixed at m/z 110. One MS/MS spectrum of a precursor mass was allowed before dynamic exclusion for 30 seconds with “exclude isotopes” on. Accurate mass measurements in MS mode were accomplished by enabling the lock-mass internal calibration of the polydimethylcyclosiloxane ions generated in the electrospray process from ambient air (m/z 445.12003).²²

Database searching and criteria for protein identification

Tandem mass spectra data were extracted with Proteome Discoverer (version 2.3.0.523, Thermo Fisher Scientific) and were searched against human, reviewed protein sequences (SwissprotKB database, release 08-2018) with Sequest HT and MS Amanda search engines. The following search criteria were used: carbamidomethylation of cysteine (fixed modification), oxidation of methionine and acetyl of the protein N-terminus (variable modifications), a maximum of two missed trypsin cleavages, 0.02-Da fragment ion mass tolerance, and 10-ppm precursor ion tolerance. Search results from PD were loaded into Scaffold 4 (version 4.9.0, Proteome Software Inc.), and all spectra were searched with the X! Tandem search engine against identified proteins to identify nonspecific trypsin cleavages.

Peptide and protein identifications were filtered to achieve a false discovery rate < 1.0% (based on searching the reversed human database). Grouping of proteins sharing identical peptides was enabled. In order to evaluate the likelihood of the predicted interactions, the following criteria were established: (1) nonspecific bindings were removed based on the negative control (without primary antibodies); (2) the number of recognized peptides was set to at least two; (3) proteins that were identified by more than one of the antibodies to CDR2L or CDR2 were considered as more likely partners; (4) the likelihood of

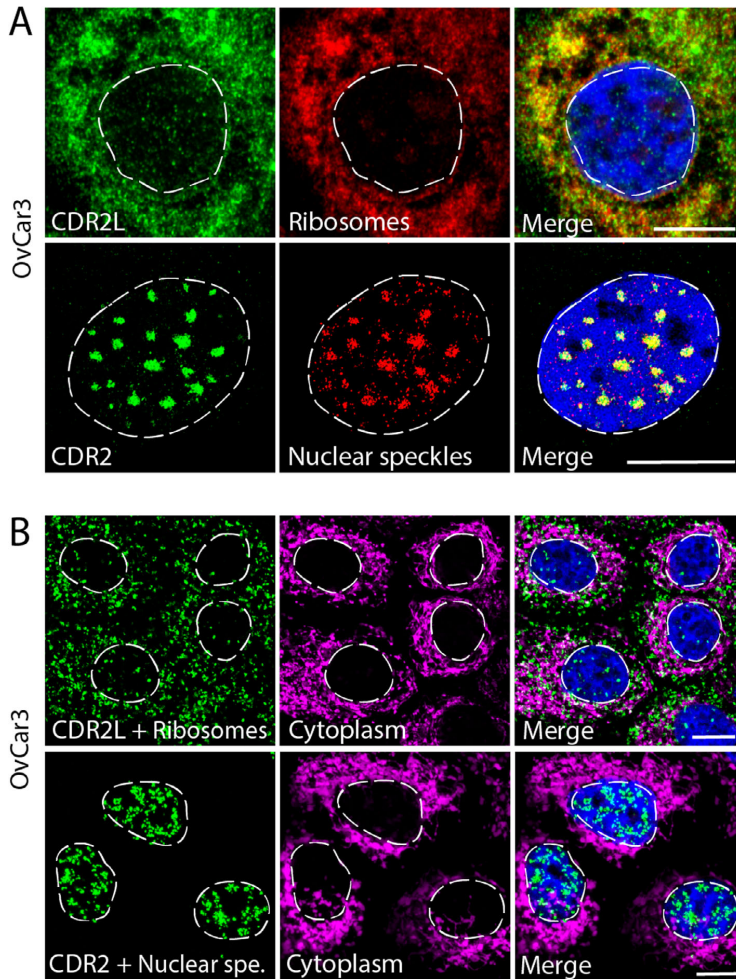


Figure 2. CDR2L co-localizes with ribosomes and CDR2 with nuclear speckles in OvCar3 cells as shown using proximity ligation assay. (A) Upper row: Co-localization of anti-CDR2L (green) and ribosomes (rp56; red) in the cytoplasm (yellow; merged image). Lower row: Co-localization of anti-CDR2 (green) and nuclear speckles (SRSF2; red) in the nucleus (yellow; merged image). (B) Upper row: Positive Duolink (green) between CDR2L and ribosomes (rp56) in the cytoplasm (hsp60 in magenta was used to show the extent of the cell cytoplasm; merged image). Lower row: Positive Duolink (green) between CDR2 and nuclear speckle marker (SRSF2) in the nuclei; no co-localization was observed with cytoplasmic marker hsp60 (magenta; merged image). DAPI was used as a marker for the nuclei (blue). Scale bars = 10 μm.

interaction was evaluated based on the predicted cellular location of each protein of interest. Protein-protein interactions were analyzed using the STRING database. STRING implements all publicly available sources of known and predicted protein-protein associations, together with computational analysis to evaluate potential connectivity networks.^{23,24}

Results

Antibody specificity

To evaluate antibody specificity, we immunoprecipitated CDR2L and CDR2 from cancer cell lysates and analyzed the precipitates using mass spectrometry-based

proteomics with the antibodies listed in Table 1. We found that the commercial antibodies raised against CDR2L and CDR2 were specific and recognized the expected antigens. Also, we confirmed our previous data showing that CDR2L is the major Yo antibody target. Analysis of lysates of OvCar3 cells, which expresses both CDR2L and CDR2, immunoprecipitated with Yo antibodies bound to magnetic beads showed that CDR2L, but not CDR2, was recognized by Yo antibodies. In similar experiments performed with a cell line that only expresses CDR2, HepG2 cells, Yo antibody did not precipitate CDR2.

CDR2L and CDR2 interaction partners identified by mass spectrometry analysis

Potential protein interaction partners were identified using mass spectrometry analysis of proteins immunoprecipitated with anti-CDR2L and anti-CDR2 antibodies from cancer cell lysates. Initially, several hundred hits were detected, and four criteria were established to determine the likelihood of the predicted interactions. Thereafter, we used the STRING database to evaluate the connectivity of the proteins that met our criteria. CDR2L was predicted to interact with 50 ribosomal proteins that were tightly connected (Fig. 1A). Of these 50 ribosomal proteins, 20 belong to the 40S subunit, and 30 belong to the 60S subunit. Proteins known to associate with nuclear speckles, eukaryotic initiation factor eIF4A3, SON, and the serine/arginine-rich splicing factor SRSF2, were identified as potential interaction partners of CDR2. According to the STRING analysis eIF4A3 interacts with SON and SRSF2 (Fig. 1B), as well as with the 40S ribosomal subunit factor rpS6 (Fig. 1C).

CDR2L Co-localizes with ribosomal proteins and CDR2 with nuclear speckle proteins in ovarian cancer cells

We used immunolabeling and proximity ligation assay to investigate the subcellular localization of CDR2L and CDR2. In OvCar3 cells, which express both CDR2L and CDR2, we found that CDR2L co-localizes with rpS6, whereas CDR2 co-localizes with nuclear speckle proteins SON, eIF4A3, and SRSF2 (Fig. 2A). These results were confirmed by proximity ligation assay in OvCar3 cells (Fig. 2B).

Co-Immunoprecipitation of CDR2L and CDR2 from OvCar3 cells confirms protein-protein interactions with ribosomal and nuclear speckle proteins

To analyze whether CDR2L directly interacts with rpS6, we performed co-immunoprecipitation assays from OvCar3 cell lysates. CDR2L specifically co-immunoprecipitated with rpS6, indicating that endogenous CDR2L forms a complex with rpS6 in cancer cells (Fig. 3A). Furthermore, we found that SON and eIF4A3 co-immunoprecipitated with CDR2 from HepG2 cells, thus indicating a strong and stable interaction between these proteins and CDR2 (Fig. 3B).

Co-localizations of CDR2L with ribosomal proteins and of CDR2 with nuclear speckle proteins occurs in Purkinje neurons in Human cerebellum sections and in Purkinje neuron cultures

In human cerebellum sections, CDR2L and Yo antibodies stained the cytoplasm in regions that overlapped with

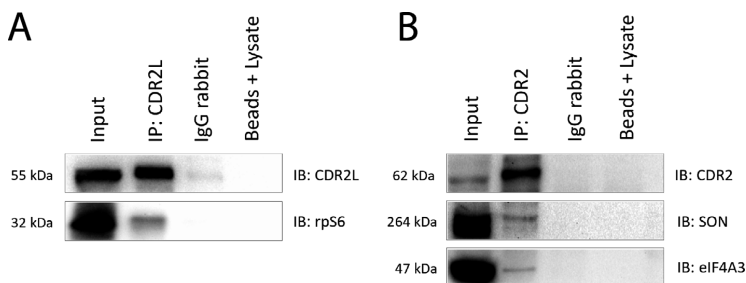


Figure 3. CDR2L co-immunoprecipitates with ribosomal protein rpS6, whereas CDR2 co-immunoprecipitates with nuclear speckle proteins SON and eIF4A3 in cancer cell lysates. (A) Immunoblot demonstrating the co-immunoprecipitation of CDR2L and rpS6 from OvCar3 cell lysates. (B) Immunoblot demonstrating the co-immunoprecipitation of CDR2, SON, and eIF4A3 from HepG2 cell lysates. Input = cancer cell lysates (OvCar3 or HepG2). Beads + lysate = samples that were not treated with primary antibody, and served as negative controls.

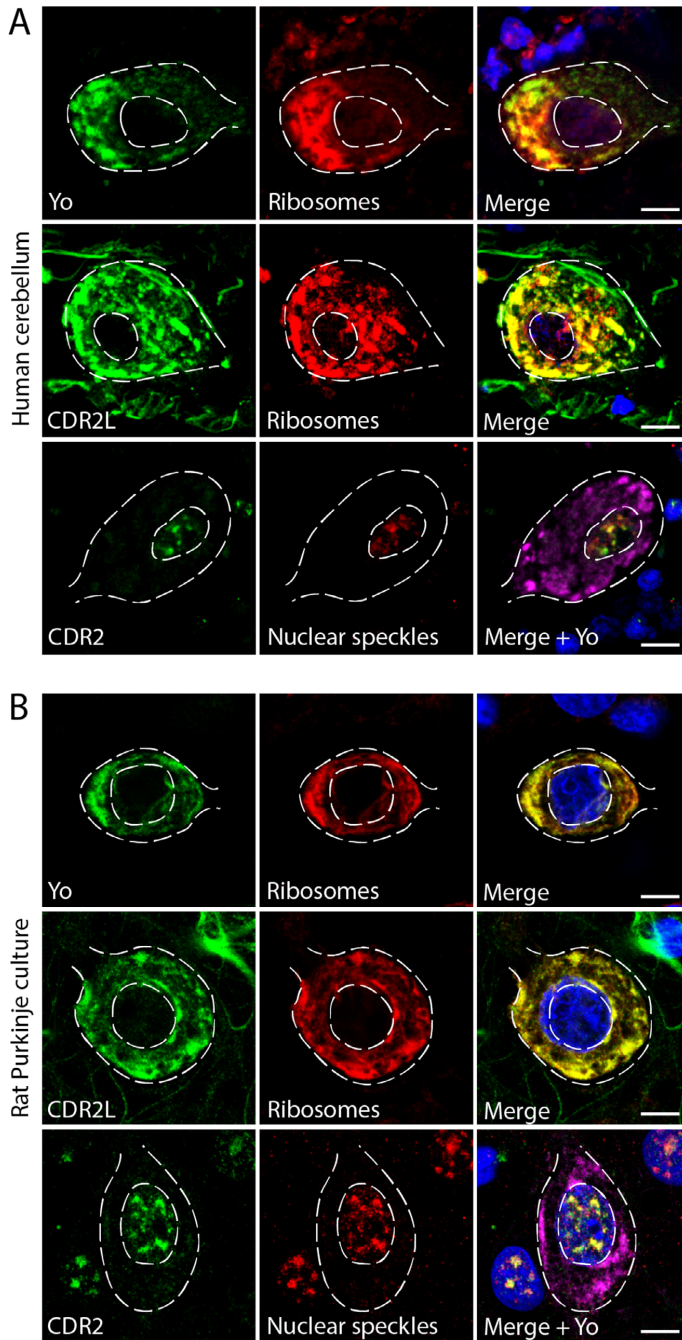


Figure 4. CDR2L and Yo co-localize with ribosomal proteins and CDR2 co-localizes with nuclear speckle proteins in cerebellar Purkinje neurons as shown by super-resolution microscopy. (A) Upper row: Human cerebellar section stained with Yo-CSF (green) and anti-rpS6 (red); the proteins co-localize in the cytoplasm (yellow; merged image). Middle row: Human cerebellar section stained with anti-CDR2L (green) and ribosomal marker anti-rpS6 (red); the proteins co-localize in the cytoplasm (yellow; merged image). Lower row: Human cerebellar section stained with anti-CDR2 (green) and nuclear speckle marker anti-SRSF2 (red); the proteins co-localize in the nucleus. No co-localization was found with anti-Yo (magenta; merged image). (B) Upper row: Rat Purkinje neuron cultures stained with anti-Yo (CSF; green) and rpS6 (ribosomes; red); co-localization was observed in the cytoplasm (yellow; merged image). Middle row: Rat Purkinje neuron cultures stained with anti-CDR2L (green) and anti-rpS6 (red); co-localization was observed in the cytoplasm (yellow; merged image). Lower row: Rat Purkinje neurons stained with anti-CDR2 (green), nuclear speckle protein (red), and anti-Yo (magenta). CDR2 and the nuclear speckle protein co-localize in the cell nucleus (yellow; merged image), whereas Yo does not. Scale bars = 10 μ m.

regions stained for the ribosomal marker rpS6, whereas CDR2 showed nuclear staining that overlapped with nuclear speckle markers (eIF4A3, SON, and SRSF2; Fig. 4A). These results were replicated in cultured rat Purkinje neurons (Fig. 4B).

Discussion

The pathogenesis of Yo-mediated PCD remains incompletely understood, but it has been postulated that the Purkinje neuron loss is due to auto-reactive T cells and a direct damaging effect of Yo antibodies.^{3,4,6,25} We demonstrated previously that CDR2L, not CDR2, is the major target of the Yo antibody⁷: Yo antibodies bind both endogenous and recombinant CDR2L, but only recombinant CDR2, not the native form. In this study, we confirmed the CDR2L specificity of Yo antibodies by mass spectrometry-based proteomics and showed that while CDR2L and CDR2 have differing localizations, it is possible to link their putative roles to ribosomal function.

The biological functions and precise subcellular localization of both CDR2L and CDR2 have been unresolved questions. Analysis of PCD patient sera has shown that Yo antibodies localize to the cytoplasm and associate with both membrane-bound and free ribosomes.^{26,27} In these studies, the Yo antigen is referred to as “CDR2.” However, based on our recent findings, we are confident that the main Yo antigen is indeed CDR2L. Here, we used available antibodies against CDR2L and CDR2, as well as anti-Yo, to characterize the cellular localization of these proteins and their potential binding partners.

Immunolabeling cells with commercially available anti-CDR2 antibodies result in various expression patterns, localizing CDR2 to both the cytoplasm and the nucleus.^{7,13} Therefore, we first evaluated the specificity of the available CDR2L and CDR2 antibodies produced to recognize the full-length protein or shorter sequences. Immunoprecipitation followed by mass spectrometry analysis confirmed antibody specificity. The previously reported inconsistent results for CDR2 may either stem from the antibody recognition of one of the four CDR2 isoforms (www.uniprot.org) or from the translocation of

CDR2 between the cytoplasm and nucleus. Furthermore, previous studies also identified PKN, MRG15, and MRGX as CDR2 binding partners. Since these proteins function both in the cytoplasm and nucleus, this raises the possibility that CDR2 might facilitate the transport of these proteins or translocate itself.^{15,18,19,28} In addition, no CDR2L-CDR2 cross-talk was observed, which supports our finding that there is no cross-talk between CDR2L and CDR2 in their native forms. Furthermore, our immunoprecipitation-mass spectrometry results showed that Yo antibodies only precipitated CDR2L and not CDR2 from cancer cells. This is in line with recent work, which shows that Yo antibodies bind to the CDR2L regions of least homology with CDR2.²⁹

In addition to confirming antibody specificity, the mass spectrometry analysis revealed potential interacting partners for CDR2L and CDR2. A number of ribosomal proteins, including rpS6, were identified as potential CDR2L binding partners. The most prominent CDR2 binding partners were three nuclear speckle proteins: SON, eIF4A3, and SRSF2. Next, we used super-resolution microscopy and proximity ligation assay to evaluate co-localization within a 40-nm range in cancer cells and Purkinje neurons. CDR2L was found to co-localize with rpS6, whereas CDR2 co-localized with nuclear speckle proteins eIF4A3, SON, and SRSF2. Co-immunoprecipitation analyses established that CDR2L directly interacts with rpS6 and that CDR2 directly interacts with eIF4A3 and SON.

Nuclear speckles are self-assembled organelles consisting of around 200 proteins involved in pre-mRNA processing including splicing, surveillance, and RNA export.³⁰ The speckles can vary in size and morphology within a single cell, but have been shown to be non-random organizations of proteins and RNAs stabilized by favorable intermolecular interactions.³⁰ SRSF2 and SON localize to the core region of the speckle; both proteins have domains enriched with arginine and serine repeats that are crucial for speckle core formation.^{30,31} Both proteins are also involved in mRNA splicing^{32,33} and interact with the ATP-dependent RNA helicase eIF4A3.³⁴ It has been suggested that eIF4A3 may provide a link between

splicing and translation in the cytoplasm through its connection to rpS6^{34,35}, which co-localizes with CDR2L.

Translation in eukaryotes relies on the assembly of the small (40S) and the large (60S) ribosomal subunit into the 80S ribosomes.³⁶ Each subunit is composed of ribosomal proteins and RNAs that work together to catalyze protein synthesis using mRNA as a template.^{37,38} Ribosomal proteins often undergo post-translational modifications and rpS6, the identified CDR2L binding partner, is regulated by phosphorylation.^{39,40} Five phosphorylation sites have been identified and these phosphorylation events could participate in regulating the translation of specific subclasses of mRNA, synaptic plasticity and behavior.⁴¹ Thus, rpS6 phosphorylation is often used to track neuronal activity.^{40,41}

Our findings linking CDR2 to nuclear speckles and CDR2L to ribosomes allow us to speculate that these two proteins may participate in a common pathway (Fig. 5). First, we show that CDR2 interacts with eIF4A3 in the nucleus. Second, eIF4A3, along with other initiation factors, facilitates mRNA binding to ribosomes.⁴² Furthermore, eIF4A3 and rpS6 have been shown to interact based on affinity-capture mass spectrometry analysis.³⁵ Third, we show that CDR2L interacts with the ribosomes through rpS6. These findings place CDR2 and CDR2L in the process of protein translation, one involved in mRNA maturation and the other directly with the synthesis of proteins.

Ensuring proper protein homeostasis is crucial to the cell.^{36,38} We show that Yo antibodies specifically bind to

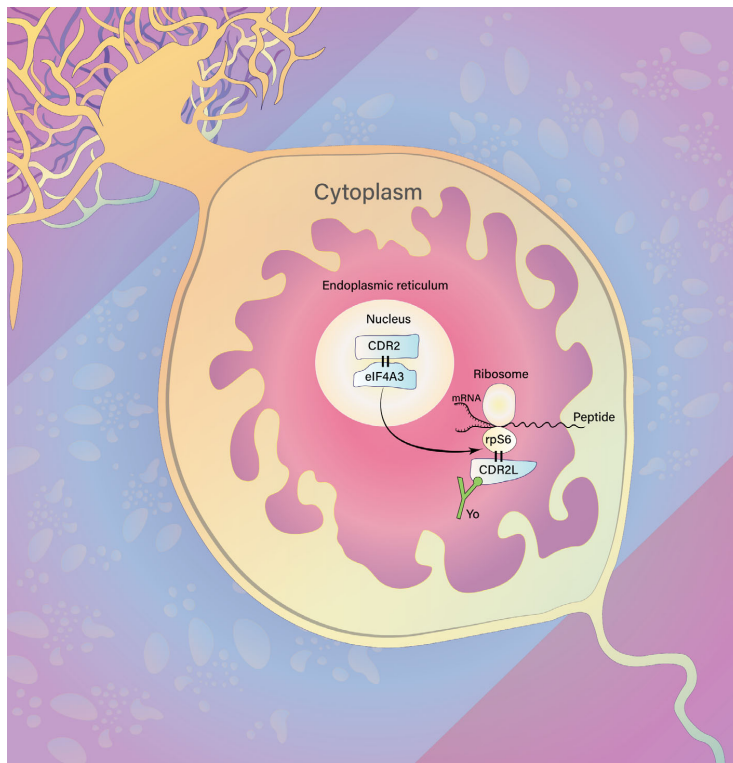


Figure 5. Hypothesis of CDR2L and CDR2 involvement in protein synthesis in Purkinje neurons. CDR2 localizes to the nucleus and directly interacts with nuclear speckle protein eIF4A3. eIF4A3, in conjunction with other cytoplasmic initiation factors, facilitates mRNA binding to the 40S ribosomal subunit. This event is important for mRNA maturation and translation, ultimately resulting in the synthesis of new proteins. CDR2L interacts with ribosomal subunit protein rpS6; therefore, we propose that CDR2L and CDR2 are both involved in the process of protein synthesis. Furthermore, Yo antibody (green) binding to CDR2L in Purkinje neurons of PCD patients may, therefore, interfere with the function of the ribosomal machinery, resulting in disrupted mRNA translation and/or protein synthesis.

CDR2L in Purkinje neurons of PCD patients where they potentially interfere with the function of the ribosomal machinery resulting in disrupted mRNA translation and/or protein synthesis. Taken together, our findings that CDR2L interacts with ribosomal proteins and CDR2 with nuclear speckle proteins is an important step toward understanding PCD pathogenesis. Future studies are needed to track the subcellular events in real-time with the aim of addressing the dynamic interaction between the CDR2L and CDR2 molecules. This will be vital to understand whether there is a functional relationship between CDR2L and CDR2 in the Purkinje neuron deterioration that occurs in PCD.

Acknowledgments

This work was supported by grants from Helse Vest, the University of Bergen, and Torbjørg Hauges Legacy. The confocal imaging was performed at the Molecular Imaging Center and was supported by the Department of Biomedicine and the Faculty of Medicine, University of Bergen, and its partners. The authors would like to thank Mette Haugen at the Department of Neurology, Haukeland University Hospital for valuable advice and discussion, and Anne Døskeland and Olav Mjaavatten at the Proteomics Unit (PROBE) at the University of Bergen for help and support related to the mass spectrometry analysis. Last but not least, we thank Dr. Laurence Bindoff for valuable discussion of our paper.

Author Contributions

All authors contributed to the conception and design of the study; I.H. and T.K. performed the acquisition, data analysis, and prepared figures; I.H., T.K., M.S., and C.V. drafted the manuscript.

Conflicts of Interest

The authors have no conflicts of interest to report.

References

- Peterson K, Rosenblum MK, Kotanides H, Posner JB. Paraneoplastic cerebellar degeneration. I. A clinical analysis of 55 anti-Yo antibody-positive patients. *Neurol*. 1992;42:1931–1937.
- Vedeler CA, Antoine JC, Giometto B, et al. Management of paraneoplastic neurological syndromes: report of an EFNS Task Force. *European J Neurol*. 2006;13:682–690.
- Rasputnig M, Haugen M, Thorsteinsdottir M, et al. Cerebellar degeneration-related proteins 2 and 2-like are present in ovarian cancer in patients with and without Yo antibodies. *Cancer immunol immunother* 2017;66:1463–1471.
- Darnell RB, Posner JB. Paraneoplastic Syndromes Involving the Nervous System. 2003;349(16):1543–54.
- Rees JH. Paraneoplastic syndromes: when to suspect, how to confirm, and how to manage. *J Neurol Neurosurg Psychiatry* 2004;75 Suppl 2(Suppl 2):ii43–ii50.
- Eichler TW, Totland C, Haugen M, et al. CDR2L antibodies: a new player in paraneoplastic cerebellar degeneration. *PLoS one*. 2013;8(6):e66002.
- Krakenes T, Herdlevær I, Rasputnig M, Haugen M, Schubert M, Vedeler CA. CDR2L is the major Yo antibody target in paraneoplastic cerebellar degeneration. *Annals of Neurol* 2019;86:316–321.
- Schubert M, Panja D, Haugen M, Bramham CR, Vedeler CA. Paraneoplastic CDR2 and CDR2L antibodies affect Purkinje cell calcium homeostasis. *Acta Neuropathol* 2014;128(6):835–852.
- Albert ML, Darnell JC, Bender A, Francisco LM, Bhardwaj N, Darnell RB. Tumor-specific killer cells in paraneoplastic cerebellar degeneration. *Nature Med* 1998;4:1321–1324.
- Greenlee JE, Clawson SA, Hill KE, Wood BL, Tsunoda I, Carlson NG. Purkinje cell death after uptake of anti-Yo antibodies in cerebellar slice cultures. *J Neuropathol Exp Neurol* 2010;69:997–1007.
- Sato S, Inuzuka T, Nakano R, et al. Antibody to a zinc finger protein in a patient with paraneoplastic cerebellar degeneration. *Biochem Biophys Res Commun* 1991;178:198–206.
- Corradi JP, Yang C, Darnell JC, Dalmau J, Darnell RB. A Post-transcriptional regulatory mechanism restricts expression of the paraneoplastic cerebellar degeneration antigen cdr2 to Immune Privileged Tissues. *J Neurosci*. 1997;17:1406.
- Totland C, Aarskog NK, Eichler TW, et al. CDR2 antigen and Yo antibodies. *Cancer Immunology Immunother* 2011;60:283–289.
- Small M, Treilleux I, Couillault C, et al. Genetic alterations and tumor immune attack in Yo paraneoplastic cerebellar degeneration. *Acta Neuropathol* 2018;135:569–579.
- Sakai K, Shirakawa T, Li Y, Kitagawa Y, Hirose G. Interaction of a paraneoplastic cerebellar degeneration-associated neuronal protein with the nuclear helix-loop-helix leucine zipper protein MRG X. *Mol Cell Neurosci* 2002;19:477–484.
- Okano HJ, Park WY, Corradi JP, Darnell RB. The cytoplasmic Purkinje onconeural antigen cdr2 down-regulates c-Myc function: implications for neuronal and tumor cell survival. *Genes Dev* 1999;13:2087–2097.
- Fathallah-Shaykh H, Wolf S, Wong E, Posner JB, Furneaux HM. Cloning of a leucine-zipper protein recognized by the sera of patients with antibody-associated

- paraneoplastic cerebellar degeneration. *Proc Natl Acad Sci USA* 1991;88:3451–3454.
18. Takanaga H, Mukai H, Shibata H, Toshimori M, Ono Y. PKN interacts with a paraneoplastic cerebellar degeneration-associated antigen, which is a potential transcription factor. *Exp Cell Res* 1998;241:363–372.
 19. Sakai K, Kitagawa Y, Saiki S, Saiki M, Hirose G. Effect of a paraneoplastic cerebellar degeneration-associated neural protein on B-myb promoter activity. *Neurobiol Dis* 2004;15:529–533.
 20. Uggerud IM, Krakenes T, Hirai H, Vedeler CA, Schubert M. Development and optimization of a high-throughput 3D rat Purkinje neuron culture. *bioRxiv*. 2020;105858.
 21. Rappsilber J, Ishihama Y, Mann M. Stop and go extraction tips for matrix-assisted laser desorption/ionization, nanoelectrospray, and LC/MS sample pretreatment in proteomics. *Analytical Chem* 2003;75:663–670.
 22. Olsen JV, de Godoy LM, Li G, *et al.* Parts per million mass accuracy on an Orbitrap mass spectrometer via lock mass injection into a C-trap. *Mol Cell Proteomics* 2005;4:2010–2021.
 23. Szklarczyk D, Morris JH, Cook H, *et al.* The STRING database in 2017: quality-controlled protein-protein association networks, made broadly accessible. *Nucleic Acids Res* 2017;45(D1):D362–d8.
 24. Szklarczyk D, Gable AL, Lyon D, *et al.* STRING v11: protein-protein association networks with increased coverage, supporting functional discovery in genome-wide experimental datasets. *Nucleic Acids Res* 2019;47(D1):D607–d13.
 25. Storstein A, Krossnes BK, Vedeler CA. Morphological and immunohistochemical characterization of paraneoplastic cerebellar degeneration associated with Yo antibodies. *Acta Neurol Scand* 2009;120:64–7.
 26. Rodriguez M, Truh LI, O'Neill BP, Lennon VA. Autoimmune-paraneoplastic-cerebellar-degeneration-Ultrastructural-localization-of-antibody-binding-sites-in-purkinje-cells. *Neurology* 1988;38:1380.
 27. Hida C, Tsukamoto T, Awano H, Yamamoto T. Ultrastructural localization of anti-Purkinje cell antibody-binding sites in paraneoplastic cerebellar degeneration. *Arch Neurol* 1994;51:555–558.
 28. Mukai H, Miyahara M, Sunakawa H, *et al.* Translocation of PKN from the cytosol to the nucleus induced by stresses. *Proc Natl Acad Sci USA*. 1996;93(19):10195–10199.
 29. O'Donovan B, Mandel-Brehm C, Vazquez SE, *et al.* High resolution epitope mapping of anti-Hu and anti-Yo autoimmunity by programmable phage display. *Brain Communications*. 2020.
 30. Fei J, Jadalila M, Harmon TS, *et al.* Quantitative analysis of multilayer organization of proteins and RNA in nuclear speckles at super resolution. *J Cell Sci* 2017;130:4180–4192.
 31. Sharma A, Takata H, Shibahara K, Bubulya A, Bubulya PA. Son is essential for nuclear speckle organization and cell cycle progression. *Mol Biol Cell*. 2010;21:650–663.
 32. Lin S, Coutinho-Mansfield G, Wang D, Pandit S, Fu X-D. The splicing factor SC35 has an active role in transcriptional elongation. *Nat Struct Mol Biol* 2008;15:819–826.
 33. Ahn E-Y, DeKolver Russell C, Lo M-C, *et al.* son controls cell-cycle progression by coordinated regulation of RNA Splicing. *Molecular Cell* 2011;42:185–198.
 34. Chan CC, Dostie J, Diem MD, *et al.* eIF4A3 is a novel component of the exon junction complex. *RNA*. 2004;10:200–209.
 35. Singh G, Kucukural A, Cenik C, *et al.* The cellular EJC interactome reveals higher-order mRNP structure and an EJC-SR protein nexus. *Cell*. 2012;151:750–764.
 36. Klaijs CL, Jayaraj GG, Hartl FU. Pathways of cellular proteostasis in aging and disease. *J Cell Biol* 2018;217:51–63.
 37. Aitken CE, Lorsch JR. A mechanistic overview of translation initiation in eukaryotes. *Nat Struct Mol Biol* 2012;19:568–576.
 38. Lehmkuhl EM, Zarnescu DC. Lost in Translation: Evidence for Protein Synthesis Deficits in ALS/FTD and Related Neurodegenerative Diseases. *Adv Neurobiol* 2018;20:283–301.
 39. Ruvinsky I, Meyuhas O. Ribosomal protein S6 phosphorylation: from protein synthesis to cell size. *Trends Biochem Sci* 2006;31:342–348.
 40. Biever A, Valjent E, Puighermanal E. Ribosomal protein S6 phosphorylation in the nervous system. From Regulation to Function. *Front Mol Neurosci* 2015;8:75.
 41. Puighermanal E, Biever A, Pascoli V, *et al.* Ribosomal protein S6 phosphorylation is involved in novelty-induced locomotion, synaptic plasticity and mRNA translation. *Front Mol Neurosci* 2017;10:419.
 42. Rogers GW Jr, Richter NJ, Lima WF, Merrick WC. Modulation of the helicase activity of eIF4A by eIF4B, eIF4H, and eIF4F. *J Biol Chem* 2001;276:30914–30922.

1 **Development and optimization of a high-throughput 3D rat Purkinje neuron culture**

2 Running head: Rat Purkinje neuron culture

3

4 Ida M. Uggerud (MSc)^{1,2}, Torbjorn Krakenes (MSc)², Hirokazu Hirai³ (MD, PhD), Christian
5 A. Vedeler (MD, PhD)^{1,2,4}, Manja Schubert (ScD)*¹

6 ¹ Department of Neurology, Haukeland University Hospital, 5021 Bergen, Norway

7 ² Department of Clinical Medicine (K1), University of Bergen, 5021 Bergen, Norway

8 ³ Department of Neurophysiology & Neural Repair, Gunma University Graduate School of
9 Medicine, Maebashi, Gunma 371-8511, Japan

10 ⁴ Neuro-SysMed - Centre of Excellence for Experimental Therapy in Neurology, Departments
11 of Neurology and Clinical Medicine, 5021 Bergen, Norway

12

13 Address correspondence to:

14 Dr. Manja Schubert, ScD
15 Department of Neurology
16 Haukeland University Hospital
17 N-5021 Bergen, Norway
18 Tel: (47) 55 58 67 15
19 Fax: (47) 55 58 64 10
20 Email: schubert_manja@hotmail.com

21

22 Title:	80	characters
23 Running head:	27	characters
24 Abstract:	564	characters
25 Article:	9644	characters
26 Material and Methods:	10507	characters
27 Statements:	754	characters
28 Figure legends:	4177	characters
29 TOTAL:	25646	characters
30 Number of figures/tables:	3	
31 Main text:	1461	words

32

33

1 **Keywords:** Purkinje neuron; neuronal culture system; neurodegeneration

2

3 **Abbreviations:** DIV = days *in vitro*; PN = Purkinje neuron; PNC = Purkinje neuron culture;

4 SCL = support cell layer

5

1 **Abstract**

2 Improved understanding of the mechanisms involved in neurodegenerative disease has been
3 hampered by the lack of robust cellular models that faithfully replicate *in vivo* features. Here,
4 we present a refined protocol for generating age-dependent, well-developed and synaptically
5 active rat Purkinje neurons, responsive to paracrine factors and supporting a 3D cell network.
6 Our model provides high experimental flexibility, high-throughput screening capabilities and
7 reliability to elucidate Purkinje neuron function, communication and neurodegenerative
8 mechanisms.

9

10 **Article**

11 Unravelling the mechanisms of neurodegeneration depends on the availability of robust
12 models that provide insight both at the single cell level and network levels, and that offer high
13 experimental flexibility. Dissociated neuronal cultures can be useful, but their quality and
14 survival depends on several factors including animal species, age of tissue that is dispersed
15 to give single cells, the surface onto which the single cells are seeded and cultured, and co-
16 factors that drive neuronal growth and development. To date, the majority of successful
17 Purkinje neuron cultures (PNC) models have used embryonic mouse cerebellum, few have
18 successfully used rat embryonic or postnatal cerebellum. Although the success rate of
19 transgenic alterations and *in vivo* modelling is lower in rats ¹, the rat is physiologically,
20 genetically and morphologically closer to humans than the mouse ², and outbred or transgenic
21 rat models mimic human neurodegenerative disease mechanisms and progressions more
22 closely ³⁻⁵ than mouse models do ^{6,7}.

23 Since neurodegeneration generally occurs in the adult or aged human brain, a
24 dissociated culture system derived from mature rather than embryonic tissue is desirable.
25 However, previous attempts to culture functional dissociated neurons from late postnatal and
26 adult tissue have been largely unsuccessful. Therefore, our goal was to develop a culture

1 protocol that provided well-developed, mature, functional and synaptically active rat Purkinje
2 neurons (PNs), interdependent of the derived tissue age, that gives maximal experimental
3 flexibility and the potential for high-throughput screening. We discovered three factors that
4 were essential for success: having a three-dimensional (3D) growth structure, pH stability and
5 co-factor supplementation.

6 The first attempt growing PNs directly on glass cover-slips coated with poly-D-lysine
7 (PDL) and the extracellular matrix protein laminin failed: the yield of PNs per cover-slip
8 declined to zero from E18 to P10 at 21 days *in vitro* (*DIV*) (Figure 1a, non 3D-SCL). We
9 reasoned that the extracellular matrix used lacked important features including other cell types
10 that provide the *in vivo* 3D cell network structure and thereby cell-cell communicate including
11 paracrine factor secretion. Therefore, in the second attempt we developed a three-
12 dimensional support cell layer (3D-SCL) approach by plating two cerebellar cell layers
13 derived of either E18, P0 or P10 tissue onto PDL coated cover-slips. We introduced a time-
14 delay by plating the second cell layer 7 to 48 days later than the first. We found that the tissue
15 age of cells used to grow the 3D-SCL (E18 to P10) had no impact on the PN yield of the
16 second layer, however, there was a strong correlation between the *in vivo* age of the support
17 cell layer and the tissue age used to grow the second cell layer, the enriched PN layer. The
18 highest survival rate of E18 derived-PNs was observed when plated onto the 3D-SCL at
19 *DIV14*, for P0 derived-PNs at *DIV21* and for P10 derived-PNs at *DIV28* (Figure 1a). These
20 findings indicate that the older the starting tissue, the more mature the 3D-SCL has to be to
21 achieve a high survival rate of PNs for a minimum of 21 to 28 *DIV*.

22 However, the use of a “double” cell layer was associated with higher metabolic
23 demand than single layer cultures and led to non-physiological pH fluctuations resulted in cell
24 death when half of the culture media was replaced ones a week. Replacing the culture media
25 more frequently, either every 3.5-days (6 well) or every 2-days (12 and 24 well) prevented
26 pathological pH fluctuations and gave a healthy well-developed neuronal network. Despite

1 this, immunofluorescent staining showed that the PNs had a poorly developed dendritic
2 morphology compared to those *in vivo*, with fewer and shorter branches in E18 and P0
3 derived-PNs (Figure 1b-c, 1b upper panel).

4 Neuronal dendrites are generated during development by a series of processes
5 involving a first step of extension and retraction of dendritic branches, and subsequently
6 stabilisation of existing dendrites through building of synaptic connections and neuronal
7 calcium homeostasis ⁸. Calcium-dependent protein kinase C (PKC) subtypes, activated by
8 synaptic inputs from the parallel fibres (granule cells) through metabotropic glutamate
9 receptors (mGluR1/4), trigger functional changes as well as long-term anatomical maturation
10 of the PN dendritic tree during cerebellar development ⁹. Altering the activity of calcium-
11 dependent PKC subtypes using PKC antagonist K252a improved dendritic branching for E18
12 and P0 derived-PNs similar to *in vivo*, but had no effect on the branching characteristics of
13 P10 derived-PNs (Figure 1b-c, 1b lower panel). Interestingly, K252a-induced PKC inhibition
14 significantly improved the low survival rate observed for P0 and particularly for P10 derived-
15 PNs in a concentration dependent manner (Figure 1d). The survival rate in P0 derived-PNs
16 was improved by a factor of 6 by blocking 20 % of PKC activity (10 nM K252a), whereas in
17 P10 derived-PNs, blocking PKC activity to 50 % (25 nM K252a) increased the survival rate
18 by a factor of 28. Inhibiting PKC activity had no effect on the survival rate of E18 derived-
19 PNs (Figure 1d).

20 PN survival and dendritic tree development are also highly dependent on paracrine
21 factors such as progesterone, insulin and insulin-like growth factor 1 (IGF1) secreted by other
22 cells or self-produced by PNs in an age-dependent manner ¹⁰⁻¹². We supplemented our culture
23 with 40 μ M progesterone and found this led to increased branched dendritic trees in E18
24 derived-PNs, but it had no impact on the branch structure of P0 and P10 derived-PNs (Figure
25 1e). Even though PN dendritic development was insufficient when either K252a inhibition or
26 progesterone were not supplied, supplementation with insulin and IGF1 were sufficient to

1 maintain the long-term growth of the other cerebellar cell types: granule, Golgi, Lugaro,
2 unipolar brush, stellate and basket cells (Figure 1f).

3 To demonstrate that our PNs expressed functional synapses, we used
4 immunocytochemistry to identify pre- and postsynaptic biomarkers of functional synapses
5 including voltage-gated calcium channels (VGCC), metabotropic glutamate receptor 1
6 (mGluR1), post-synaptic density protein 95 (PSD95), glutamate-decarboxylase 65 (GAD65),
7 glycine transporter 2 (GlyT2), α -synuclein and bassoon. All these markers were present
8 indicating a level of maturity of both the PNs and the surrounding network (Figure 1g).

9 Next, we tested the functional activity of these PNs. *In vivo*, PNs fire spontaneous
10 action potentials at frequencies of about 40-50 Hz with a complex trimodal pattern of tonic
11 firing, bursting, and silent modes that depend on anatomically and functionally maturity^{13,14}.
12 E18 derived-PNs cultured in a 24 well multielectrode array first revealed spontaneous
13 bioelectrical activity on *in vitro* day 11. The spike rate increased constantly from 0.15 ± 0.03
14 Hz (*DIV11*) to 2.56 ± 0.59 Hz (*DIV21*). After *DIV28*, the spike activity become erratic with
15 long periods of silence, but overall, a frequency of 2.79 ± 0.55 Hz was maintained until
16 *DIV63* (Figure 1h). We observed uniform, highly non-uniform spike intervals and trains with
17 silent periods between bursts and spike frequencies of up-to 140 Hz within the burst.
18 Exchanging the PNC media at *DIV28* to one previously used in organotypic brain slice culture
19¹⁵, prevented the erratic spike activity and stabilized the spike frequency at 6.35 ± 1.85 Hz for
20 up-to 63 *DIV*.

21 In addition to immunocytochemical and high-throughput electrophysiological studies,
22 this 3D PN model system will provides the potential for cell-type-specific genetic
23 engineering. For example, by using lentiviral particles to express PN-specific green
24 fluorescence protein (GFP) via implementation of the L7 promoter^{16,17}. To test this, we
25 applied L7-GFP inducing viral particles to dissociated PNs on the day of seeding. Within 3
26 days, we found PNs expressing GFP and hardly any off-targets (<0.02%). At *DIV14*, 61.5 %

1 of the PN population were GFP positive and these cells did not differ in dendritic structure and
2 stably expressed GFP for up-to 169 *DIV* (Figure 1i). Using our culture system, we also found
3 a sufficiently high transfection rate of PNs when lentiviral particles were added to the culture
4 at *DIV14* and *DIV28*, however the rate of transfection and speed of expression fell
5 progressively the later the genetic manipulation was implemented. The GFP positive PNs in
6 the culture revealed a very similar development to *in vivo*, as we were able to observe the
7 fusion phase (E17-P5), the phase of stellate cells with disoriented dendrites (P5-P7), as well
8 as the phase of orientation and flattening of the dendritic tree (P7-P21)^{18,19} (Figure 1i).

9 We present a 3D, rat PNC model for growing Purkinje neurons that is independent of
10 derived tissue age, and which provides a complex and robust system that allows maximal
11 experimental flexibility. The combined use of 3D network structures (3D-SCL) with
12 optimized concentrations and time-dependent addition of hormones, paracrine factors and
13 activity regulators (progesterone, insulin, IGF-1, K252a), created ideal conditions to grow a
14 balanced cerebellar network in miniature (Figure 2). As a proof-of-principle, we
15 demonstrated the usefulness of this culture model as a high-throughput screening tool to
16 investigate disease mechanisms including drug/compound testing. The long-term stability and
17 neuronal complexity of our culture will facilitate the study of cell- and network-dependent
18 cerebellar degeneration related to paraneoplastic cerebellar degeneration and ataxia.

19

20 **Material and Methods**

21

22 **Neuronal culture preparation.**

23 All procedures were performed according to the National Institutes of Health Guidelines for
24 the Care and Use of Laboratory Animals Norway (FOTS 20135149/20157494/20170001).
25 Wistar Hannover GLAST rat pups (n = 328), embryonic day 18 (E18) to postnatal day 10
26 (P10), were used for neuronal culture preparation.

1 Briefly, following anaesthesia and decapitation, the brains were rapidly transferred into
2 preparation solution: ice-cold EBSS solution (Gibco, #24010043) containing 0.5% glucose
3 (Sigma, #G8769) and 10 mM HEPES (Gibco, #15630056). Under a dissection microscope,
4 carefully remove the meninges, cut off the medulla oblongata and separate the cerebellum
5 from the pons and the midbrain. Depending on the culture, Purkinje neuron or structural layer,
6 transfer either only the cerebellum or the cerebellum including pones to a 15 mL tube
7 containing 20 U/mL papain (Worthington, #LK003178) solved in preparation solution and
8 warmed up to 36 °C. Place the tube into the incubator for 15 minutes at 36°C with
9 occasionally swirling to digest the tissue. Remove the papain solution carefully with a fire
10 polished Pasteur pipette and stop the digestion by adding pre-warmed stop media (36°C):
11 advanced DMEM/F12 solution (Gibco, #12634010) containing 0.5% glucose (Sigma,
12 #G8769) and 10% foetal bovine serum (FBS, Gibco, #10500064). After 5 minutes of
13 deactivation, remove the stop media and add 250 µL growth media containing 10% FBS per
14 cerebellum and pipette the tissue/media suspension with a fire polished Pasteur pipette 100X
15 until cells are separated.

16

17 **3D Support Cell Layer (3D-SCL).**

18 375000 cells/mL from cerebellum including pones were seeded on pre-coated coverslides
19 from Neuvitro (#GG-12-1.5-PDL, 24 well, 500 µL/well; #GG-18-1.5-PDL, 12 well, 1
20 mL/well; #GG-25-1.5-laminin, 6 well, 2 mL/well). Culture were maintained in 6-,12- or 24-
21 well plates in growth media consisting of 45% advanced DMEM/F12 solution (Gibco, #
22 126340010), 45% NBM solution (Miltenyibiotec, #130-093-570), 1.5% B-27 serum-free
23 supplement (Gibco, #17504044), 1.5% NB-21 serum-free supplement (Miltenyibiotec, #130-
24 093-566), 1% NaPyruvate (Invitrogen, #11360088), 1% heat-inactivated FBS (Invitrogen,
25 #10500064), 2% GLUTAMAX (Gibco, #35050038), 5 mg/mL D-glucose and 10 mM HEPES
26 (Invitrogen, #15630056) at 36°C. Half of the culture medium was replaced every 7 days.

1

2 **Purkinje neuron layer.**

3 E18 and P0 derived Purkinje neuron culture: 500000 cells/mL from cerebellum without pones
4 were seeded on the 3D support cell layer of different *in vitro* ages. P10 derived Purkinje
5 neuron culture: 750000 cells/mL from the vermis of the cerebellum were seeded on the 3D
6 support layer of different *in vitro* ages. The growth media was supplemented with insulin
7 (Invitrogen, #12585014; 1:250, stock 4 mg/mL), progesterone (Sigma, #P8783, 1:2000, stock
8 80 mM), insulin-like growth factor 1 (IGF1; Promokine, #E-60840, 1:40000, stock 1 µg/µL)
9 and Protein kinase C inhibitor K252a (Alomone, # K-150; IC₅₀ 25 nM). In long-term cultures
10 that were maintained for more than 28 days *in vitro* the IGF1 and progesterone concentration
11 were reduced to 10 ng/mL and 20 µM, respectively. K252a was supplemented for 21 days
12 before the washout process started, its optimal concentration was experimental evaluated for
13 each tested culture type. Half of the culture medium was replaced every 3.5 (6 well) and 2
14 (12/24 well) days, respectively. All experiments testing the Purkinje neuron yield dependent
15 on derived tissue age, *in vitro* age of the 3D-SCL and K252a concentration were performed
16 randomly, containing 3 to 6 probes per experimental setting and 5 independently repeats for
17 each group and condition.

18

19 **Lentiviral gene editing.**

20 L7 promoter (full length 1005 bp) were custom cloned by SBI System Bioscience into
21 construct pCDH-L7-MCS-copGFP (#CS970S-1) and viral particle with a yield of 2.24×10^9
22 ifus/mL were produced. Freshly prepared Purkinje neurons of E18 or P0 cerebellum
23 suspended in growth media containing no serum were incubated for 10 minutes at 37 °C with
24 1.22×10^6 viral particle/mL before seeded onto the supplement structure layer containing
25 cover-slip or live cell imaging µ-dish (#80136, 35 mm, Ibidi). Media was changed after 3
26 days and transfection efficiency evaluated by live cell imaging microscopy 24h post

1 transfection, daily up to 21 days and weekly up to 169 days in culture, respectively.
2 Additional, lentiviral transfection of Purkinje neurons in culture were performed 1 day after
3 feeding at DIV15 and DIV29 by applying 2.5×10^6 viral particle/mL to evaluate the
4 efficiency and effects of age-dependent genetic manipulations. The neuronal development of
5 the GFP expressing Purkinje neurons was followed by obtaining 10 independent 3x3 tile scan
6 using the Zyla camera configuration (2048x2048) with the CFI Plan Apochromat Lambda dry
7 objective 10x0.45 (pixel size 603 nm) or 20x0.75 (pixel size 301 nm) at the Andor Dragonfly
8 microscope system (Oxford Instruments company). The experiments of DIV0, DIV15 and
9 DIV29 were repeated three times.

10

11 **Immunohistochemical cell type characterisation.**

12 To evaluate Purkinje neuron yield and the distribution ratio of other cell types of the
13 cerebellum, including their synaptic interactions, the culture was washed with pre-warmed 0.1
14 M PBS (1xPBS; Gibco, #70013016) and fixed with 1.5-4% paraformaldehyde (PFA, pH 6-
15 7.2; ThermoScientific, #28908) containing 0.5% sucrose for 15 minutes at 36°C. Tris-based
16 or citric acid-based heat induced antigen retrieval (pH 9 and pH 6; 45 min, 85 °C)²⁰ were
17 perform when necessary (see Table 1). Culture were quenched with 1xPBS containing 50 mM
18 NH₄Cl (PBS_N), permeabilised with 0.2% Triton X-100 (Sigma, #T9284) in PBS_N (5 min,
19 36°C), rinsed with PBS_N containing 0.5% cold water fish gelatine (Sigma, #G7041)(PBS_{NG},
20 3x15 min), and incubated with primary antibody over-night at 4°C in PBS_{NG} containing 10%
21 Sea Block (SB; ThermoScientific, #37527), 0.05% Triton X-100 and 100 μM glycine
22 (Sigma, #G7126) to visualise the different cerebellar cell types, including Purkinje neurons
23 and their synaptic interactions (Table 1). The cover-slips were rinsed with PBS_{NG} (3x20 min)
24 and incubated with highly cross-absorbed donkey secondary antibodies conjugated to
25 CFTM488/594/647-Dye (1:400; Biotium, #20014, #20115, #20046, #20015, #20152, #20047,
26 #20074, #20075, #20169, #20170) for 2 hours at 22°C in PBS_{NG} containing 2.5% SB. To

1 remove unbound secondary antibody cover-slips were rinsed with PBS_N (3x20 min), and
2 briefly tipped into MilliQ water before mounted in hardening ProlongTM Glass Antifade
3 Reagent (Invitrogen, #P36981) onto cover-slides. After 2 days of hardening at 18-21°C in the
4 dark, cover-slides were stored at 4°C until imaging.

5

6 **Purkinje neuron count and imaging.**

7 Purkinje neurons were counted manually and blind by screening the cover-slips using a Leitz
8 Diaplan Fluorescence microscope equipped with CoolLED pE-300white. For dendritic tree
9 branch analysis and determination of maturity and synaptic interaction, 10 Purkinje neuron
10 Z-stack images per cover-slide were collected in 5 independent and randomized experiments
11 at 0.5-1 μm intervals with the Zyla camera configuration (2048x2048) at the Andor Dragonfly
12 microscope system using either a CFI Plan Apochromat Lambda S LWD 40x1.14 water
13 objective (pixel size 151 nm), 60x1.20 oil objective (pixel size 103 nm) or CFI SR HP Apo TIRF
14 100x1.49 oil objective (pixel size 60 nm) to detect DAPI and CFTM488/594/647 dye emission
15 and superimposed with Fusion software (Oxford Instruments). 3D surface visualization of
16 synapses was performed using Oxford Instruments analysis software IMARIS 9.3.1 and the
17 filament tracer tool²¹.

18

19 **Dendritic tree branch analysis.**

20 The Purkinje neuron dendritic tree development was evaluated by analysing group
21 dependent 10 Purkinje neurons per experiment in 10 independent experiments towards the
22 order and length of the dendritic arbours by using an open-source ImageJ and Fiji plugin
23 Simple_Neurit_Tracer (Neuroanatomy)²².

24

25 **Micro-electrode array (MEA) recordings.**

1 Primary cultures of E18 derived-PNs at a concentration of 500000 cells/mL were
2 plated onto PDL precoated 24 well format plate of the Multiwell-MEA-system (Multi
3 Channel System-MCS, Reutlingen, Germany). Each well contains 12 PEDOT coated gold
4 micro-electrodes (30 μm diameter, 300 μm space, 3 x 4 geometrical layout) on glass base to
5 facilitate visual checking (#890850, 24W300/30G-288). The amplifier (data resolution: 24 bit;
6 bandwidth: 0.1 Hz to 10 kHz, modifiable via software; default 1 Hz to 3.5 kHz; sampling
7 frequency per channel: 50 kHz or lower, software controlled; input voltage range: \pm 2500
8 mV), stimulator (current stimulation: max. \pm 1 mA; voltage stimulation: max. \pm 10 V;
9 stimulation pattern: pulse or burst stimulation sites freely selectable) and heating element
10 (regulation: \pm 0.1 $^{\circ}\text{C}$) is integrated in the Multiwell-MEA-headstage which is driven by the
11 MCS-Interface Board 3.0 Multiboot. The Multiwell recording platform is covered by a mini
12 incubator to provide 5% CO_2 and balanced air. Electrophysiological signals were acquired at a
13 sampling rate of 20kHz through the commercial software Multiwell-Screen. Plates were
14 tested every second day for spontaneous activity from day 5 *in vitro*. Raw voltage traces were
15 recorded for 120 seconds, saved and analysed using offline MCS-Multiwell-Analyzer to
16 calculate spike rate and burst activity, including network properties. Two experimental
17 settings were tested: number 1 recording of spontaneous spike activity in Purkinje neuron
18 culture media (45% advanced DMEM/F12 solution, 45% NBM solution, 1.5% B-27 serum-
19 free supplement, 1.5% NB-21 serum-free supplement, 1% NaPyruvate, 1% heat-inactivated
20 FBS, 2% GLUTAMAX, 5 mg/mL D-glucose, 10 mM HEPES, 16 $\mu\text{g}/\text{mL}$ insulin, 25 ng/mL
21 IGF1, 40 μM progesterone, 5 nM K252a) for 63 days and number 2 recording spontaneous
22 spike activity for the first 28 days in Purkinje neuron culture media but then exchanged to
23 organotypic brain slice culture media¹⁵ (30% advanced DMEM/F12 solution, 20% MEM
24 solution (#41090028; Gibco), 25% EBSS solution (#24010043; Gibco), 25% heat-inactivated
25 horse serum (#H1138; Sigma), 2% GLUTAMAX, 5 mg/ml D-glucose and 2% B-27 serum-
26 free supplement) for the remaining 45 days.

1

2 **Notes to provide stable high yield Purkinje neuron culture.**

3 (1) All media should be prepared fresh on the day of use.

4 (2) Prevent repeated thaw-freeze cycles of the supplements

5 (3) 3D-SCL should be fed 24 hours prior plating of the second cell layer, PN layer, to
6 provide stable pH at 6.8 to 7.0 on the day of seeding.

7

8 **ACKNOWLEDGMENT**

9 The authors thank Y.Ishizuka and C.E.Bramham for providing the E18 cerebellum tissue, C.
10 Elliott for discussion, and the Molecular Imaging Centre (MIC), where the imaging
11 experiments were performed (Department of Biomedicine and the Faculty of Medicine and
12 Dentistry of University of Bergen). This work was funded by grants from HelseVest Norway
13 and University of Bergen.

14

15 **AUTHOR CONTRIBUTIONS**

16 M.S. devised the conceptual framework. I.M.U., T.K and M.S planned and performed the
17 experiments and analysed the obtained data sets. H.H. provided the lentiviral approach. The
18 paper was written by M.S, H.H. and C.A.V. with editing contributions from all the authors.

19

20 **COMPETING FINANCIAL INTERESTS**

21 The authors declare no competing financial interests.

22

1 **REFERENCES**

2

3 1. Bugos, O., Bhide, M. & Zilka, N. Beyond the rat models of human neurodegenerative
4 disorders. *Cell. Mol. Neurobiol.* **29**, 859–869 (2009).

5 2. Jacob, H. J. & Kwitek, A. E. Rat genetics: attaching physiology and pharmacology to the
6 genome. *Nat. Rev. Genet.* **3**, 33–42 (2002).

7 3. Drummond, E. & Wisniewski, T. Alzheimer’s disease: experimental models and reality.
8 *Acta Neuropathol. (Berl.)* **133**, 155–175 (2017).

9 4. Nuber, S. *et al.* A progressive dopaminergic phenotype associated with neurotoxic
10 conversion of α -synuclein in BAC-transgenic rats. *Brain J. Neurol.* **136**, 412–432 (2013).

11 5. von Hörsten, S. *et al.* Transgenic rat model of Huntington’s disease. *Hum. Mol. Genet.* **12**,
12 617–624 (2003).

13 6. Ellenbroek, B. & Youn, J. Rodent models in neuroscience research: is it a rat race? *Dis.*
14 *Model. Mech.* **9**, 1079–1087 (2016).

15 7. Dawson, T. M., Golde, T. E. & Lagier-Tourenne, C. Animal models of neurodegenerative
16 diseases. *Nat. Neurosci.* **21**, 1370–1379 (2018).

17 8. Metzger, F. Molecular and cellular control of dendrite maturation during brain
18 development. *Curr. Mol. Pharmacol.* **3**, 1–11 (2010).

19 9. Metzger, F. & Kapfhammer, J. P. Protein kinase C: its role in activity-dependent Purkinje
20 cell dendritic development and plasticity. *Cerebellum Lond. Engl.* **2**, 206–214 (2003).

21 10. Wessel, L. *et al.* Long-term incubation with mifepristone (MLTI) increases the spine
22 density in developing Purkinje cells: new insights into progesterone receptor mechanisms.
23 *Cell. Mol. Life Sci. CMLS* **71**, 1723–1740 (2014).

24 11. Croci, L. *et al.* Local insulin-like growth factor I expression is essential for Purkinje
25 neuron survival at birth. *Cell Death Differ.* **18**, 48–59 (2011).

- 1 12. Hami, J. *et al.* Stereological study of the effects of maternal diabetes on cerebellar
2 cortex development in rat. *Metab. Brain Dis.* **31**, 643–652 (2016).
- 3 13. Armstrong, D. M. & Rawson, J. A. Activity patterns of cerebellar cortical neurones
4 and climbing fibre afferents in the awake cat. *J. Physiol.* **289**, 425–448 (1979).
- 5 14. Womack, M. & Khodakhah, K. Active Contribution of Dendrites to the Tonic and
6 Trimodal Patterns of Activity in Cerebellar Purkinje Neurons. *J. Neurosci.* **22**, 10603–
7 10612 (2002).
- 8 15. Schubert, M., Panja, D., Haugen, M., Bramham, C. R. & Vedeler, C. A. Paraneoplastic
9 CDR2 and CDR2L antibodies affect Purkinje cell calcium homeostasis. *Acta Neuropathol.*
10 *(Berl.)* **128**, 835–852 (2014).
- 11 16. Hirai, H. Basic research on cerebellar gene therapy using lentiviral vectors.
12 *Cerebellum Lond. Engl.* **11**, 443–445 (2012).
- 13 17. Nitta, K., Matsuzaki, Y., Konno, A. & Hirai, H. Minimal Purkinje Cell-Specific
14 PCP2/L7 Promoter Virally Available for Rodents and Non-human Primates. *Mol. Ther.*
15 *Methods Clin. Dev.* **6**, 159–170 (2017).
- 16 18. McKay, B. E. & Turner, R. W. Physiological and morphological development of the
17 rat cerebellar Purkinje cell: Purkinje cell output parallels dendritic development. *J. Physiol.*
18 **567**, 829–850 (2005).
- 19 19. Kapfhammer, J. P. Cellular and molecular control of dendritic growth and
20 development of cerebellar Purkinje cells. *Prog. Histochem. Cytochem.* **39**, 131–182 (2004).
- 21 20. Emoto, K., Yamashita, S. & Okada, Y. Mechanisms of heat-induced antigen retrieval:
22 does pH or ionic strength of the solution play a role for refolding antigens? *J. Histochem.*
23 *Cytochem. Off. J. Histochem. Soc.* **53**, 1311–1321 (2005).
- 24 21. De Bartolo, P., Florenzano, F., Burello, L., Gelfo, F. & Petrosini, L. Activity-
25 dependent structural plasticity of Purkinje cell spines in cerebellar vermis and hemisphere.
26 *Brain Struct. Funct.* **220**, 2895–2904 (2015).

1 22. Longair, M. H., Baker, D. A. & Armstrong, J. D. Simple Neurite Tracer: open source
2 software for reconstruction, visualization and analysis of neuronal processes. *Bioinforma.*
3 *Oxf. Engl.* **27**, 2453–2454 (2011).

4

5

6

1 **FIGURE LEGEND**

2 **Figure 1** | Evaluation of age-dependent rat Purkinje neuron culture. **(a)** Interdependent
3 relationship of Purkinje neuron yield and *in vitro* age of the 3D support cell layer (3D-SCL:
4 DIV 7 to 48) for E18, P0 and P10 derived-Purkinje neurons. **(b)** Representative Purkinje
5 neuron skeletons dependent on derived neuron age, 3D-SCL and protein kinase C (PKC)
6 antagonist K252a. Scale bar, 20 μm ; **(c)** Analysis of dendritic branch structure towards length
7 and branch orders for Purkinje neurons derived from E18, P0 and P10 tissue without and with
8 25 μM K252a to modulate PKC activity. **(d)** Interdependent relationship of Purkinje neuron
9 yield and concentration-dependent PKC activity modulation for E18, P0 and P10 derived-
10 Purkinje neurons. **(e)** Representative skeleton of an E18 derived-Purkinje neurons visualizing
11 the effect of 40 μM progesterone on dendritic branching. Scale bar, 20 μm ; **(f)**
12 Immunohistochemical representation of the major cell types (white) forming the 3D-SCL:
13 unipolar brush cells (CAL- calretinin), granule cells (GABAAR α 6), Golgi cells (NG-
14 neurogranin, GlyT2), Lugaro cells (GlyT2), stellate and basket cells (PAV-parvalbumin),
15 fibres such as mossy and climbing (VGluT2, PP-peripherin), oligodendrocytes (CNP1) as
16 well as microglia (IBA1). Nuclei staining DAPI (blue). Scale bar, 50 μm ; **(g)**
17 Immunohistochemical representation of mature Purkinje neurons (green; CB-calbindin, PCP2
18 - Purkinje cell specific protein 2) positive for post- and presynaptic biomarkers (magenta).
19 Postsynaptic: VGCC, mGluR1, and PSD95 including 3D IMARIS cartoon reconstruction of
20 the protein positive synapses on one chosen Purkinje neuron dendrite; Pre-synaptic: α -
21 synuclein (α -syn) – marker of glutamatergic synaptic terminals from granule cells (parallel
22 fibres) and unipolar brush cells (type I/II); GAD65- marker of axon terminals from stellate
23 and basket cells; bassoon – marker of the active zone of mossy fibre terminals and parallel
24 fibre terminals between Golgi cells and granule cells, and between basket cells and Purkinje
25 neurons; and synapsin I – synaptic vesicle phosphoprotein of mature CNS synapses; Nuclei
26 staining DAPI (blue). Scale bar, 20 μm ; **(h)** MEA recorded spike patterns (10s) with a cut-out

1 (1s) at day 21 *in vitro* following Purkinje neuron maturity. (i) Live-cell imaging of E18
2 derived-Purkinje neuron expressing lentiviral-induced GFP from day of seeding (DIV0) up to
3 2 months (DIV53). The Purkinje neuron development to maturity was very similar to *in vivo*,
4 as the fusion phase (E17 - P5 \approx DIV0 – DIV7), the phase of stellate cells with disoriented
5 dendrites (P5 - P7 \approx DIV7 – DIV9), as well as the phase of orientation and fluttering of the
6 dendritic tree (P7 - P21 \approx DIV9 – DIV23) were observed. Scale bar, 50 μ m

7

8 **Figure 2** | Optimized 3D rat Purkinje neuron culture protocol. Each tested culture desired
9 different conditions of support and activity interdependent of the starting tissue age. Whereas
10 the supplementation of insulin-like growth factor 1 (IGF1) and progesterone (PROG) induced
11 a stable environment to obtain high survival rates of Purkinje neurons, PKC activity
12 modulation mainly shaped the dendritic tree development, with the exception of P10 tissue
13 derived neurons where the survival was highly dependent on the inhibition of PKC but not
14 their dendritic tree development. The optimized protocol for all tested tissues relies on the
15 time point of placing the second cell layer, the Purkinje neuron enriched layer, and media that
16 is supplemented with IGF1, progesterone and K252a, where K252a starting concentration is
17 altered dependent on the used tissue to start the culture as follow; DIV1-10: E18 - 5 nM, P0 -
18 10 nM, P10 - 25 nM; DIV10-22: the K252a concentration is raised to 25 nM for E18 and P0
19 until the dendritic tree is well-developed and mature; DIV22-28: washout phase, K252a
20 supplementation is stopped (DIV22-24: 12.5 nM, DIV24-26: 6.75 nM, DIV26-28: 3.35 nM).
21 At DIV 28 the IGF1 and progesterone concentration is reduced by factor, 2.5 and 2,
22 respectively, to proceed to long-term culture conditions. The developed protocol allows to
23 grow a stable Purkinje neuron 3D culture for up to 6 months (DIV163) in a 6 to 24 well
24 format.

Table 1 | Primary antibodies. The signal to noise ratio for the antibodies were evaluated for the following conditions: 4% PFA at pH 7.2 diluted in 100 mM PBS; 1.5% PFA at pH 6 diluted in 100mM sodium acetate buffer (NaAcB); without heat-induced antigen retrieval (HIAGR); and with HIAGR either TRIS-based (pH 9) or citric acid-based (pH 6). The best conditions for each used antibody are described below.

Antibody	Species	Company	Cat. No.	LOT No.	RRID	Dilution [µg/mL]	PFA fixation	HIAGR	Marker
A-Synuclein	chicken	EnCorBio	CPCA-SNCA	71113	AB_2572385	1.0	1.5%; pH 6; NaAcB	No	Pre-synapse, granule and unipolar brush cells /PNS
Bassoon	chicken	SYSY	141016	141016/1-1	AB_2661779	Serum 1:500	4%, pH 7.2; PBS	No	Pre-synapse; Golgi / granule cells, or basket cells / PNS
Calbindin	guinea pig	SYSY	214005	214005/1-5	AB_2619902	0.5	4%, pH 7.2; PBS	No	Purkinje neurons
	chicken	SYSY	214006	214006/1-3	AB_2619903	Serum 1:750	4%, pH 7.2; PBS	No	Purkinje neurons
Calretinin	chicken	SYSY	214106	214106/2	AB_2619909	Serum 1:500	4%, pH 7.2; PBS	No	Unipolar-brush cells
CNP1	rabbit	SYSY	355003	355003/1-2	AB_2620112	1.0	4%, pH 7.2; PBS	No	Oligodendrocytes
GABA _A Rα6	rabbit	SYSY	224603	224603/3	AB_2619945	5.0	4%, pH 7.2; PBS	pH 9	Granule cells
GAD65	mouse	BD Bio-science	559931	4283665	AB_397380	2.5	1.5%; pH 6; NaAcB	No	Pre-synapse, stellate and basket cells / PNS
GlyT2	guinea pig	SYSY	272004	27004/2	AB_2619998	Serum 1:250	4%, pH 7.2; PBS	pH 6	Golgi cells; Lugaro cells
IBA1	rabbit	EnCorBio	RPCA-IBA1	266_100517	AB_2722747	1.0	4%, pH 7.2; PBS	No	microglia
mGluR1	guinea pig	FRONTIER	2571801		AB_2571801	2.5	1.5%; pH 6; NaAcB	No	PNS, Lugaro cells
Neurogranin	rabbit	SYSY	357003	357003/1	AB_2620115	2.5	4%, pH 7.2; PBS	No	Golgi cells
Parvalbumin	guinea pig	SYSY	195004	195004/1-21	AB_2156476	Serum 1:500	4%, pH 7.2; PBS	No	PNS, basket and stellate cells
PCP2	rabbit	Takara	M194	1AFXJ002.0		1.0	4%, pH 7.2; PBS	No	Purkinje neurons
Peripherin	rabbit	EnCor Bio	RPCA-Peri	0208_070316	AB_2572375	0.5	4%, pH 7.2; PBS	No	Mossy and climbing fibers
PSD95	mouse	Neuro mab	75-028	455.71D.22G	AB_2292909	5.0	1.5%; pH 6; NaAcB	No	Post-synapse
Synapsin 1/2	chicken	SYSY	106006	106006/1-4	AB_2622240	Serum 1:500	1.5%; pH 6; NaAcB	No	Pre-synapse
VGCC-PQ α-1A	guinea pig	SYSY	152205	152205/3	AB_2619842	4.0	1.5%; pH 6; NaAcB	No	Purkinje neuron synapse
VGluT2	guinea pig	SYSY	135404	135404/2-32	AB_887884	Serum 1:500	4%, pH 7.2; PBS	pH 6	Mossy and climbing fibers

EnCorBio: EnCor Biotechnology; SYSY: synaptic systems; PN: Purkinje neuron

Figure 1

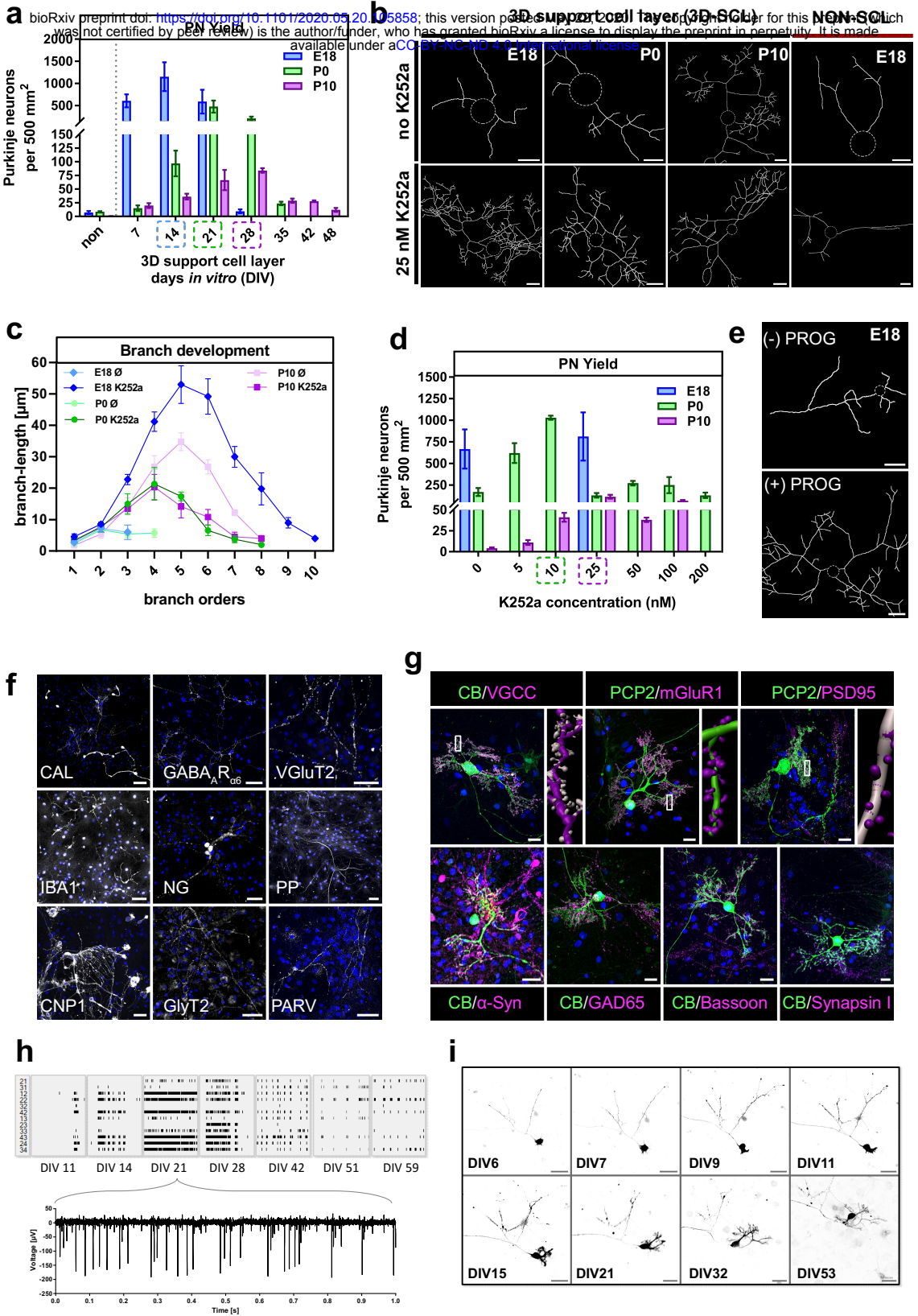
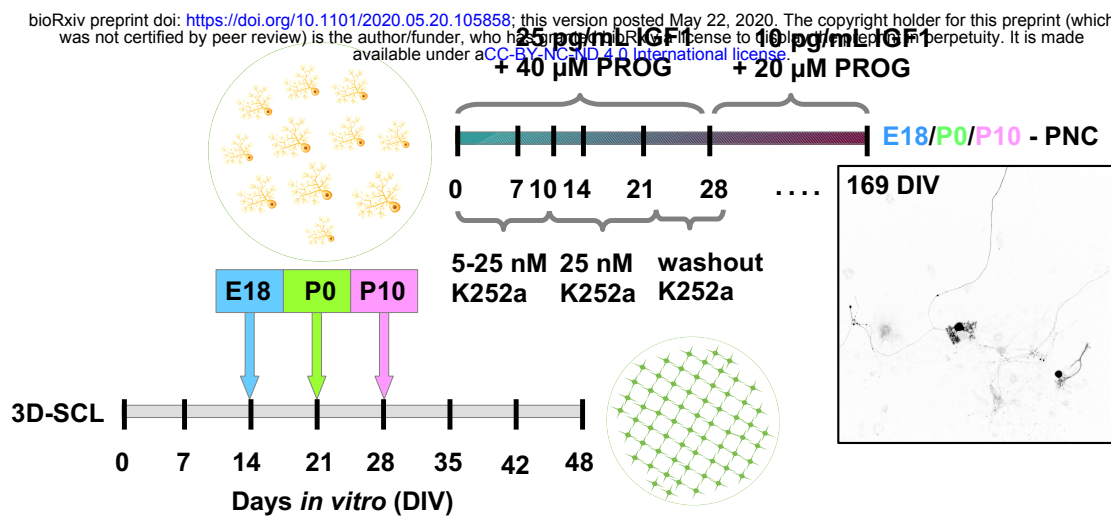


Figure 2

bioRxiv preprint doi: <https://doi.org/10.1101/2020.05.20.105858>; this version posted May 22, 2020. The copyright holder for this preprint (which was not certified by peer review) is the author/funder, who has granted bioRxiv a license to display the preprint in perpetuity. It is made available under aCC-BY-NC-ND 4.0 International license.





Graphic design: Communication Division, UIB / Print: Skjipes Kommunikasjon AS



uib.no

ISBN: 9788230867761 (print)
9788230849231 (PDF)